GAS TURBINE & PLASMA DYNAMICS LABORATORY
MASSACHUSETTS INSTITUTE OF TECHNOLOGY
CAMBRIDGE, MASSACHUSETTS

Optimal Mistuning for Enhanced Aeroelastic Stability of Transonic Fans

by

Kenneth C. Hall

Edward F. Crawley

GTL Report No. 176 November 1983

This research was carried out in the Gas Turbine and Plasma Dynamics Laboratory, MIT, supported by the NASA Lewis Research Center under grant NSG-3079

Abstract

An inverse design procedure was developed for the design of a mistuned rotor. The design requirements are that the stability margin of the eigenvalues of the aeroelastic system be greater than or equal to some minimum stability margin, and that the mass added to each blade be positive. The objective was to achieve these requirements with a minimal amount of mistuning. Hence, the problem was posed as a constrained optimization problem. The constrained minimization problem was solved by the technique of mathematical programming via augmented Lagrangians. The unconstrained minimization phase of this technique was solved by the variable metric method of Broyden, Fletcher, and Shanno.

The bladed disk was modelled as being composed of a rigid disk mounted on a rigid shaft. Each of the blades were modelled with a single tosional degree of freedom. Adamcyzk and Goldstein's linearized aerodynamic model for the unsteady moment coefficients in a supersonic cascade was applied at the typical section. The resulting non-self-adjoint eigenvalue problem is of the form $Aq = \lambda Bq$. The eigenvalues and eigenvectors of this eigenvalue problem were found by a fourth-order Runge-Kutta line integration of the derivatives of the eigenvalues and eigenvectors.

It was shown that mass mistuning does not introduce damping into the system, and that a necessary but not sufficient condition for stability is that the blade be self damped. The results of the optimization showed that an optimally mistuned rotor can achieve a given stability margin

for a much lower level of mistuning than alternate mistuning. However, it was shown that optimal mistuning is sensitive to errors in mistuning. Small errors in the implementation of optimal mistuning can severely reduce the gains in stability achieved by optimal mistuning. Alternate mistuning, on the other hand, is relatively insensitive to errors in mistune.

Acknowledgements

This work is supported by grant NSG-3079 from NASA Lewis Research Center, and has been monitored by Dr. John Adamcyzk and Mr. Donald Boldman.

Support was also provided to Kenneth Hall by the Fannie and John Hertz Foundation.

Table of Contents

Nomenclature

a	location of elastic axis
a_{pn}	coupling of the pth to the nth right eigenvector
$\underset{\sim}{A}$	matrix in eigenvalue problem $\underset{\sim\sim}{A}\underset{\sim}{q} = \lambda\underset{\sim\sim}{B}\underset{\sim}{q}$
b	semichord
b_{pn}	coupling of the pth to the nth left eigenvector
$\underset{\sim}{B}$	matrix in eigenvalue problem $\underset{\sim\sim}{A}\underset{\sim}{q} = \lambda\underset{\sim\sim}{B}\underset{\sim}{q}$
c	chord
c	stepsize
$\bar{c}$	maximimum stepsize
$\underset{\sim}{d}_K$	search direction
$\underset{\sim}{e}$	error in mistuning
$\underset{\sim}{E}$	transformation matrix
E	root mean square of errors in mistuning
$\underset{\sim}{g}$	gradient of cost function
$\underset{\sim}{H}$	Hessian matrix
i_a	active inequality constraint
i_b	inactive inequality constraint
I	number of Runge-Kutta integration steps
I_i	moment of inertia of typical section of ith blade
j	$\sqrt{-1}$
J	Lagrangian cost function
J_a	augmented Lagrangian cost function
k	reduced frequency
k_{α_i}	torsional stiffness of typical section of ith blade

l_{β_n}	unsteady moment coefficient acting on zeroth blade due to nth interblade phase angle travelling wave
$\underset{\sim}{L}$	influence coefficient matri.
L_K	the Kth influence coefficient
m	mass of typical section of blade
M	Mach number
$M^D_{\alpha_i}$	unsteady moment acting on ith blade due to disturbances
$M^M_{\alpha_i}$	unsteady moment acting on ith blade due to motion of blades
n	number of optimization parameters
N	number of blades
P	equality penalty function weights
q_i	displacement of ith blade
q_{β_n}	displacement of travelling wave of nth interblade phase angle
r	nondimesional radius of gyration
s	$s = j\Omega$
$\tilde{s}$	$s = j + \tilde{s}$
t	time
u	real part of s
v	imaginary part of s
V	reduced velocity
W	inequality penalty function weight
x	in the x direction
x_i	the ith optimization parameter
z	in the z direction
β	interblade phase angle

γ	reduction factor in stepsize control
δ_i	stiffness mistune of the ith blade
ϵ_i	mass mistune of the ith blade
ζ_i	stability margin of the ith eigenvalue
$\bar{\zeta}$	required stability margin
ν	inequality constraint Lagrange multiplier
θ	inequality constraint function
ϕ	objective cost function
λ	eigenvalue
μ	nondimensional mass of typical section of blade
η	equality constraint Lagrange multiplier
ξ	stagger angle
σ	solidity of cascade
σ	used in step size control
ψ	equality constraint function
ω_i	ith natural blade frequency
ω_R	reference blade frequency
Ω_N	rotational speed of rotor
Ω	nondimensional eigenfrequency

List of Tables

List of Figures

1. INTRODUCTION

The aeroelastic phenomenon of flutter in a transonic rotor is unusual in the field of airfoil aeroelasticity in that the instability is not of the frequency coalescence type which is common in isolated airfoils. The instability in a rotor is due to the destabilizing effect of the cascade aerodynamics. The motion of a single blade will cause unsteady aerodynamic forces on all the other blades. These forces can cause the rotor to be unstable. It has been shown by several researchers that the effect of mistuning, that is the altering of the natural frequencies of the blades of a rotor, generally has a benificial effect on the stability of the rotor [1-3]. In the past, however, the analysis of mistuned rotors has been limited to the determination of the aeroelastic behavior of a rotor whose mistuning has been specified. In this investigation, the inverse problem is solved. A method is presented for the determination of the mistuning arrangement which provides the greatest stability for the least amount of mistuning.

Recently, Kaza and Kielb [1,2] have used a bending-torsion coupled model of the blades to examine the effects of mistuning on subsonic and supersonic rotors. They showed that if the elastic axis is at the midchord of the blade, and the first bending frequency and the first torsional frequency of the blades are not nearly equal, then the flutter speed predicted by a single torsional mode agrees well with

the results of the two degree of freedom bending-torsion model. This indicates that the flutter of rotors is not of the clasical bending-torsion frequency coalescence type. Furthermore, their work has demonstrated that the effect of mistuning is generally stabilizing.

The phenomenon of flutter in transonic rotors is dependent on the unsteady aerodynamic forces acting on the blades of the rotor. Several authors have studied the unsteady forces acting on blades in supersonic flows [4-6]. The aerodynamic conditions modelled were steady uniform flows over flat, nonturning airfoils with unsteady perturbations of the flow due to the motion of the airfoils. The flow was modelled as irrotational, isentropic, and two-dimensional. The blades undergo simple harmonic motion but are phased such that the motion of the blades can be described in terms of travelling waves. This representation of the blade motion is useful for deriving these unsteady forces. However, it will be shown that this representation is not as useful for studying the mistuned aeroelastic behavior of the rotor.

The unsteady aerodynamic forces can, through a Fourier transformation, be converted into an influence coefficient form. The coefficients indicate the force felt on a reference blade for a unit amplitude displacement of any other blade on the rotor. In this form, one can clearly identify the origin of the forces acting on a blade. As early as 1969, Samoylovich [7] used such transformations to determine the

influence coefficients of an infinite cascade. In 1980, Srinivasan [8] used a similar transformation to study the influence of mistuning on blade torsional flutter of a shrouded fan. In that same year, Hanamura, Tanaka, and Yamaguchi [9] used the inverse of this transform to convert experimental data from individual blade generalized coordinates to travelling wave coordinates. Recently, Kaza and Kielb [1,2] have used a similar transformation to transform the mass and stiffness matrices from the individual blade coordinates to the travelling wave coordinates to study the effects of mistune on the flutter and forced response of rotors.

In Chapter 2 of this report, the basic theory of rotor aeroelasticity is reviewed. The blades are modelled with one degree of freedom per blade to study the effects of structural mistuning on the aeroelastic phenomenon of flutter. The mistuned rotor stability problem is cast as a matrix eigenvalue problem. By making use of the properties of the eigenvalue problem, it will be shown that structural mistuning does not introduce damping into the system, but rather makes use of the damping already present in the system to delay the onset of flutter. Hence, there are limits to the usefulness of mistuning as a mechanism for the preventition of flutter.

In Chapter 3, a method of determining the eigenvalues and eigenvectors of the mistuned system is presented. The first step in the process is to determine the derivatives of the

eigenvalues with respect to the mistune parameters. Once these derivatives are known, one can then integrate these derivatives to another mistuned state to determine the new eigenvalues and eigenvectors. This integration is carried out using a fourth-order Runge-Kutta algorithm. It was necessary to develop this method of evaluation of the eigenvalues for use with the inverse design procedure discussed in Chapter 4. Conventional methods of evaluating the eigenvalues of such a system (such as the inverse power method or the QR method) are shown to be unacceptable for use in the inverse design procedure.

The inverse design procedure is presented in Chapter 4. When designing a rotor which will not flutter, one would like to minimize the amount of mistuning required to achieve a flutter free system. For this reason, the inverse design procedure was posed as a constrained minimization problem. The minimized quantity is the amount of mistune in the rotor and the constraint insures an adequate stability margin. This inverse design problem can be divided into two parts: the definition of the problem statement; and the efficient solution for the constrained minimum. As part of the problem definition, a cost function must be defined which represents the level of mistune which is present in the rotor. The design specifications are then cast as constraints. For instance, one such design requirement is that the rotor be free of flutter at its aeroelastic design point. The second

part of the problem is to find the solution for this constrained minimization problem. The solution is defined as that mistune pattern which minimizes the cost function while satisfying all the design requirements. The technique used to solve this problem is mathematical programming via augmented Lagrangians [10,11].

Finally, in Chapter 5, the results of the optimization are presented. It will be shown that optimal mistuning can achieve the design requirements at a relatively low level of mistuning compared to alternate mistuning. However, several other issues need to be addressed before the designer can implement these optimal mistune patterns. For example, the optimal mistune patterns found in this investigation are very sensitive to errors in implementation. If the rotor is not mistuned very precisely, the rotor will lose the stability margin gained in the optimal mistuning. This and facets of the problem of practical implementation will be discussed, leading to a realistic assessment of the practical value and realizable optimization of rotor mistuning.

2. AEROELASTIC EQUATIONS OF MOTION FOR A BLADED DISK

In this chapter, the equations of motion which govern the aeroelastic behavior of a bladed disk are developed and the implications these equations have on stability are examined. The bladed disk is modelled as a rigid disk mounted on a rigid shaft. Each of the N flexible blades are aerodynamically identical but may have small differences in structural properties from one blade to the next. This structural nonuniformity is known as mistuning. Mistuning may be of a statistical nature due to manufacturing tolerances or material differences from blade to blade, or it may be designed into the rotor by introducing deliberate changes in blade materials or dimensions.

2.1 STRUCTURAL DYNAMIC MODEL OF THE BLADED DISK

The disk considered in this investigation is assumed to be rigid and mounted on a rigid shaft rotating at rotational speed Ω_N. Each blade is assumed to have a single torsional degree of freedom. In this investigation, this degree of freedom was taken to be the first torsional mode of the blade. The structural model does not include the effects of disk flexibility, rotation, or blade to blade coupling through shrouds. However, the principles of mistuning can be extended to include such effects as discussed by Kaza and Kielb [12]. In the absence of aerodynamic forces, each blade is uncoupled from every other blade and behaves like an uncoupled

oscillator. In this typical section analysis, the resulting equations of motion are

$$I_i \ddot{q}_i + \omega_{\alpha_i}^2 I_i q_i = 0, \quad i = 0, 1, 2, \ldots N-1 \tag{2.1}$$

where I_i is the typical section moment of inertia, ω_{α_i} is the first natural torsional frequency of the ith blade, and q_i is the torsional degree of freedom of the ith blade about the elastic axis as shown in Figure 2.1. In the presence of aerodynamic forces, the blades are recoupled since the forces acting on one blade depend on the time history of all the other blades.

$$I_i \ddot{q}_i + \omega_{\alpha_i}^2 I_i q_i = M_{\alpha_i}(q, \dot{q}, \ldots, M, k, \sigma, \xi, a, \ldots), \quad i = 0, 1, 2, \ldots, N-1 \tag{2.2}$$

where M = the relative Mach number

k = the reduced frequency of vibration

σ = the solidity of the rotor at the typical section

ξ = the stagger angle of the typical section

a = the location of the pitch axis

In matrix form this becomes

$$\left[I_i\right]\left\{\ddot{q}_i\right\} + \left[\omega_{ai}^2 I_i\right]\left\{q_i\right\} = \left\{M_{ai}^D\right\} + \left\{M_{ai}^M\right\} \qquad (2.3)$$

The right hand side of Equation (2.3) includes the effect of both forces due to external forcing and forces arising from the motion of the blades. Or said another way, the blades are subjected to both inhomogeneous and homogeneous forces. The stability of this system is governed by the homogeneous terms. Therefore, when analyzing the aeroelastic stability of the system, only the motion dependent forces need to be included.

To determine the solution to Equation (2.3), it is assumed that all the blades undergo simple harmonic motion. This assumption is made for two reasons. First, unsteady aerodynamics coefficients are derived assuming the airfoils of a cascade undergo uniform harmonic motion. Second, even though such an analysis does not strictly give the damping ratios of the different modes, such an analysis will correctly predict the neutral stability modes since the blades undergo simple harmonic motion at the stability boundary. With the assumption of simple harmonic motion, the displacement of the blades is expressed as

$$q_i = Re\left(\bar{q}_i e^{j\omega t}\right), \quad i = 0, 1, 2, \ldots, N-1 \qquad (2.4)$$

Substitution of Equation (2.4) into the equations of motion results in the eigenvalue problem

$$-\omega^2\left[I_i\right]\left\{\bar{q}_i\right\}e^{j\omega t} + \left[\omega_{\alpha_i}^2 I_i\right]\left\{\bar{q}_i\right\}e^{j\omega t} = \pi\rho b^4\omega^2\left[L\right]\left\{\bar{q}_i\right\}e^{j\omega t} \tag{2.5}$$

The aerodynamic influence coefficients, [L], are as yet undetermined. However, by the symmetry of the cascade, it must be that [L] is a circulant matrix [3]. That is, all the columns of [L] are identical except that each succesive column is shifted down by one row since the effect of blade 2 on blade 1 must be the same as the effect of blade 3 on blade 2, etc. Of course, [L] is still a function of ω since the unsteady aerodynamics are a function of the reduced frequency of vibration, $k = \omega b/U$. Dugundji and Bundas [13] have shown how to approximate the unsteady aerodynamic forces over a wide range of frequency k using Pade approximates and have included this effect into a standing wave flutter analysis. However, for the present analysis it is assumed that [L] is independent of ω since, for small amounts of mistune, the reduced frequency of the various modes varies by a small amount.

2.2 NONDIMENSIONAL FORM OF THE EIGENVALUE PROBLEM

Some insight into the problem of flutter can be gained by examining the eigenvalue equations in nondimensional form. Toward this end, Equation (2.5) is divided by $I_R\omega_R^2$ where ω_R is the first torsional frequency of the nominal reference blade and I_R is the typical section moment of inertia. Then the nondimensional eigenvalue problem becomes

$$\left[\widehat{(1+\delta_i)}\right]\{\bar{q}_i\} = \Omega^2\left[\left[\widehat{(1+\epsilon_i)}\right] + \frac{1}{\mu r^2}[L]\right]\{\bar{q}_i\} \qquad (2.6)$$

where ϵ_i = the fractional mass mistune of the ith blade

δ_i = the fractional stiffness mistune of the ith blade

$\Omega = \omega/\omega_R$ = the nondimensional eigenfrequency

μ = the nondimensional mass of the blade compared to the mass of the surrounding fluid

$= m/\pi\rho b^2$

r = the nondimensional radius of gyration

$= \sqrt{I/mb^2}$

m = the mass of the typical section of the nominal blade

In Equation (2.6), the matrix [L] appears as an apparent inertial term. This is a result of the choice of notation since the aerodynamic forces were assumed to be proportional to $\omega^2[L]$. If instead the aerodynamic forces were chosen to be proportional to $\omega_R{}^2[L]$, where ω_R is the natural frequency of the nominal blade, then [L] would appear as an apparent stiffness term. However, both are good approximations at the stability boundary for small levels of mistune. Dugundji and Bundas [13] have used Padé approximates to obtain better approximations to the aerodynamic forces both close to and away from the stability boundary and for a large range of reduced frequency.

Note that this eigenvalue problem is of the form

$$[A]\{\bar{q}\} = \lambda[B]\{\bar{q}\} \tag{2.7}$$

This form of the eigenvalue equation is slightly more difficult to work with than the standard eigenvalue form, $\underset{\sim}{A}\underset{\sim}{q} = \lambda\underset{\sim}{q}$. Some useful properties of Equation (2.7) are developed in Section 3.1.

In general, the eigenvalues λ will be complex and hence, Ω will also be complex. The fact that Ω is not purely real but will have a small imaginary part violates the assumption of simple harmonic motion. Strictly speaking, these eigenvalues do not give the correct damping ratio of the different eigenmodes. However, the assumption of simple harmonic motion is only violated slightly since the imaginary part of Ω is usually very small compared to the real part. Bundas [14] has shown that for small damping ratios, the damping ratio predicted by assumming simple harmonic motion gives a good approximation to the actual damping ratio.

This approach of assuming simple harmonic motion, only to find that the eigenvalues do not represent simple harmonic motion, is similar to the traditional V-g diagram analysis often used in analyzing the stability of isolated airfoils. The damping ratio of each eigenvalue found from Equation (2.6) is interpreted as the damping ratio which must be subtracted from that mode so that the mode will undergo simple harmonic motion.

An alternative formulation to the eigenvalue equation

given in Section 2.2 is to pose the eigenvalue problem in terms of travelling wave coordinates. Formulation of the nondimensional eigenvalue problem in this fashion gives

$$[E]^{-1}[(1+\delta_i)][E]\{q_{\beta_n}\} = \Omega^2\left[[E]^{-1}[(1+\epsilon_i)][E] + \frac{1}{\mu r^2}[\lambda_{\beta_n}]\right]\{q_{\beta_n}\} \tag{2.8}$$

where [E] is a linear transformation matrix (see Section 2.3), and q_{β_n} is a travelling wave with an interblade phase angle of $\beta_n = 2\pi n/N$. This form has been used by other investigators to study the effects of mistune on rotor stability and forced response [1,2]. The principle advantage to this form is that the eigenvalues and eigenvectors of the tuned system are readily determined. For ϵ_i and $\delta_i = 0$, the eigenvalue problem becomes

$$[I]\{q_{\beta_n}\} = \Omega^2\left[[I] + \frac{1}{\mu r^2}[\lambda_{\beta_n}]\right]\{q_{\beta_n}\} \tag{2.9}$$

The characteristic equation is then

$$\det\left([I] - \Omega^2\left[[I] + \frac{1}{\mu r^2}[\lambda_{\beta_n}]\right]\right) = 0 \tag{2.10}$$

Since all the matrices in Equation (2.9) are diagonal, the determinant is equal to zero if and only if one or more of the diagonal entries is equal to zero. This is equivalent to

$$\Omega_k^2\left(1 + \frac{\lambda_{\beta_k}}{\mu r^2}\right) = 1 \qquad k = 0, 1, 2, \ldots, N-1 \tag{2.11}$$

Hence, the eigenfrequencies are

$$\Omega_k = \frac{1}{+\sqrt{1 + \frac{l\beta_k}{\mu r}}} \qquad (2.12)$$

It is seen from Equation (2.12) that the tuned rotor will flutter if any one of the unsteady moment coefficients l_{β_n} has a positive imaginary part. This formulation of the eigenvalue problem is not as useful when ϵ_i and δ_i are not equal to zero. In the mistuned case, the matrices $[E]^{-1}\,[1+\epsilon_i][E]$ and $[E]^{-1}\,[1+\delta_i][E]$ will, in general, be fully populated.

2.3 DETERMINATION OF THE AERODYNAMIC INFLUENCE COEFFICIENT MATRIX

When describing simple harmonic motion of the blades, there are many equally valid generalized coordinate systems one can use to represent their motion. The three common choices are the travelling wave representation, the standing wave representation, and the individual blade coordinates where each blade is represented by its own degree of freedom. Of course, one may easily transform from one coordinate system to another by simple coordinate transformations. The choice of coordinate system will generally depend on the nature of the problem being solved. For instance, when analyzing a flexible disk, the natural choice is the standing wave coordinate system since for the tuned rotor, the eigenmodes are standing waves which can be classified by the number of

nodal diameters and nodal circumferences.

When deriving unsteady aerodynamic forces which act on a blade, it is easiest to work in travelling wave coordinates. However, describing the force acting on a reference blade as a function of interblade phase angle does not yield a physical understanding of the origin of these forces. One would like to look at the unsteady air loads as influence coefficients, i.e., forces which act on a given blade due to the motion of other individual blades. Looking at the forces in this manner gives a clearer picture of the mechanisms of flutter.

Consider the cascade shown in Figure 2.2. Suppose there is a travelling wave moving through the cascade with an interblade phase angle of $\beta_n = 2\pi n/N$. The deflection of the ith blade is then

$$q_i = q_{\beta_n} e^{j(\omega t + \beta_n i)} \tag{2.13}$$

As β_n has been defined, the travelling wave moves in the direction of rotor rotation with a wave speed of ω/n. Of course, it is equally valid to consider this motion as a backward travelling wave with an interblade phase angle of $2\pi - \beta_n$. To completely describe all possible combinations of sinusoidal motion of the N individual blades requires N interblade phase angles,

$$q_i = \sum_{n=0}^{N-1} q_{\beta_n} e^{j(\omega t + \beta_n i)} \tag{2.14}$$

This is conveniently expressed in matrix form as

$$\{q_i\} = [E]\{q_{\beta_n}\} e^{j\omega t} \tag{2.15}$$

where the matrix [E] is

$$[E] = \begin{bmatrix} E_{0,0} & E_{0,1} & E_{0,2} & \cdots & E_{0,N-1} \\ E_{1,0} & E_{1,1} & E_{1,2} & \cdots & \vdots \\ E_{2,0} & E_{2,1} & E_{2,2} & \cdots & \\ \vdots & \vdots & \vdots & \ddots & \\ \vdots & \vdots & \vdots & & \\ E_{N-1,0} & \cdots & & & E_{N-1,N-1} \end{bmatrix} \tag{2.16}$$

where $E_{k,l} = e^{j\frac{2\pi kl}{N}}$

The unsteady aerodynamic moment acting on the zeroth blade for a given travelling wave with amplitude q_{β_n} and interblade phase angle β_n is

$$M_{a_0} = \pi \rho b^4 \omega^2 l_{\beta_n} q_{\beta_n} e^{j\omega t} \tag{2.17}$$

But the force acting on the ith blade due to travelling wave mode n is just the force acting on the zeroth blade but shifted in phase by $\beta_n i$. Summing the contributions made from all the interblade phase angles gives

$$M_{a_i} = \pi \rho b^4 \omega^2 \sum_{n=0}^{N-1} l_{\beta_n} q_{\beta_n} e^{j(\omega t + \beta_n i)} \tag{2.18}$$

This is expressed more succinctly in matrix form.

$$\{M_{\alpha i}\} = \pi \rho b^4 \omega^2 [E][\lambda_{\beta_n}]\{q_{\beta_n}\} e^{j\omega t} \tag{2.19}$$

Next, Equation (2.15) is used to eliminate q_{β_n} from Equation (2.19). This gives the desired result of describing the unsteady aerodynamics in terms of the motion of the individual blades

$$\{M_{\alpha i}\} = \pi \rho b^4 \omega^2 [E][\lambda_{\beta_n}][E]^{-1}\{q_i\} \tag{2.20}$$

where the entries of the matrix $[E]^{-1}$ are given by

$$E^{-1}_{k,l} = \frac{1}{N} e^{-j\frac{2\pi kl}{N}} \tag{2.21}$$

So that finally the influence coefficient matrix [L] is given by

$$[L] = [E][\lambda_{\beta_n}][E]^{-1} \tag{2.22}$$

Multiplication of the right hand side yields that [L] is in fact a circulant matrix.

$$[L] = \begin{bmatrix} L_0 & L_{N-1} & L_{N-2} & \cdots & L_1 \\ L_1 & L_0 & L_{N-1} & \cdots & L_2 \\ L_2 & L_1 & L_0 & \cdots & L_3 \\ \vdots & \vdots & \vdots & \ddots & \vdots \\ L_{N-1} & L_{N-2} & L_{N-3} & \cdots & L_0 \end{bmatrix} \tag{2.23}$$

where $$L_K = \frac{1}{N}\sum_{n=0}^{N-1} l_{\beta_n} e^{+j\frac{2\pi K n}{N}} \qquad (2.24)$$

Equation (2.24) shows that L_K is just the Kth coefficient in a discrete Fourier series representation of l_{β_n}.

$$l_{\beta_n} = \sum_{K=0}^{N-1} L_K e^{-j\frac{2\pi K n}{N}} \qquad (2.25)$$

So for example, if [L] is a tridiagonal matrix, then the physical interpretation is that only the two blades adjacent to a given blade and the blade itself have any direct effect on the blade. Then from Equation (2.25), l_{β_n} will contain only cos(Ø), cos(β), and sin(β) components. In other words, the plot of the real and imaginary parts of l_{β_n} when plotted as a function of β will have a D.C. offset and will have components of cos(β) and sin(β). If the influence coefficient matrix has a larger bandwidth, then l_{β_n} will contain higher harmonics of cos(β) and sin(β).

As early as 1969, Samoylovich [7] used a similar Fourier transform to convert from travelling wave coordinates to individual blade coordinates. In 1980, Hanamura, Tananka, and Yamaguchi [9] reversed the process. They experimentally measured the influence coefficients of a cascade of blades in incompressible flow by vibrating a single blade and measuring the resulting forces on all the other blades. They then converted these forces to interblade phase angle coordinates

by the use of the Fourier series representation, Equation (2.25)

2.4 IMPORTANCE OF BLADE SELF DAMPING

As stated earlier, the matrix [L] is circulant. Hence, every term on the diagonal is equal. This term, denoted by L_0 , reflects the aerodynamic effect the motion of the blade has on itself. To show the importance of this term, consider the case of mass mistune only (i.e., no stiffness mistune, $\delta_i = \emptyset$). Then the eigenvalue problem can be written as

$$\frac{1}{\Omega^2}\left\{\bar{q}_i\right\} = \left[\left[(1+\epsilon_i)\right] + \frac{1}{\mu r^2}\left[L\right]\right]\left\{\bar{q}_i\right\} \qquad (2.26)$$

Here, $1/\Omega^2$ represents the eigenvalues of the matrix on the right hand side of Equation (2.26). Next, making use of the familiar matrix property that the sum of the eigenvalues of a matrix is equal to the trace of the matrix, it must be that

$$\frac{1}{N}\sum_{k=0}^{N-1}\frac{1}{\Omega_k^2} = 1 + \frac{L_0}{\mu r^2} + \frac{1}{N}\sum_{i=0}^{N-1}\epsilon_i \qquad (2.27)$$

Recall that the nominal reference blade in the absence of aerodynamic forces vibrates at the nondimensional frequency $\Omega = 1$. Since the unsteady aerodynamic forces are small compared to the elastic and inertial forces, we expect that the complex nondimensional eigenfrequencies Ω will be very close to unity. For convenience, let $j\Omega = s$. This gives the

familar s-plane interpretation of the poles or eigenfrequencies. If any pole lies in the right half of the complex plane, then the system is unstable.

In the remainder of this section, necessary conditions for stability will be derived. For stability, all poles must lie in the left half of the complex s-plane. Since Ω is approximately equal to unity, s will be nearly equal to j. Let s be represented by $s = j + \tilde{s}$ where $\tilde{s}$ is a complex number much less than unity. Then

$$\begin{aligned} \Omega &= -js \\ &= -j(j+\tilde{s}) \end{aligned} \tag{2.28}$$

so that

$$\begin{aligned} \frac{1}{\Omega^2} &= \frac{-1}{(-1+2j\tilde{s}+\tilde{s}^2)} \\ &= 1+2j\tilde{s}+O(\tilde{s}^2) \end{aligned} \tag{2.29}$$

Next the centroid of the poles in the complex plane, denoted by <s>, is found. Substitution of Equation (2.29) into (2.27) gives

$$\begin{aligned} \frac{1}{N}\sum_k (1+2j\tilde{s}_k) &\approx 1+\frac{L_0}{\mu r_1}+\frac{1}{N}\sum_i \epsilon_i \\ \langle s\rangle &\approx j\left(1-\frac{1}{2}\frac{L_0}{\mu r_1}-\frac{\langle\epsilon\rangle}{2}\right) \end{aligned} \tag{2.30}$$

The centroid of the poles is $\langle s \rangle$ so that from Equation (2.30)

$$\begin{aligned} Re\langle s\rangle &\approx \frac{1}{2} Im\left(\frac{L_0}{\mu r^2}\right) \\ Im\langle s\rangle &\approx 1 - \frac{1}{2} Re\left(\frac{L_0}{\mu r^2}\right) - \frac{\langle \epsilon \rangle}{2} \end{aligned} \tag{2.31}$$

Equation (2.31) shows, at least for small amounts of mistune and large μr^2, that the centroid of the poles lie in the left half of the complex plane if and only if $Im(L_0)$ is less than zero. This is equivalent to saying that a necessary but not sufficient condition for stability is that the blades must be self damped. Or said another way, if all the blades were perfectly rigid except for a single flexible reference blade, that blade must not flutter. This condition is the fundamental limitation to the usefulness of mistuning as a mechanism for stabilizing a bladed disk. Note that $Re\langle s \rangle$ is independent of ϵ_i. Physically, this is because mistuning does not introduce any damping into the system.

On the other hand, $Im\langle s \rangle$ does depend on ϵ_i. The lowering of the centroid by $\langle \epsilon \rangle/2$ in the complex plane just reflects the fact that the natural frequency of each blade is inversely proportional to the square root of $1 + \epsilon_i$. Similarly, the term $Re(L_0/\mu r^2)$ can be thought of as an effective mass added to the blade due to the unsteady aerodynamics, or alternatively, as an aerodynamic destiffening of the blade.

2.5 EXAMPLES OF TUNED AND MISTUNED ROTORS

As an example, consider the unsteady loads acting on a typical section of a blade. The aerodynamic model used in this example and throughout this investigation is that of Adamczyk and Goldstein's [4]. In this model, linearized theory is used to obtain the unsteady loads on flat plate airfoils undergoing small amplitude harmonic oscillations. Shocks are modelled as isentropic Mach waves and there is no steady pressure rise across the cascade. The typical section has a single torsional degree of freedom and pitches about its midchord. In this example, the reduced frequency, k, is equal to Ø.495, the Mach number, M, is equal to 1.317, the solidity, σ, is equal to 1.4Ø9, and the number of blades, N, is equal to 14. These rotor parameters are tabulated in Table 2.1. The unsteady moments for this model are plotted in Figure 2.3 as a function of interblade phase angle. Note that for interblade phase angles 25.71°, 51.43°, 77.14°, and $1Ø2.86^{\circ}$, the imaginary part of l_{β_n} is positive. Therefore, the rotor will flutter at this reduced velocity and Mach number in its tuned position. However, the average value of l_{β_n} is less than zero. This indicates that the centroid of eigenvalues lies in the left half of the s-plane and hence, it may be possible to achieve aeroelastic stability through the use of mistuning.

Next, Equation (2.24) is used to transform the unsteady moments from interblade phase coordinates to influence coefficient form. These influence coefficients are plotted in

Figure 2.4. Several interesting features of the influence coefficients deserve mention. First of all, the term L_0 has a negative imaginary part. This again reflects the fact that the average value of the imaginary part of 1_{β_n} is negative, or that the blade self damping is stabilizing, and hence, the potential for stability exists. Secondly, the largest coefficients are seen to be L_0, L_1, and L_{13}. It is clear that only the near field neighbors of a given blade exert a significant influence on the blade. The L_1 and L_{13}terms are the first off diagonal terms of [L]. Examination of Equation (2.25) reveals that a dominantly tridiagonal [L] results in an 1_{β_n} which has a strong first harmonic dependence in β_n. Figure (2.3) shows that this is in fact the case.

The previous discussion suggests that alternate mistuning may be an effective mistuning arrangement since one would expect such a pattern to reduce the influence adjacent blades have on each other. Figure 2.5 shows the eigenvalues of the tuned system plotted in the s-plane. Figure 2.6 shows the eigenvalues of the alternately mass mistuned rotor. The even numbered blades have $\varepsilon_i = \emptyset$ while the odd numbered blades have $\varepsilon_i = \emptyset.1$. This mistune pattern does in fact stabilize this rotor. However, it remains to be seen whether or not alternate mistuning is a near optimal mistuning arrangement. This discussion is deferred to Chapter 5.

3. EVALUATION OF EIGENVALUES AND THEIR DERIVATIVES

In the previous chapter, the stability of a rotor was found to be dependent on the eigenvalues of the aeroelastic eigenvalue problem. In the next chapter, an optimization procedure will be described. The goal of this optimization will be to find the mistune pattern which provides the most stability for the least amount of mistuning. In this optimizaton, it will be necessary to identify each of the eigenvalues uniquely. The technique used is this investigation to evaluate the eigenvalues while insuring unique identification will now be described.

Consider for the moment the tuned rotor under the influence of unsteady aerodynamic forces. For this system, there are N eigenvalues. Corresponding to each eigenvalue is an eigenmode. The nth eigenmode is a travelling wave with an interblade phase angle of $2\pi n/N$. However, as soon as the system is mistuned, the eigenmodes are no longer pure travelling waves of a single interblade phase angle. The problem is to in some sense identify each eigenvalue of the subsequent mistuned system with the eigenvalues of the original tuned system.

As an analogy, consider that the mistune introduced into the system is a gain and that the eigenvalues in the complex s-plane are the poles of a control system. As the gain is increased, i.e., as the level of mistune is increased in a continuous way, the poles, or eigenvalues, trace out root loci

in the complex plane. Hence, in some sense, one of the eigenvalues of the mistuned system will be identified with the nth eigenvalue of the tuned system since they both are on the same root locus.

It is not, however, an easy task to identify in this sense the nth mistuned eigenvalue. In general, the eigenmode of the nth mistuned eigenvalue will be composed of travelling waves of all N interblade phase angles. It is not generally possible to identify the the loci of roots that a particular root belongs by inspection of the eigenmodes. For these reasons, routines such as EISPACK [15] are not acceptable for the purposes of this investigation.

Therefore, before the optimization of Chapter 4 could be performed, a scheme had to be developed which could evaluate the eigenvalues of the aeroelastic eigenvalue problem while uniquely identifying the root locus to which each eigenvalue belongs. That method of determining the eigenvalues and eigenvectors of the aeroelastic equations of motion is the topic of this chapter. In Section 3.1, it is shown how the derivatives of the eigenvalues and eigenvectors with respect to the mistune parameters are determined. Once the derivatives of the eigenvalues and eigenvectors are known, one can integrate these quantities from one mistune level to another through the use of an explicit fourth-order Runge-Kutta operator. The details of such an integration are given in Section 3.2. Finally, an illustrative example is

presented in Section 3.3 which demonstrates the use of this technique.

3.1 NONDEGENERATE PERTURBATION THEORY APPLIED TO THE NON-SELF-ADJOINT EIGENVALUE PROBLEM

In this section, the derivatives of the N eigenvalues of the aeroelastic eigenvalue will be found with respect to the mistune parameters ε_i. First, some properties of the eigenvalue problem will be reviewed. These properties will then be used in a perturbation analysis of the eigenvalue problem. At a given level of mistune, a pertubation parameter will be introduced into the problem. The end result of the perturbation analysis will be that the derivatives of the eigenvalues and eigenvectors of the mistuned system will be known with respect to the single perturbation parameter. Finally, the derivatives will be generalized to produce the derivatives of the eigenvalues and eigenvectors with respect to each and every mistune parameter.

The eigenvalue problem

$$[A]\{q_{Rn}\} = \lambda_n [B]\{q_{Rn}\} \tag{3.1}$$

is known as a non-self-adjoint eigenvalue problem whenever one or both of the matrices A and B are not symmetric. Under these circumstances, the eigenvectors of Equation (3.1) are not in general the same as the eigenvectors of the adjoint

eigenvalue problem [16]:

$$\left[q_{Lm} \right]^T [A] = \lambda_m \left[q_{Lm} \right]^T [B] \tag{3.2}$$

However, both eigenvalue problems have the same set of eigenvalues since they both have the same characteristic equation

$$\det\left([A] - \lambda [B] \right) = 0 \tag{3.3}$$

The eigenvectors of Equations (3.1) and (3.2) are known as the right and left eigenvectors respectively. To obtain the relationship between the right and left eigenvectors, Equation (3.1) is premultiplied by the mth left eigenvector $\underset{\sim}{q}_{Lm}^T$, Equation (3.2) is postmuitiplied by the nth right eigenvector $\underset{\sim}{q}_{Rn}^T$, and the resulting equations are then subtracted one from another to obtain

$$(\lambda_m - \lambda_n) \left[q_{Lm} \right]^T [B] \{ q_{Rn} \} = 0 \tag{3.4}$$

It is assumed at this time that there are no repeated eigenvalues. Therefore, the only way for Equation (3.4) to be nontrivially satisfied is if

$$\left[q_{Lm} \right]^T [B] \{ q_{Rn} \} = 0 \qquad \begin{matrix} m \neq n \\ \lambda_m \neq \lambda_n \end{matrix} \tag{3.5}$$

This is known as the biorthogonality condition [16] and will be useful in the perturbation analysis which follows.

In Chapter 4, a procedure for optimally mistuning a rotor is described. As will be shown, it will be necessary to evaluate the derivatives of the eigenvalues and eigenvectors to perform this optimization. The remainder of this section deals with the determination of these derivatives through a perturbation analysis.

Suppose that the eigenvalues and eigenvectors of the general eigenvalue problem (3.1) are known. Next the matrices $\underset{\sim}{A}$ and $\underset{\sim}{B}$ are changed slightly. These changes are due to the introduction of a perturbation parameter γ. It is assumed that the matrices $\underset{\sim}{A}$ and $\underset{\sim}{B}$ can be expressed in terms of a Taylor series in γ. Then

$$A = A^{(0)} + \gamma A^{(1)} + \gamma^2 A^{(2)} + \cdots \tag{3.6}$$

$$B = B^{(0)} + \gamma B^{(1)} + \gamma^2 B^{(2)} + \cdots \tag{3.7}$$

where $\underset{\sim}{A}^{(0)}$, $\underset{\sim}{B}^{(0)}$, $\underset{\sim}{A}^{(1)}$, $\underset{\sim}{B}^{(1)}$, and so on are known quantities. Next it is assumed that the eigenvalues and eigenvectors of the problem can also be represented in terms of a Taylor series in γ:

$$\lambda_n = \lambda_n^{(0)} + \gamma \lambda_n^{(1)} + \gamma^2 \lambda_n^{(2)} + \cdots \tag{3.8}$$

$$q_{Rn} = q_{Rn}^{(0)} + \gamma \sum_{l=0}^{N-1} a_{ln} q_{Rl}^{(0)} + \cdots \tag{3.9}$$

$$q_{Ln} = q_{Ln}^{(0)} + \gamma \sum_{l=0}^{N-1} b_{ln} q_{Ll}^{(0)} + \cdots \tag{3.10}$$

where all the terms appearing in Equations (3.6) to (3.10) are of order unity except for γ. The terms like $a_{ln}\underset{\sim}{q}_{Rl}^{(0)}$ in Equations (3.9) and (3.10) represent a convenient change of basis for representing the changes in the eigenvectors. Substitution of Equations (3.6) to (3.9) into Equation (3.1) gives the following asymptotic relationship:

$$\begin{aligned}&(\underset{\sim}{A}^{(0)} + \gamma \underset{\sim}{A}^{(1)} + \cdots)(q_{Rn}^{(0)} + \gamma \sum_l a_{ln} q_{Rl}^{(0)} + \cdots) \sim \\ &(\lambda_n^{(0)} + \gamma \lambda_n^{(1)} + \cdots)(\underset{\sim}{B}^{(0)} + \gamma \underset{\sim}{B}^{(1)} + \cdots)(q_{Rn}^{(0)} + \gamma \sum_l a_{ln} q_{Rl}^{(0)} + \end{aligned} \tag{3.11}$$

Collecting terms in Equation (3.11) of equal order gives

$$\begin{aligned}\underset{\sim}{A}^{(0)} q_{Rn}^{(0)} - \lambda_n^{(0)} \underset{\sim}{B}^{(0)} q_{Rn}^{(0)} \sim \gamma(&-\underset{\sim}{A}^{(1)} q_{Rn}^{(0)} - \underset{\sim}{A}^{(0)} \sum_l a_{ln} q_{Rl}^{(0)} \\ &+ \lambda_n^{(1)} \underset{\sim}{B}^{(0)} q_{Rn}^{(0)} + \lambda_n^{(0)} \underset{\sim}{B}^{(1)} q_{Rn}^{(0)} + \lambda_n^{(0)} \underset{\sim}{B}^{(0)} \sum a_{ln} q_{Rl}^{(0)}) \\ &+ O(\gamma^2)\end{aligned} \tag{3.12}$$

For this asymptotic relationship to hold true, each coefficient of every order of γ must vanish. This results in the equalities

$$\gamma^0: \quad \underset{\sim}{A}^{(0)} q_{Rn}^{(0)} = \lambda_n^{(0)} \underset{\sim}{B}^{(0)} q_{Rn}^{(0)} \tag{3.13}$$

$$\begin{aligned}\gamma^1: \quad &\underset{\sim}{A}^{(1)} q_{Rn}^{(0)} + \underset{\sim}{A}^{(0)} \sum_l a_{ln} q_{Rl}^{(0)} = \\ &\lambda_n^{(1)} \underset{\sim}{B}^{(0)} q_{Rn}^{(0)} + \lambda_n^{(0)} \underset{\sim}{B}^{(0)} \sum a_{ln} q_{Rl}^{(0)}\end{aligned} \tag{3.14}$$

Equations (3.13) and (3.14) give the zeroth and first order perturbation relationships between the known quantities $\underset{\sim}{A}^{(0)}$, $\underset{\sim}{B}^{(0)}$, $\underset{\sim}{A}^{(1)}$, $\underset{\sim}{B}^{(1)}$ and the unknown quantities $\lambda_n^{(0)}$, $\lambda_n^{(1)}$, $\underset{\sim}{q}_{Rn}^{(0)}$, a_{1n}. Notice that the zeroth order equation is just the unperturbed eigenvalue problem, and $\lambda_n^{(0)}$ and $\underset{\sim}{q}_{Rn}^{(0)}$ can be found from its solution. This indicates that this is a regular perturbation problem.

To determine the first order changes in the eigenvalues, Equation (3.14) is premultiplied by $\underset{\sim}{q}_{Ln}^{(0)}$ and the biorthogonality condition is imposed to eliminate terms equal to zero with the result that

$$\underset{\sim}{q}_{Ln}^{(0)T}\underset{\sim}{A}^{(1)}\underset{\sim}{q}_{Rn}^{(0)} = \lambda_n^{(1)}\underset{\sim}{q}_{Ln}^{(0)T}\underset{\sim}{B}^{(0)}\underset{\sim}{q}_{Rn}^{(0)} + \lambda_n^{(0)}\underset{\sim}{q}_{Ln}^{(0)T}\underset{\sim}{B}^{(1)}\underset{\sim}{q}_{Rn}^{(0)} \tag{3.15}$$

Solving for the unknown quantity $\lambda_n^{(1)}$ gives

$$\lambda_n^{(1)} = \frac{\underset{\sim}{q}_{Ln}^{(0)T}(\underset{\sim}{A}^{(1)} - \lambda_n^{(0)}\underset{\sim}{B}^{(1)})\underset{\sim}{q}_{Rn}^{(0)}}{\underset{\sim}{q}_{Ln}^{(0)T}\underset{\sim}{B}^{(0)}\underset{\sim}{q}_{Rn}^{(0)}} \tag{3.16}$$

Hence, if $\underset{\sim}{A}$ and $\underset{\sim}{B}$ are perturbed about some point $\underset{\sim}{A}^{(0)}$ and $\underset{\sim}{B}^{(0)}$, the value of the nth eigenvalue can now be estimated with errors of order γ^2 by substitution of equation (3.16) into Equation (3.8).

The perturbed eigenvectors are found in a similar fashion. Equation (3.13) is premultiplied by $\underset{\sim}{q}_{Lp}^{(0)T}$. Again, the biorthogonality relations are used with the result that

$$q_{Lp}^{(0)T} \underset{\sim}{A}^{(1)} q_{Rn}^{(0)} + a_{pn}\lambda_p^{(0)} q_{Lp}^{(0)T} \underset{\sim}{B}^{(0)} q_{Rp} = \lambda_n^{(0)} q_{Lp}^{(0)T} \underset{\sim}{B}^{(1)} q_{Rn}^{(0)} + a_{pn}\lambda_n^{(0)} q_{Lp}^{(0)T} \underset{\sim}{B}^{(0)} q_{Rp}^{(0)} \quad (3.17)$$

Or solving for a_{pn} gives

$$a_{pn} = \frac{q_{Lp}^{(0)T}(\underset{\sim}{A}^{(1)} - \lambda_n^{(0)} \underset{\sim}{B}^{(1)}) q_{Rn}^{(0)}}{(\lambda_n^{(0)} - \lambda_p^{(0)}) q_{Lp}^{(0)T} \underset{\sim}{B}^{(0)} q_{Rp}^{(0)}} \quad (3.18)$$

The left eigenvalue perturbation terms are found in a completely analogous fashion.

$$b_{pn} = \frac{q_{Ln}^{(0)T}(\underset{\sim}{A}^{(1)} - \lambda_n^{(0)} \underset{\sim}{B}^{(1)}) q_{Rp}^{(0)}}{(\lambda_n^{(0)} - \lambda_p^{(0)}) q_{Lp}^{(0)T} \underset{\sim}{B}^{(0)} q_{Rp}^{(0)}} \quad (3.19)$$

Note that Equation (3.18) is valid only if $p \neq n$ and $\lambda_p^{(0)} \neq \lambda_n^{(0)}$. This analysis is therefore known as nondegenerate perturbation theory [17] since the eigenvalues must be distinct.

The scalar a_{pn} indicates the degree to which the pth eigenvector is coupled to the nth eigenvector through the introduction of a small perturbation. Note that eigenvectors with closely spaced eigenvalues are more easily coupled than those whose eigenvalues are far apart due to the $(\lambda_n^{(0)} - \lambda_p^{(0)})$ term appearing in the denominator of Equation (3.18). From Equation (3.16) it is observed that the eigenvalue perturbations do not exibit this amplification due to the proximity of other eigenvalues.

The range of validity of this perturbation analysis is that range for which $\gamma\lambda_n^{(1)}$, $\gamma \underset{\sim}{q}_{Rn}^{(1)}$, and $\gamma \underset{\sim}{q}_{Ln}^{(1)}$ are less than

order unity. Hence, from Equations (3.18) and (3.19), it is clear that for this to hold, it must be that γ is small compared to $\min(\lambda_n^{(0)} - \lambda_p^{(0)})$, the spacing of the closest eigenvalues. It is this fact which ultimately limits the usefulness of such an approximation.

An interesting feature of this first order perturbation analysis is that a_{nn} and b_{nn} are not determined. This is due to the fact that there is some degree of freedom in choosing an eigenvector. Recall an eigenvector specifies a direction in N-space but not a length. Furthermore, to order γ, a small perturbation of the eigenvector in the direction of the eigenvector only produces a change in direction of order γ^2. Hence, one is free to choose any values for a_{nn} and b_{nn} so long as they are no greater than O(1). For convenience, the values of a_{nn} and b_{nn} are taken to be zero.

Although the first order coefficients $\lambda_n^{(1)}$, $\underset{\sim}{q}_{Rn}^{(1)}$, and $\underset{\sim}{q}_{Ln}^{(1)}$ were derived from a perturbation analysis, Plaut and Huseyin [18] have shown that these are in fact the first derivatives of the eigenvalues and the right and left eigenvectors with respect to the variable γ. In the mass mistuning problem, there are N independent variables denoted by the mass mistune vector $\underset{\sim}{\varepsilon}$. The results of the previous section can be generalized to give the derivatives with respect to every mistune variable:

$$\frac{\partial \lambda_n}{\partial \epsilon_i} = \frac{q_{Ln}^T \left(\frac{\partial A}{\partial \epsilon_i} - \lambda_n \frac{\partial B}{\partial \epsilon_i} \right) q_{Rn}^T}{q_{Ln}^T \underline{B} \, q_{Rn}} \tag{3.20}$$

$$\frac{\partial q_{Rn}}{\partial \epsilon_i} = \sum_{l \neq n} \left[\frac{q_{Ll}^T \left(\frac{\partial A}{\partial \epsilon_i} - \lambda_n \frac{\partial B}{\partial \epsilon_i} \right) q_{Rn}}{(\lambda_n - \lambda_l) q_{Ll}^T B q_{Rl}} \right] q_{Rl} \tag{3.21}$$

$$\frac{\partial q_{Ln}}{\partial \epsilon_i} = \sum_{l \neq n} \left[\frac{q_{Ln}^T \left(\frac{\partial A}{\partial \epsilon_i} - \lambda_n \frac{\partial B}{\partial \epsilon_i} \right) q_{Rl}}{(\lambda_n - \lambda_l) q_{Ll}^T B q_{Rl}} \right] q_{Ll} \tag{3.22}$$

3.2 INTEGRATION OF EIGENVALUES AND EIGENVECTORS FROM THEIR DERIVATIVES

In the previous section, the derivatives of the eigenvalues and eigenvectors were found with respect to the mistune parameters. Equations (3.20) through (3.22) make up a system of $N^2 + 2N^3$ first order, coupled, partial differential equations for the N unknown eigenvalues and 2N unknown eigenvectors. There are N independent variables ϵ_i. If the derivatives of the eigenvalues and eigenvectors are known everywhere along a line, then a line integration can be performed to evaluate the eigenvalues and eigenvectors at a point along this line. This method of solving for the eigenvalues and eigenvectors has two advantages. First, if the matrices $\underset{\sim}{A}$ and $\underset{\sim}{B}$ are changed slightly, then the new eigenvalues and eigenvectors can be evaluated by integrating over a short distance with less computational effort than the effort required to completely re-solve the eigenvalue problem. Secondly, the eigenvalues are automatically kept track of in the root locus sense. The problem of eigenvalue identity discussed in the introduction to this chapter is completely eliminated. This was the main reason for choosing this method

of eigenvalue evaluation.

Now that the derivatives are known, they may be used in a line integration of the eigenvalues and eigenvectors. Assume the line of integration to be the line in parameter space that connects some old value of the independent variable $\underset{\sim}{\epsilon}_K$ to the new value $\underset{\sim}{\epsilon}_{K+1}$. The path of integration can then described in terms of a single scalar variable h:

$$\begin{aligned}\left\{\epsilon_i\right\}_{K+1} &= \left\{\epsilon_i\right\}_K + h\left(\left\{\epsilon_i\right\}_{K+1} - \left\{\epsilon_i\right\}_K\right) \\ &= \left\{\epsilon_i\right\}_K + h\left\{\Delta\epsilon_i\right\}_K\end{aligned} \tag{3.23}$$

where h is a scalar value which varies from zero to one along the path of integration. Equations (3.20) through (3.22) can be reduced to a system of $N + 2N^2$ coupled, first order, ordinary differential equations by the chain rule.

$$\frac{d}{dh} = \frac{d\epsilon_1}{dh}\frac{\partial}{\partial\epsilon_1} + \frac{d\epsilon_2}{dh}\frac{\partial}{\partial\epsilon_2} + \cdots + \frac{d\epsilon_N}{dh}\frac{\partial}{\partial\epsilon_N} \tag{3.24}$$

The derivatives of the dependent variables along the line of integration and the distance along the path of integration can now be expressed in terms of a single scalar variable h. For example, the derivative of λ_n with respect to h is

$$\frac{d\lambda_n}{dh} = \left[\Delta\epsilon_i\right]_K \begin{Bmatrix} \frac{\partial\lambda_n}{\partial\epsilon_1} \\ \frac{\partial\lambda_n}{\partial\epsilon_2} \\ \frac{\partial\lambda_n}{\partial\epsilon_3} \\ \vdots \\ \frac{\partial\lambda_n}{\partial\epsilon_N} \end{Bmatrix} \tag{3.25}$$

where the terms $\partial\lambda_n/\partial\varepsilon_i$ are given by Equation (3.20).

The numerical scheme used to compute the line integrals is a fourth order Runge-Kutta scheme [19]. Truncation errors are then of the order of step size to the fifth power. This type of scheme is one of a class of explicit predictor-corrector methods. The method is carried out in four steps:

$$\begin{aligned}
\lambda_{n_{K+1}} &= \lambda_{n_K} + \frac{1}{6}\left(J_{\lambda_n}^{(1)} + 2J_{\lambda_n}^{(2)} + 2J_{\lambda_n}^{(3)} + J_{\lambda_n}^{(4)}\right) \\
\underset{\sim}{q}_{R_{n_{K+1}}} &= \underset{\sim}{q}_{R_{n_{K+1}}} + \frac{1}{6}\left(\underset{\sim}{J}_{q_{Rn}}^{(1)} + 2\underset{\sim}{J}_{q_{Rn}}^{(2)} + 2\underset{\sim}{J}_{q_{Rn}}^{(3)} + \underset{\sim}{J}_{q_{Rn}}^{(4)}\right) \\
\underset{\sim}{q}_{L_{n_{K+1}}} &= \underset{\sim}{q}_{L_{n_{K+1}}} + \frac{1}{6}\left(\underset{\sim}{J}_{q_{Ln}}^{(1)} + 2\underset{\sim}{J}_{q_{Ln}}^{(2)} + 2\underset{\sim}{J}_{q_{Ln}}^{(3)} + \underset{\sim}{J}_{q_{Ln}}^{(4)}\right) \\
& \qquad n = 0, 1, 2, \ldots, N-1
\end{aligned} \tag{3.26}$$

where

$$\begin{aligned}
J_{\lambda_n}^{(1)} &= \frac{d\lambda_n}{dh}\left(\underset{\sim}{\varepsilon}_{i_K}, \lambda_0, \lambda_1, \ldots, \underset{\sim}{q}_{R0}, \underset{\sim}{q}_{R1}, \ldots\right) \\
J_{\lambda_n}^{(2)} &= \frac{d\lambda_n}{dh}\left(\underset{\sim}{\varepsilon}_{i_K} + \tfrac{1}{2}\Delta\underset{\sim}{\varepsilon}_{i_K}, \lambda_0 + \tfrac{1}{2}J_{\lambda_0}^{(1)}, \lambda_1 + \tfrac{1}{2}J_{\lambda_1}^{(1)}, \right. \\
&\qquad \left. \ldots, \underset{\sim}{q}_{R0} + \tfrac{1}{2}\underset{\sim}{J}_{q_{R0}}^{(1)}, \ldots\right) \\
J_{\lambda_n}^{(3)} &= \frac{d\lambda_n}{dh}\left(\underset{\sim}{\varepsilon}_{i_K} + \tfrac{1}{2}\Delta\underset{\sim}{\varepsilon}_{i_K}, \lambda_0 + \tfrac{1}{2}J_{\lambda_0}^{(2)}, \lambda_1 + \tfrac{1}{2}J_{\lambda_1}^{(2)}, \right. \\
&\qquad \left. \ldots, \underset{\sim}{q}_{R0} + \tfrac{1}{2}\underset{\sim}{J}_{q_{R0}}^{(2)}, \ldots\right) \\
J_{\lambda_n}^{(4)} &= \frac{d\lambda_n}{dh}\left(\underset{\sim}{\varepsilon}_{i_K} + \Delta\underset{\sim}{\varepsilon}_{i_K}, \lambda_0 + J_{\lambda_0}^{(3)}, \lambda_1 + J_{\lambda_1}^{(3)}, \right. \\
&\qquad \left. \ldots, \underset{\sim}{q}_{R0} + \underset{\sim}{J}_{q_{R0}}^{(3)}, \ldots\right) \\
\underset{\sim}{J}_{q_{Rn}}^{(1)} &= \frac{d\underset{\sim}{q}_{Rn}}{dh}\left(\underset{\sim}{\varepsilon}_{i_K}, \lambda_0, \lambda_1, \ldots, \underset{\sim}{q}_{R0}, \underset{\sim}{q}_{R1}, \ldots\right) \\
&\vdots
\end{aligned} \tag{3.27}$$

To integrate over larger distances, say from $\underset{\sim}{\varepsilon}_I$ to

$\underset{\sim}{\varepsilon}_{II}$, the path of integration is divided into some number of intervals, I, as shown in Figure 3.1. These intervals are picked sufficiently small to avoid significant truncation error but large enough to keep the amount of computation required at a reasonable level. The line integration is then carried out using I fourth order Runge-Kutta integration steps.

This method of evaluating the eigenvalues and eigenvectors of the equations of motion is not efficient when the number of integration intervals is large. However, when I is small, this method requires computation time on the same order as EISPACK. Generally, when evaluating the eigenvalues and eigenvectors of the mistuned system in the constrained optimization procedure discussed in Chapter 4, I is less than or equal to two. Under these circumstances, this procedure is reasonably efficient. But more importantly, the identities of the eigenvalues are determined in the process of the integration. This is a requirement for the constrained optimization of the flutter problem.

3.3 EVALUATION OF THE ALTERNATELY MISTUNED ROTOR BY RUNGE-KUTTA INTEGRATION

In the previous section, it was shown how to evaluate the eigenvalues and eigenvectors of the aeroelastic eigenvalue problem by a Runge-Kutta integration. In this section, a numerical example of that technique is presented which

demonstrates the accuracy of this technique.

The example will proceed as follows: first the exact eigenvalues of an alternately mistuned rotor will be found. Then the Runge-Kutta integration technique will be used with the path of integration divided into 1, 2, 3, and 10 intervals as described in the previous section.

The aeroelastic properties of this rotor are listed in Table 2.1. This is the same 14-bladed rotor first introduced in Chapter 2. The rotor was alternately mistuned in mass. The masses of the even numbered blades was increased by 10 percent while the masses of the odd numbered blades were unchanged. EISPACK was used to determine the exact values of the 14 eigenvalues.

Next, the Runge-Kutta scheme was used to evaluate the eigenvalues of the system described above. The tuned eigenvalues and eigenvectors were use as the starting point of the integration since the eigenvalues and eigenvectors are easily determined at this point. Of course the accuracy of the integration will be determined by the step size of the intervals (inversely proportional to the number of intervals) used in the integration. The step size controls the level of truncation error. Hence, a smaller step size produces smaller total integrated errors. However, one must balance accuracy with computational efficiency. Integrations with small step sizes generally imply many steps and, hence, a large amount of computation.

Figures 3.2 through 3.5 show graphically the effect of step size on integration accuracy. Figures 3.2, 3.3, and 3.4 show the results of the integration where the path of integration has been divided into one, two, and three intervals respectively. Notice that some of the eigenvalues evaluated by this approximate integration are very different than the exact eigenvalues as determined by EISPACK. This is due to the large step size used in the numerical integration. If the number of intervals is increased to 10, the approximate eigenvalues found from integration are virtually indistinguishable from the exact eigenvalues as indicated in Figure 3.5.

The most useful feature of this method of evaluating the eigenvalues is not its efficiency since in fact for an integration which requires many intervals, this method is computationally very expensive. Its utility is in its ability to to retain the identities of the eigenvalues no matter how severe the mistuning. For this reason, this is the method used for evaluating the eigenvalues in the optimization procedure described in the next chapter.

4. OPTIMAL MISTUNING OF A BLADED DISK TO PREVENT FLUTTER

When mistuning a rotor to prevent flutter, one would like, in some sense, to minimize the amount of mistuning while maximizing the stability of the rotor. Not only does such an optimization make the production of a mistuned rotor more attractive but the results of this minimization may provide some insight into the nature of mistuning.

In this chapter, such an optimization procedure is outlined. The objective of the optimization is to determine that mistune pattern which delivers the most stability for the least amount of mistuning. A cost function is devised which is a measure of the level of mistune in the rotor. This cost function is to be minimized subject to certain physical constraints on the problem. Although the desired effect is to maximize the stability of the rotor, it is more appropriate to modify the above optimization statement to make stability a constraint rather than a maximized quantity. The problem is then to minimize the level of mistuning in the rotor while meeting some minimum requirement of stability. Although these conditions may be stated very easily in mathematical terms, the solution to the problem is a computationally difficult task.

Other authors have shown the useful benefits of alternate mistuning [1-3]. It has been suggested that the alternate mistune pattern may be nearly optimal [3]. The results of the optimization procedure presented in this chapter will be

presented in Chapter 5. It will be shown that in fact, alternate mistune is not nearly optimal, but does have other favorable properties that optimal mistuning does not always have.

4.1 FORMULATION OF THE MISTUNING PROBLEM AS A NONLINEAR CONSTRAINED OPTIMIZATION

In this section, the mistuning problem is formulated as a nonlinear constrained minimization problem. The steps to be taken are: first, chose an appropriate cost function which represents the level of mistuning in the rotor. Second, define the set of minimum requirements which must be met. These are known as constraints. Together, the objective cost function and the constraints form the constrained optimization problem.

The first task in formulating the formal constrained optimization problem is to define the objective cost function. The objective cost function will be chosen to be a measure of the amount of mistuning in the rotor. As a simple case, suppose the cost of mistuning, ϕ, is chosen to be the absolute value of the mass fraction added to the blade with the greatest amount of mistuning. Then

$$\phi(\underline{\epsilon}) = \max\left(|\epsilon_0|, |\epsilon_1|, |\epsilon_2|, \ldots, |\epsilon_{N-1}|\right) \tag{4.1}$$

This cost function, although conceptually meaningful, is not

amenable to many nonlinear programming methods due to the discontinuities in the gradient of the cost at various locations in the domain. Note, however, that this cost function is equivalent to the cost function

$$\phi(\underset{\sim}{\epsilon}) = \sqrt[I]{\frac{\sum_{i=0}^{N-1} \epsilon_i^I}{N}} \quad ; \quad I \to \infty \tag{4.2}$$

where I is a positive even integer. For large but finite I this function closely approximates the cost function in Equation (4.1) but has no discontinuities anywhere. For this investigation, I was taken to be 4.

$$\phi(\underset{\sim}{\epsilon}) = \sqrt[4]{\frac{\sum_{i=0}^{N-1} \epsilon_i^4}{N}} \tag{4.3}$$

Originally, I was chosen to be 2, making the cost the root mean square value of the mass mistuning. In this case, the cost function is then just proportional to the length of the mass mistune vector $\underset{\sim}{\epsilon}$. However, it was found that this cost function, when optimized, does not penalize strongly enough large amounts of mistune in a single blade. The result is that the mass of one of the blades may become much too large to be practical. For this reason, I was increased to 4. This gave a more physically realizable distribution of mistuning.

As will be shown, the optimization procedure outlined in this chapter requires that the derivatives of the cost

function and the constraints be evaluated. The gradient of this cost function is

$$\nabla\phi = \frac{\phi^{-3}}{\sqrt[4]{N}} \begin{Bmatrix} c_0^3 \\ c_1^3 \\ c_2^3 \\ \vdots \\ c_{N-1}^3 \end{Bmatrix} \tag{4.4}$$

Having defined the cost function, the next step in formulating the constrained optimization problem is to define the appropriate set of constraints. As previously mentioned, the cost function will be minimized subject to minimum stability requirements. These stability requirements are interpreted as constraints. The measure of stability will be the damping ratio of the eigenvalues of the eigenvalue problem given by Equation (2.6). Recall that these damping ratios are not the physical damping ratios of the eigenmodes but rather are damping ratios in the sense of a V-g analysis. If the eigenvalue of the ith mode of Equation (2.6) is $j\Omega_i = s_i = u_i + jv_i$, then the damping ratio of the ith mode is given by

$$\gamma_i = \frac{-U_i}{\sqrt{U_i^2 + V_i^2}} \quad , \quad i = 0, 1, 2, \ldots, N-1 \tag{4.5}$$

One set of constraints is then that each and every mode of the rotor must have a damping ratio greater than or equal to some minimum damping ratio, $\bar{\zeta}$, as shown in Figure 4.1. This is expressed in the standard inequality form

$$\theta_i(\underline{b}) = f_i - \bar{f} \geq 0 \quad , \quad i = 0, 1, 2, \ldots, N-1 \tag{4.6}$$

which gives N constraints to be satisfied, represented by the functions θ_i.

Another set of constraints used in this investigation is that mass can be added to a blade to mistune the blade but mass cannot be removed. This constraint was used because it was felt that a practical way to mistune blades would be to add mass to the tip of the blade or to reduce the stiffness of the root. Both of these methods tend to lower the natural frequency of the blade. In this problem, the stiffness of each blade was held fixed. It is believed that the natural frequencies of the individual blades dominates the mistuning effects. Hence, one may work with either mass or stiffness mistunings or a combination of the two with little difference in the resulting natural frequencies of the mistuned blades.

This second set of constraints is expressed simply as

$$\theta_{i+N}(\underline{\epsilon}) = \epsilon_i \geq 0 \quad , \quad i = 0, 1, 2, \ldots, N-1 \tag{4.7}$$

which gives an additional N constraints to be satisfied.

Together these two sets of constraints provide a total of 2N inequality constraints for the minimization of a cost function of N variables. There were no equality constraints used in this investigation.

The first derivative of the eigenvalue constraints

(Equation (4.6)) are

$$\frac{\partial \theta_i}{\partial \epsilon_j} = \frac{-V_i}{(U_i^2+V_i^2)^{3/4}}\left[V_i \frac{\partial U_i}{\partial \epsilon_j} - U_i \frac{\partial V_i}{\partial \epsilon_j}\right] \tag{4.8}$$

where $$\frac{\partial U_i}{\partial \epsilon_j} = \frac{-1}{2(U_i^2+V_i^2)}\left(U_i \frac{\partial \lambda_{Re_i}}{\partial \epsilon_j} + V_i \frac{\partial \lambda_{Im_i}}{\partial \epsilon_j}\right)$$

$$\frac{\partial V_i}{\partial \epsilon_j} = \frac{-1}{2(U_i^2+V_i^2)}\left(U_i \frac{\partial \lambda_{Im_i}}{\partial \epsilon_j} - V_i \frac{\partial \lambda_{Re_i}}{\partial \epsilon_j}\right)$$

where recall that $\lambda = \Omega^2$ and the derivatives of λ are given by Equation (3.20). The derivatives of the mass inequality constraints (Equation (4.7)) are

$$\frac{\partial \theta_{inv}}{\partial \epsilon_j} = \Delta_{ij} \tag{4.9}$$

where Δ_{ij} is the Kronecker delta.

To summarize, the purpose of the optimization procedure is to provide the most stability for a given rotor at its aeroelastic operating point for the lowest level of mistune. The formal mathematical statement of the problem is slightly different. The mistuned rotor must meet damping ratio requirements at a minimum cost which reflects the amount the rotor is mistuned. Furthermore, mass changes or mistunings in each blade must, in this investigation, be positive.

4 2 FORMULATION OF THE CONSTRAINED OPTIMIZATION PROBLEM USING LAGRANGE MULTIPLIERS

The general problem of nonlinear programming is to find

the minimum of some cost function subject to constraints. The cost function ϕ is a function of the n variables $\underset{\sim}{x}$:

$$\phi = \phi(\underset{\sim}{x}) \tag{4.10}$$

In general, there may be two types of constraints which must be satisfied: equality and inequality constraints. Equality constraints are of the form

$$\gamma_i(\underset{\sim}{x}) = 0 \;, \quad i = 1, 2, \ldots, p \quad p < n \tag{4.11}$$

while inequality constraints are of the form

$$\theta_j(\underset{\sim}{x}) \geq 0 \;, \quad j = 1, 2, \ldots, q \quad q \gtreqless n \tag{4.12}$$

As indicated above, there may be any number of inequality constraints but there must be fewer equality constraints than the number of independent variables, n. The region in x-space where these constraints are satisfied is called the feasible region. The cost function ϕ is said to have a constrained minimum [10] at x if there exists some positive α such that

$$\phi(\underset{\sim}{x}) \leq \phi(\underset{\sim}{x} + \Delta\underset{\sim}{x}) \tag{4.13}$$

for all Δx in the set -

$$\left\{ \Delta\underset{\sim}{x} \;\middle|\; 0 < \|\Delta\underset{\sim}{x}\| < \alpha \;;\; \gamma_i(\underset{\sim}{x} + \Delta\underset{\sim}{x}) = 0, \; i = 1, 2, \ldots, p; \right.$$
$$\left. \theta_j(\underset{\sim}{x} + \Delta\underset{\sim}{x}) \geq 0, \; j = 1, 2, \ldots, q \right\}$$

Or said another way, a constrained minimum exists at a point x if x is in the feasible region and a small change in x in any direction in the feasible region causes an increase in ϕ. If at such a minimum an inequality constraint function satisfies $\theta_i = 0$, then that constraint is said to be active. If on the other hand, $\theta_i > 0$, then the constraint is said to be inactive.

Mathematically, it is convenient to add p+q additional variables to the problem by introducing Lagrange multipliers. Let the Lagrangian cost be

$$J = \phi + \underset{\sim}{\nu}^T \underset{\sim}{\psi} + \underset{\sim}{\eta}^T \underset{\sim}{\theta} \tag{4.14}$$

where

$\underset{\sim}{\nu}$ = the vector of equality Lagrange multipliers

$\underset{\sim}{\eta}$ = the vector of inequality Lagrange multipliers

It can be shown [10], except for rare circumstances known as abnormal cases, that the necessary conditions for a constrained minimum are given by

$$\nabla J = 0 \tag{4.15}$$

$$\psi_i = 0 \,, \quad i = 1, 2, \ldots, p \tag{4.16}$$

$$\left.\begin{aligned} \eta_j \theta_j &= 0 \qquad (4.17)\\ \eta_j &\leq 0 \qquad (4.18)\\ \theta_j &\geq 0 \qquad (4.19) \end{aligned}\right\} j = 1, 2, \ldots, q$$

These conditions are known as the Kuhn-Tucker conditions.

The addition of the product of the Lagrange multipliers and the constraint functions to the objective cost function ϕ results in the Lagrangian cost J which has a slope of zero at the constrained minimum. In other words, the Lagrangian cost has a stationary point at the constrained minimum. Since the value of the constraint is zero at the constrained minimum, the Lagrangian cost J equals the cost ϕ at that point. However, the stationary point which is a constrained minimum will not necessarily be a minimum of the Lagrangian cost. In fact, this point may be a saddle point or even a maximum of the Lagrangian cost. In other words, the Hessian of the Lagrangian cost (the Hessian is the matrix of second derivatives) will not necessarily be positive definite at the constrained minimum. This means that one cannot look for a stationary point by searching for a minimum of J. This problem is easily remedied by adding penalty functions to the Lagrangian cost, J, to form the augmented Lagrangian cost, J_a. For the moment, consider only equality constraints. We wish the augmented Lagrangian cost to equal the Lagrangian cost everywhere along the constraints. But the Hessian of the new cost should be positive definite at the stationary point. This suggests adding a quadratic-like quantity to the Lagrangian cost which is zero everywhere along the constraint. Hence, we let

$$J_a = \phi + \underset{\sim}{\nu}^T \underset{\sim}{\psi} + \frac{1}{2} P \sum_{i=1}^{p} \psi_i^2 \qquad (4.20)$$

where P must be greater than some minimum value to ensure that the Hessian of J_a will be positive definite at the minimum.

Figure 4.2 shows graphically the concepts discussed above. Consider the one-dimensional problem where $\phi(x) = 2 - x$ and $\psi(x) = x - 1$. The cost, Lagrangian cost, and augmented Lagrangian cost functions are plotted versus x. By inspection the solution is $x = 1$ and the Lagrange multiplier is easily found to be $\nu = 2$. The Lagrangian cost is seen to have a stationary point at $x = 1$. However, the Lagrangian cost is a maximum at the constrained minimum. Next, the penalty function is added to the Lagrangian cost. In this case, we let $P = 5$. Now the augmented Lagrangian cost has a stationary point at the constrained minimum and the second derivative is positive. Note that all three costs have the same value at the constrained minimum.

4.3 SIGNIFICANCE OF THE LAGRANGE MULTIPLIERS

Not only are Lagrange multipliers an effective and elegant method of including constraints into the optimization problem, but as with many problems solved with Lagrange multipliers, they provide special information about the system being optimized. To show this, consider the optimization problem with equality constraints only. At the constrained

minimum

$$\nabla J = \nabla \phi + \underset{\sim}{y}^T \nabla \underset{\sim}{\psi} = 0 \tag{4.21}$$

Hence, it must be that

$$\nabla \phi = -\underset{\sim}{y}^T \nabla \underset{\sim}{\psi} \tag{4.22}$$

But the change in cost for a small change in x is

$$\Delta \phi = \nabla \phi^T \Delta \underset{\sim}{x} \tag{4.23}$$

Substitution of Equation (4.22) into (4.23) gives the result that

$$\Delta \phi = -\underset{\sim}{y}^T \nabla \underset{\sim}{\psi} \Delta \underset{\sim}{x} = -\underset{\sim}{y}^T \Delta \underset{\sim}{\psi} \tag{4.24}$$

Therefore, it is seen from Equation (4.24) that the Lagrange multiplier indicates the sensitivity of cost to a change in constraints. A similar result holds for the inequality constraints.

4.4 UNCONSTRAINED MINIMIZATIONS

Optimization problems can be divided into two distinct categories: constrained function minimizations and unconstrained function minimizations. In Section 4.6, the

method of mathematical programming via augmented Lagrangians [10] will be discussed. With this technique, the constrained optimization problem is solved as a series of unconstrained optimization problems. In this section, and in Section 4.5, the methods used for solving the unconstrained portion of the constrained optimization problem are discussed.

Suppose one wishes to minimize the cost function ϕ not subject to any constraints. The goal is to find that $\underset{\sim}{x}$ which produces a minimum ϕ. A necessary condition for function minimization is that the gradient of the function be equal to zero. The simplest method of searching for a minimum ϕ in x-space is to first start at some point $\underset{\sim}{x}_K$ and evaluate the gradient at this point. Since we are looking for a minimum, and hence a decrease in ϕ, the negative of the gradient is taken as the search direction. Then along this semi-infinite line, a minimum will exist. A line search is carried out to find the location $\underset{\sim}{x}_{K+1}$ of this minimum. Then the gradient of $\underset{\sim}{g}_{K+1}$ is found at this new point and the entire process is repeated until $\nabla\phi$ is approximately equal to zero. This is known as a steepest descent gradient search.

Although the steepest descent search is very simple to implement, the convergence to the minimum can be very slow, especially when used in conjunction with the method of mathematical programming via augmented Lgarangians. Hence, a more elegant search routine is needed. The method chosen for this research is attributed to Broyden [20] and is one of a

class of variable metric methods, also know as quasi-Newton methods. The motivation for these methods is illustrated by the Taylor series expansion of the gradient of the cost.

$$\nabla\phi_{k+1} \approx \nabla\phi_k + \nabla\nabla\phi_k \Delta\underset{\sim}{\chi}_k \tag{4.25}$$

where $\Delta\underset{\sim}{\chi}_k = \underset{\sim}{\chi}_{k+1} - \underset{\sim}{\chi}_k$

The vector operators in Equation (4.25) are

$$\nabla = \left\{\frac{\partial}{\partial\chi_i}\right\} \tag{4.26}$$

and

$$\nabla\nabla = \left[\frac{\partial^2}{\partial\chi_i\partial\chi_j}\right] \tag{4.27}$$

The matrix $\nabla\nabla\phi$ is the so-called Hessian matrix, A. To determine the location where the gradient of the cost is zero in this Taylor series approximation implies taking a step $\Delta\underset{\sim}{x}$ where

$$\begin{aligned}\Delta\underset{\sim}{\chi}_k &= -\underset{\sim}{A}^{-1}\nabla\phi_k \\ &= -\underset{\sim}{A}^{-1}\underset{\sim}{g}_k\end{aligned} \tag{4.28}$$

Notice that this is just a Newton-Raphson step. Figure 4.3 shows graphically the benefits of using quasi-Newton procedure

near the minimum. First of all, the gradient is the vector which points in the direction of greatest slope. It does not point in the direction of the minimum. Secondly, the gradient contains no information about the step size one should take to get to the minimum along the gradient search direction. On the other hand, near a minimum, a Newton-Raphson search direction vector points directly to the minimum, both in direction and magnitude. Hence, a search which uses a variable metric procedure is usually much more efficient, albeit more complicated, than a simple gradient search.

There exist many schemes for determining the inverse Hessian matrix $\underset{\sim}{H}$ by iteration. These schemes use the position vector and the gradients at current and previous steps to iterate on the $\underset{\sim}{H}$ matrix. The method used in this study is attributed to Broyden [20] and is one in a general class of variable metric methods formulated by Broyden. To perform a minimization of ϕ using Broyden's method, one first chooses some positive definite matrix $\underset{\sim}{H}_K$ as an initial guess. Often, for convenience, this is a multiple of the identity matrix. Next the search direction $\underset{\sim}{d}_K$ is found.

$$\underset{\sim}{d}_K = -\underset{\sim}{H}_K \underset{\sim}{g}_K \tag{4.29}$$

This direction and the point $\underset{\sim}{x}_K$ define the line

$$\underset{\sim}{x} = \underset{\sim}{x}_K + c\underset{\sim}{d}_K \qquad c \geq 0 \tag{4.30}$$

where c is the scalar step size. Along this semi-infinite line, a minimum is found, or at least a significant improvement in ϕ. This new point is $\underset{\sim}{x}_{K+1}$. The gradient at this position is $\underset{\sim}{g}_{K+1}$. The new $\underset{\sim}{H}$ matrix is then taken to be

$$H_{K+1} = H_K + \left(1 + \frac{\Delta g_K^T H_K \Delta g_K}{\Delta \underset{\sim}{x} \Delta g_K}\right) \frac{\Delta \underset{\sim}{x}_K \Delta \underset{\sim}{x}_K^T}{\Delta \underset{\sim}{x}_K^T \Delta g_K} - \frac{H_K \Delta g_K \Delta \underset{\sim}{x}_K^T}{\Delta \underset{\sim}{x}_K^T \Delta g_K} - \frac{\Delta \underset{\sim}{x}_K \Delta g_K^T H_K}{\Delta \underset{\sim}{x}_K^T \Delta g_K} \tag{4.31}$$

where

$$\Delta g_K = g_{K+1} - g_K$$

This equation is known as the Broyden-Fletcher-Shanno (BFS) formula. If the cost function ϕ is quadratic, it can be shown that $\underset{\sim}{H}$ and the minimum will be found exactly in n or fewer steps if exact line minimizations are performed during each line search. It is assumed that these good qualities will apply to a non-quadratic function sufficiently near a minimum.

There are several useful qualities of the BFS variable metric search routine. First, only the value of ϕ and its first derivatives need to be found. This saves both analytical work and computation time since second derivatives are not explicitly evaluated as in a true Newton-Raphson search. Secondly, unlike other variable metric methods, notably the method of Davidon, Fletcher, and Powell (DFP) [11], exact line minimizations need not be found. In the DFP method, the H matrix may become semi-definite near a minimum

if line minimizations are not performed very precisely. To find the exact minimum along a line can be computationally expensive and, hence, the BFS routine was chosen since line minimizations need not be computed exactly to insure a positive definite $\underset{\sim}{H}$ matrix and a finite convergence rate [21].

4.5 STEPSIZE CONTROL

At every step of the search routine a search direction is determined. Then, along this line, the vector $\underset{\sim}{x}$ is a function of the step size c as given by Equation (4.30). Along this line, ϕ may be considered a function of the single scalar c. Figure 4.3 shows the contours of a sample cost function in x-space. The vector starting at $\underset{\sim}{x}_K$ is the search vector. One must search, that is vary c through a dicrete set of values, to find a step size which produces an acceptable reduction in $\phi(c)$. Naturally, one would like to determine that step size with the least amount of computational effort. A line search for a local minimum of ϕ can be very time consuming since ϕ must be evaluated many times to find the minimum precisely.

Dixon [21] has shown that exact line minimizations may be unnecessary to achieve good convergence times when using the BFS method. In fact, some of the best results (i.e., fastest convergence to the minimum) were obtained while using an acceptable step size rule. The Armijo rule [22] used in this investigation is nearly identical to the rule used in Dixon's

study.

The Armijo rule says that step size used at each iteration will be c such that

$$c = \bar{c}\gamma^m \tag{4.32}$$

where γ is a positive number less than unity and $\bar{c}$ satisfies the conditions that

$$\phi(\underset{\sim}{x}_k) - \phi(\underset{\sim}{x}_k + \bar{c}\underset{\sim}{d}_k) < -\sigma\bar{c}\nabla\phi(\underset{\sim}{x}_k)^T\underset{\sim}{d}_k \qquad \bar{c} > 0 \tag{4.33}$$

and m is the smallest nonnegative integer which satisfies the condition that

$$\phi(\underset{\sim}{x}_k) - \phi(\underset{\sim}{x}_k + \bar{c}\gamma^m\underset{\sim}{d}_k) \geq -\sigma\bar{c}\gamma^m\nabla\phi(\underset{\sim}{x}_k)^T\underset{\sim}{d}_k \tag{4.34}$$

For this study, $\gamma = 0.35$ and $\sigma = 0.45$.

Figure 4.4 shows graphically the interpretation of the Armijo rule. The curved line is the left hand side of Equation (4.34) while the straight line is the right hand side. For c to be an acceptable step size, the difference between $\phi(c)$ and $\phi(0)$ at the point c must be less than the value of a line drawn through the origin with a slope equal to σ times $\partial\phi(0)/\partial c$. This can always be satisfied if the step size is made small enough. One can see clearly that although this rule does not attempt to find an exact line minimum, it

does force the search routine to move closer and closer to a minimum with each succesive iteration since only improvements in the cost function are accepted.

In summary, the method of solving for the unconstrained minimum has two main parts: the search direction phase and the line search phase. At each step of the search, a search direction is found by premultiplying the negative of the gradient with the current estimate of the inverse Hessian. Once the search direction has been determined, the Armijo rule is used to find the stepsize in that direction which provides a significant reduction in the cost function. This procedure is repeated until the gradient of the cost is zero, indicating a minimum has been found.

4 6 CONSTRAINED OPTIMIZATIONS

As mentioned earlier, the constrained optimization problem can be solved as a series of unconstrained problems. The general procedure is to form the augmented Lagrangian cost function by adding penalty functions to the Lagrangian cost. These penalities, in essence, add a large cost to the Lagrangian cost if the constraints are not met. This tends to force the solution to satisfy the constraints.

The augmented Lagrangian cost J_a is

$$J_a = \phi + \underline{\psi}^T \underline{I} + \underline{\eta}^T \underline{\theta} + \frac{1}{2} P \underline{\psi}^T \underline{\psi} + \frac{1}{2} W \sum_{i \in i_a} \theta_i^2 + \frac{1}{2} W \sum_{i \in i_b} (\theta_i - |\theta_i|)\theta_i \qquad (4.35)$$

where i_a indicates active inequality constraints

i_b indicates inactive inequality constraints

P is a positive number

W is a positive number

Hence the gradient of the augmented Lagrangian cost is

$$\nabla J_a = \nabla\phi + \underset{\sim}{\nu}^T \nabla \underset{\sim}{\psi} + \underset{\sim}{\eta}^T \nabla \underset{\sim}{\theta} + P \underset{\sim}{\psi}^T \nabla \underset{\sim}{\psi} + W \sum_{i \in i_a} \theta_i \nabla \theta_i + W \sum_{i \in i_b} (\theta_i - |\theta_i|) \nabla \theta_i \tag{4.36}$$

The procedure for solving for the constrained minimum is as follows. Initial guesses are chosen for the Lagrange multipliers $\underset{\sim}{\nu}$ and $\underset{\sim}{\eta}$. Initial values for the penalty function coefficients P and W are also selected. The augmented Lagrangian cost function is then considered an unconstrained function of $\underset{\sim}{x}$ only. This function is then minimized by an appropriate unconstrained minimization procedure. What is meant by appropriate will be discussed shortly. Once the minimum of J_a is found for the given values of $\underset{\sim}{\nu}$, $\underset{\sim}{\eta}$, P, and W, the Lagrange multipliers and penalty function coefficients are then updated and the entire process is repeated until convergence.

The iterative updating of the Lagrange multipliers occurs immediately after each unconstrained minimum of the augmented Lagrangian cost. To demonstrate how this procedure works, consider the gradient of the Lagrangian and augmented Lagrangian costs with equality constraints only. The gradient of the Lagrangian cost is

$$\nabla J = \nabla \phi + \underset{\sim}{\nu}^T \nabla \underset{\sim}{\psi} \tag{4.37}$$

The gradient of the augmented Lagrangian cost is

$$\begin{aligned} \nabla J_a &= \nabla \phi + \underset{\sim}{\nu}^T \nabla \underset{\sim}{\psi} + P \underset{\sim}{\psi}^T \nabla \underset{\sim}{\psi} \\ &= \nabla \phi + (\underset{\sim}{\nu}^T + P \underset{\sim}{\psi}^T) \nabla \underset{\sim}{\psi} \end{aligned} \tag{4.38}$$

In the limit of infinite P, with the Lagrange multipliers set to zero, the minimum of the augmented Lagrangian cost is a constrained minimum of the objective cost function. The value of $P\underset{\sim}{\psi}$ acts like a Lagrange multiplier and in fact will equal the true multiplier in the limit of infinite P. For large but finite P, we expect that the quantity $\underset{\sim}{\nu} + P\underset{\sim}{\psi}$ will be approximately equal to the true Lagrange multiplier at the minimum of J_a. Hence, the update for the equality Lagrange multipliers is

$$\underset{\sim}{\nu}_{new} = \underset{\sim}{\nu}_{old} + P\underset{\sim}{\psi} \tag{4.39}$$

Similarly, the update for the inequality constraint multipliers is

$$\begin{aligned} \text{For } \eta_{i_{old}} = 0 \qquad \eta_{i_{new}} &= \begin{cases} W(\theta_i - |\theta_i|) & \text{if } < 0 \\ 0 & \text{otherwise} \end{cases} \\ \text{For } \eta_{i_{old}} < 0 \qquad \eta_{i_{new}} &= \begin{cases} \eta_{i_{old}} + W\theta_i & \text{if } < 0 \\ 0 & \text{otherwise} \end{cases} \end{aligned} \tag{4.40}$$

Immediately after each update stage, the Kuhn-Tucker conditions for optimality are checked. If these conditions are satisfied, then the iteration procedure is stopped since the necessary conditions for optimality have been met. Of course, this does not guarantee that the constrained stationary point will be a minimum. But in practice, this is generally the case.

Note that to solve the constrained minimization problem, one need not work with Lagrange multipliers at all. One can simply pick P and W to be very large. Then the minimum of the cost plus the penalty function will be approximately equal to the constrained minimum of the cost function. This method of solution, however, will not work well due to the extremely slow convergence rates one encounters in the search for a minimum. In a two-dimensional problem, one can imagine that the augmented cost function is an elevation map. The valleys created by the use of penalty functions can be very narrow with steep walls. Gradient methods tend to search across the valleys and not along them. Hence, convergence to a minimum can be very slow. Even the variable metric methods will not work well except for regions very close to the minimum.

However, if the Lagrange multipliers are known approximately, the penalty functions need not be so severe and the variable metric methods tend to converge faster. This is the motivation for the technique of nonlinear programming via augmented Lagrangians. Note that a steepest descent search is

still not appropriate, however, because the augmented cost still will show some of the poor conditioning of contours as dicussed above. A variable metric method is required for good convergence.

The values of the penalty functions can be increased with each iteration to further increase the requirement that the constraints be met. By starting the values of W and P at moderate levels at the start of the optimization and increasing them at each iteration, one takes full advantage of the method of augmented Lagrangians. A simple scheme for the update for P and W is given in [11]:

$$P_{NEW} = k P_{OLD} \tag{4.41}$$

$$W_{NEW} = k W_{OLD} \tag{4.42}$$

where k is a number greater than or equal to one.

In summary, the rotor optimization problem was formulated and the method of solution was outlined. A cost function was defined which is a measure of the severity of mistune in the rotor. The stability requirements of the problem were introduced as constraints which must be satisfied. The cost function is to be minimized subject to these contraints. Finally, a review of the optimization theory used in this study was presented. The results of this optimization

procedure will be given in Chapter 5.

5. RESULTS OF THE CONSTRAINED OPTIMIZATION PROCEDURE

In this chapter, the optimization procedure described in Chapter 4 is used to determine optimal mass mistune patterns. When implemented, these patterns provide the greatest stability margin at the aeroelastic design point for the least amount of mistuning. In Section 5.1, the procedure for optimizing the rotor is outlined and the behavior of the optimized rotor at its aeroelastic design point is presented. In section 5.2, the off-design behavior of the rotor is analyzed. The next two sections address the issue of the actual implementation of mistuning in a rotor. Although the designer may specify a certain mistune pattern, the actual mistune pattern of the rotor will be different due to manufacturing tolerances and changes in the natural frequencies of the blade which occur over the life of the blade, due to its operating environment. In Section 5.3, the sensitivities of the stability margin to small errors in mistune are examined. Finally, the use of optimal mistune patterns as a guide to design of near-optimal rotors is considered in Section 5.4. For a 14-bladed rotor, the optimally mistuned rotor will in general have 14 different natural frequencies of the 14 blades. In this section, the optimal mistune pattern is approximated by two, three, and four tones or frequencies of blades.

5.1 OPTIMAL MISTUNE PATTERNS FOR A ROTOR AT ITS AEROELASTIC DESIGN POINT

The rotor which was optimized in this study is the same rotor which was first introduced in Section 2.5. The geometric and aerodynamic properties at the typical (85 percent span) section are given in Table 2.1.

The procedure for optimizing the rotor in this investigation was as follows. First, an initial guess was chosen for the optimal mass mistune pattern. Also, initial guesses were chosen for the Lagrange multipliers. A constrained minimum was then found for the case requiring a minimum damping ratio greater than or equal to $\bar{\zeta} = -0.005$. A second set of constraints requires that all mass changes be positive. It should be noted that there are in fact many constrained local minima. Which minimum found depends on many factors including the initial guess of the optimal mistune, the initial choice of Lagrange multipliers, $\underset{\sim}{\eta}$, the values of the penalty function coefficients, W, the details of the step size rule, and the method used to perform the unconstrained optimization phase of the algorithm. Only one local minimum was found in the search for optimal mistune patterns of the 14-bladed rotor studied in this report. No attempt was made to find other local minima. However, a 13-bladed case and a 12-bladed case were also examined. In the 12-bladed case, several local minima were discovered. That work will not be presented in this report except to say that the minima found in these cases had approximately same level of mistune as the

optimally mistuned 14-bladed case. It does not appear, therefore, that a rotor with an odd number of blades performs significantly better or worse than a rotor with an even number of blades when the rotors are optimally mistuned.

As the next step, the optimal mistune pattern for a minimum damping ratio greater than $\bar{\zeta} = -0.004$ was found. The initial guesses for the optimal mass mistune and the Lagrange multipliers were taken to be the result of the optimization of the $\bar{\zeta} = -0.005$ optimization problem. The optimal mistune patterns for the cases of $\bar{\zeta} = -0.003, -0.002, -0.002, 0.0, 0.001, 0.002$ were found sequentially in a completely analogous fashion, using the preceding optimization results for the initial conditions of the next successive optimization. Of these cases, the $\bar{\zeta} = 0.002$ case did not fully converge. The Lagrange multipliers at this point were not found, and the actual damping ratio produced by the partially converged solution was $\bar{\zeta} = 0.00188$.

It was not possible to obtain converged solutions to the constrained optimization problem for stability margin requirements greater than $\bar{\zeta} = 0.001$. The difficulty arises in the evaluation of the eigenvalues by integration of the derivatives of the eigenvalues and eigenvectors. As the system is mistuned, some of the eigenvalues of the system may become very close to one another. This is especially true of those eigenvalues which lie on the stability margin constraint. When the eigenvalues become very closely spaced,

the first order approximation to the eigenvalue derivatives is valid in a very small region of mass mistuning space and the accuracy of the integration becomes poor. Furthermore, if two eigenvalues should become equal or very nearly equal, the integration will break down altogether. The integration scheme was not sophisticated enough to avoid these pitfalls by dynamically adjusting the integration step size or to avoid singularities by rerouting the integration path around them. This turned out to be the limiting factor on the usefulness of the optimization procedure.

As stated in Chapter 4, the goal of this analysis is to determine the optimal mistune pattern which produces a required minimum damping ratio. Figure 5.1 shows the mistune patterns found for the eight cases described above: $\bar{\zeta}$ = -Ø.ØØ5, -Ø.ØØ4, ..., Ø.ØØ1, Ø.ØØ188.

Consider the case of $\bar{\zeta}$ = -Ø.ØØ5 (see Figure 5.1). This type of mistune pattern is called almost alternate mistuning. Notice that the odd numbered blades have no change in mass from their nominal mass (i.e., ε_i = Ø). The even blades all have nearly nearly equal masses except for blade 2, which has a mass mistune of zero, and blade 14, which has a mass mistune of about half that of the other even numbered blades.

This almost alternate mistune pattern grows in magnitude for increasing $\bar{\zeta}$ but does not change in nature until $\bar{\zeta}$ = Ø.Ø. At this value of required damping ratio, the mass of blade 9 becomes nonzero. At $\bar{\zeta}$ = Ø.ØØ1, the mass of blade

number 2 becomes nonzero but still very small compared to the mass of the other even numbered blades.

Notice that the mistune patterns shown in Figure 5.1 all resemble, to some degree, the truly alternate mistune pattern where all the odd numbered blades have $\varepsilon_i = 0$ and all the even numbered blades have equal nonzero ε_i. One might expect, therefore, that although the mistune patterns found in this investigation may be optimal, they are not significantly more cost effective than the truly alternate mistune pattern. However, as demonstrated by Figure 5.2, this is clearly not the case. The figure shows the cost of mistuning (as defined by Equation (4.3)) versus the stability margin achieved by the mistuning. The upper curve is the cost of the truly alternate mistune pattern and the lower curve is the cost of the optimal mistune pattern. The optimal mistune pattern is seen to deliver much more stability for a given level of mistune or, alternatively, a much lower cost for the same level of stability. To achieve a damping ratio of 0.00188, the optimal mistune pattern requires about 45 percent less mistuning than alternate mistuning.

Some insight into why the optimal mistune patterns are so effective can be gained by looking at the eigenvalues in the complex plane. Figures 5.3a-i show the eigenvalue for $\bar{\zeta} = -0.00602$ (tuned), -0.005, -0.004, -0.003, ..., 0.001, 0.00188. As the stability margin becomes greater, more and more eigenvalues just barely satisfy the constraint that all

eigenvalues lie to the left of the ray emanating from the origin with a damping ratio of $\bar{\zeta}$. For a damping ratio of $\bar{\zeta}$ = Ø.ØØ188 (see Figure 5.3i), four of the 14 eigenvalues lie on the stability margin constraint. This indicates that the mistune pattern is very efficient, since it does not do unnecessary work by pushing some of these eigenvalues further to the left than required. In contrast, only one of the 14 eigenvalues of the alternate mistune pattern will, in general, lie on the constraint.

As a by-product of the optimization procedure, the Lagrange multipliers of the active constraints are determined. Recall from Section 4.3 that the Lagrange multipliers indicate the change in the optimal cost for a small change in the constraints. Hence, by summing the negative of the Lagrange multipliers associated with the damping ratio constraints, the local slope of the cost versus damping ratio curve (see Figure 5.2) is determined. To check this result, the slope of the optimal cost curve was determined by using second order finite difference operators. These results are plotted in Figure 5.4, along with the slope predicted by the Lagrange multipliers. Note the generally good agreement between the two. The difference between the two can be attributed to the relatively large $\Delta\bar{\zeta}$ used in the differencing and the limited accuracy to which the Lagrange multipliers were computed.

5.2 OFF DESIGN PEFORMANCE OF OPTIMALLY MISTUNED ROTOR

The rotor has been mistuned to achieve given stability requirements at the aeroelastic design point of the rotor. It remains to be seen if this mistuned rotor will be stable over the entire operating range. To determine this, a modified V-g diagram was constructed. The negative of the damping ratio of the rotor is plotted versus the reduced velocity. For stability, the damping ratio must be positive, i.e., the curve must lie below $\bar{\zeta} = 0$. Two cases were examined. In the first case, the reduced velocity was varied while all other parameters, including the Mach number, were held constant. In the second case, the Mach number and reduced velocity were varied together to simulate a fan rotor running up its operating line.

Plotted in Figure 5.5 are three important stability curves for the constant Mach number case. The upper curve is the tuned damping ratio plotted against the relative reduced velocity of the rotor. Bendiksen [3] has shown that for rotors which can be modelled well with only one degree of freedom per blade, the tuned position is always the least stable. The lower curve is the damping ratio of the the centroid of the tuned eigenvalues. Recall from Section 2.4 that this is to first order the best damping ratio that one can achieve by mistuning. Hence, the mistuned damping ratios should lie between these two curves. Finally, the center curve is the rotor which has been optimally mistuned at the aeroelastic design point. As expected, this curve lies

between the tuned damping ratio curve and the blade self damping curve.

As Figure 5.5 clearly shows, the rotor has been stabilized for all reduced velocities less than or equal to the aeroelastic design reduced velocity. For the worst case (the tuned case), the rotor flutters at a reduced velocity of V = 1.7. The best case (the centroid of the eigenvalues) produces a flutter speed of V = 2.9. The use of optimal mistuning has increased the flutter speed from the worst case to V = 2.Ø5. Hence, the flutter speed has been increased by about 2Ø percent over the tuned flutter speed. In the best possible case, one could mistune the rotor to achieve a 7Ø percent increase in flutter speed.

In this example, the flutter speed of the rotor has been increased by 2Ø percent. This increase in flutter speed can prevent a rotor which would flutter in its tuned state from fluttering at its aerodynamic design point. On the other hand, if a rotor does not flutter in its tuned state, the increase in flutter speed could be used to reduce the chord of the blades without inducing flutter due to the subsequent increase in reduced velocity.

As a second example the case of a given fan running up an operating line was considered. In this case, the Mach number and the reduced velocity were held proportional to one another. Figure 5.6 shows a "V-M-g diagram" (damping ratio versus reduced velocity and Mach number). Again the upper and

lower curves are the tuned damping ratios, and the damping ratio of the centroid of the tuned eigenvalues, respectively. The middle curve is the optimally mistuned rotor. Notice that again, the mistuned damping ratios lie between the tuned damping ratio and the centroid damping ratio. In this example, however, although the rotor was stabilized at a reduced velocity of 2.Ø2 and a Mach number of 1.317, the rotor appears unstable at reduced velocities and Mach numbers lower than the aeroelastic design point. Note that there is a single region of instability just before the operating point is reached. It is possible that if the rotor had been more severly mistuned, the mistuned damping ratio curve would not have gone from positive to negative before the operating point is reached. Unfortunately, as previously dicussed, the optimization procedure failed to converge for damping ratios greater than $\bar{\zeta} = Ø.ØØ1$.

5.3 SENSITIVITY TO ERRORS IN MISTUNING

An important issue, which must be addressed before an optimally mistuned rotor is actually used in aeroelastic experiments, is the question of sensitivity to manufacturing errors. Although the designer may specify a certain mistune pattern, he must accept the fact that in the manufacturing process there will be certain tolerances which cannot be obtained. Hence, the actual mistune pattern which is implemented will be somewhat less than optimal. The actual

mistune pattern will be

$$\underset{\sim}{\epsilon}_i = \underset{\sim}{\epsilon}_{i_{specified}} + \underset{\sim}{e}_i \tag{5.1}$$

where $\underset{\sim}{e}_i$ is the error in mistuning the rotor.

To investigate this problem, errors in mistuning were introduced into the optimally mistuned rotor with a stability margin of Ø.ØØ188. The gradient of the damping ratio of each eigenvalue was found with respect to the mistune variables $\underset{\sim}{\epsilon}_i$. The actual mistune patterns were then taken to be

$$\underset{\sim}{\epsilon}_i = \underset{\sim}{\epsilon}_{i_{specified}} - \frac{E\sqrt{N}\,\nabla\zeta_n}{\|\nabla\zeta_n\|}, \quad n = 0, 1, \ldots, N-1 \tag{5.2}$$

In Equation (5.2), the term $-\nabla\zeta_n/\|\nabla\zeta_n\|$ is the vector which points in the most destabilizing direction of the nth eigenvalue. This vector is normalized to have a length of unity. The vector is multiplied by $E\sqrt{N}$, where E is the root mean square of the entries of the mistune error vector, then added to the nominal mistune pattern. A typical value of E for an actual rotor is about Ø.Ø1. The rotor was mistuned using the pattern specified by Equation (5.2) with the N different gradients corresponding to the N different eigenvalues. Then the case with the worst damping ratio after the errors had been introduced is, to first order, the worst possible case for a given value of E. It was found that for E = Ø.Ø1, the stability is reduced from Ø.ØØ188 to -Ø.ØØ317

(see Figures 5.7). Hence it is seen that the optimal mistune pattern for $\bar{\zeta}$ = Ø.ØØ188 is very sensitive to small changes in mistuning.

The eigenvalues of the perfectly mistuned and the worst case imperfectly mistuned systems are plotted in Figure 5.8. In this case, the eigenvalue which moves the most to the right in the complex plane is the eigenvalue on the root locus of the tuned 77.14° interblade phase angle eigenvalue. Before the introduction of mistuning error, this is one of the eigenvalues which lies on the stability margin constraint.

In a sense, the optimal mistune pattern is very sensitive to errors because it is an optimal mistune pattern. Figure 5.7 shows that the optimal cost curve has a very shallow slope at $\bar{\zeta}$ = Ø.ØØ188. This implies that for a small increase in mistuning, a large improvement can be made in the stability margin. But for this same reason, a small change in mistuning can greatly reduce the stability margin.

This same sort of sensitivity analysis was carried out on the alternately mistuned rotor with a perfectly mistuned stability margin of $\bar{\zeta}$ = Ø.ØØ171. Again the error vector was chosen to be in the worst possible direction for an error vector with a root mean square of Ø.Ø1. The stability margin in this case was degraded from Ø.ØØ171 to Ø.ØØØ47 as shown in Figure 5.7. As it turns out, alternate mistuning is less sensitive to mistuning errors than optimal mistune. By the

symmetry of the problem, the gradients of the damping ratios all are in the direction of an alternate mistuning direction. Since alternate mistuning does not give large improvements in the minimum damping ratio for a small change in mistune, one would not expect the errors in mistuning to produce a large change in the stability margin since the worst errors are in an alternate mistune direction.

An interesing result of the perturbation analysis presented in Chapter 3 is that small amounts of mistuning do not significantly change the stability of the system from the originally tuned configuration. To show this, recall that the derivatives of the eigenvalues of the system are:

$$\frac{\partial \lambda_n}{\partial \epsilon_i} = \frac{q_{Ln}^T \left(\frac{\partial \underline{\underline{A}}}{\partial \epsilon_i} - \lambda_n \frac{\partial \underline{\underline{B}}}{\partial \epsilon_i} \right) q_{Rn}}{q_{Ln}^T \underline{\underline{B}} \, q_{Rn}} \tag{5.3}$$

For the case of mass mistuning, Equation (5.3) becomes

$$\frac{\partial \lambda_n}{\partial \epsilon_i} = -\frac{\lambda_n \, q_{Ln}^T \frac{\partial \underline{\underline{B}}}{\partial \epsilon_i} q_{Rn}}{q_{Ln}^T \underline{\underline{B}} \, q_{Rn}} \tag{5.4}$$

It can be shown that, for the tuned case, the quantity on the right hand side of Equation (5.4) is equal to -1/N. Hence, for small mass perturbations about the tuned position, the change in an eigenvalue is equal to

$$\lambda_n \approx \lambda_{n_{tuned}} - \frac{1}{N} \sum_{i=0}^{N-1} \epsilon_i \tag{5.5}$$

Therefore, the eigenvalues of the slightly mistuned system

depend only on the net mass added to the system, and not on the mistune pattern. But if equal masses are added to all the blades, one would not expect the damping ratios of the eigenvalues to change significantly since the system is still tuned. Therefore, the stability margin of the tuned system is insensitive to small amounts of mistune, no matter what mistune pattern is used. This is shown clearly in Figure 5.7. Both the optimal mistuning and the alternate mistuning cost curves are very steep at the tuned postion. Relatively large amounts of mistune are required to cause small changes in stability about the initially tuned position.

5.4 TWO, THREE, AND FOUR TONE APPROXIMATIONS TO OPTIMAL MISTUNE PATTERNS

The cost function minimized in this optimization reflects the practical difficulty associated with reaching a certain magnitude of mistuning. However, the difficulty with constructing a mistuned rotor is not only in the level of mistuning, but also in the complexity of the mistune pattern. For example, for the rotor examined in this study, the optimal mistune pattern required that there be nine different blade natural frequencies for the 14 blades on the rotor. Hence, to actually construct an optimally mistuned rotor, one would have to construct approximately N/2 different types of blade for a single rotor. This would prove to be very costly. In this section, several suboptimal mistuning patterns are created by

approximating the optimal mistune patterns by two, three, and four tone mistune patterns, and the performance of these mistune patterns are presented.

The procedure for picking the approximations to the optimal mistune was to use the $\bar{\zeta} = 0.00188$ optimal pattern as a guide to provide insight for picking suboptimal mistune patterns. First, the two tone approximations were chosen. In Table 5.1, the optimal mistune pattern and the two tone approximations which were investigated are given. Of course, the goal of these suboptimal patterns is the same as the goal for the optimal patterns, i.e., to provide the greatest stability margin for the lowest cost. Figure 5.9 shows the cost versus stability margin of the two tone patterns. Note that two of the patterns result in costs which lie between the optimal and alternate mistune costs. The third is about the same cost as the alternate mistune pattern.

Next, several three tone approximations were examined. These patterns are presented in Table 5.2. All of the mistune patterns tried had a lower cost per stability margin than the alternate mistune pattern as seen in Figure 5.10, although not dramatically lower. This is an indication that the fine detail of the optimal mistune pattern is important. Large amounts of mistune will not be effective in preventing flutter if this detail is missing.

Finally, four tone approximations were examined. Table 5.3 lists the four tone patterns used to approximate the

optimal mistune pattern. In Figure 5.11, it is seen that again, the four tone patterns perform slightly better than alternate mistuning, but not as well as optimal mistuning. Even with four tone approximations, there is not sufficient similarity to the optimal mistune pattern to achieve results that are nearly optimal.

In this chapter, it has been shown that optimal mistune patterns can achieve a given stability margin for a relatively low level of mistuning. Approximations to these optimal mistune patterns using two, three, and four discrete blade frequencies, however, perform only slightly better than alternate mistuning. Furthermore, optimal mistuning is not very robust to small mistuning errors. Alternate mistuning, on the other hand is relatively insensitive to errors in mistuning. For these reasons, it appears that a practical mistune pattern for implementation is the alternate mistune pattern.

6. CONCLUSIONS

1. The aeroelastic poles or eigenfrequencies can be thought of as forming a pattern around their centroid. The location of the centroid is controlled by the average blade mechanical properties and the aerodynamic blade self damping. It was shown that a necessary but not sufficient condition for aeroelastic stability is that the blades be self damped.

2. The distribution of the poles about the centroid is due to the unsteady aeroelastic influence of the neighboring blades. This pattern of poles can be modified by mistuning the rotor, increasing the stability of the less stable poles. However, mistuning does not introduce additional damping into the system, since the damping ratio of the centroid is unaffected. Mistuning makes use of the existing damping to stabilize the rotor by decreasing the blade to blade aerodynamic influences, thereby increasing the stability of the least stable poles.

3. There are two main mechanisms which can lead to the onset of flutter in transonic fans: The first is the loss of the blade self damping, as in the case of high incidence stall flutter. In such instances, the centroid and the entire pattern of poles shifts to the right in the complex plane eventually causing the least stable poles to become unstable. The second mechanism is due to the increasing destabilizing effect of the neighboring blades with increasing reduced velocity. The off diagonal influence coefficients, which

reflect the influence of one blade in the cascade on its neighbors, cause the eigenvalues to spread out away from the centroid of the poles. Some of the eigenvalues will become more stable than the centroid, and some will become less stable than the centroid. Hence, in the presence of cascade effects, the least stable eigenvalue will necessarily be less stable than the centroid of the eigenvalues, the value of which is determined only by the blade self damping terms of the influence coefficient matrix.

4. The unsteady aerodynamic forces, derived in terms of travelling wave coordinates, can be transformed into a form which expresses the force on each blade explicitly in terms of the motion of the other blades in the cascade. This linear transformation is simply a Fourier decomposition of the forces as expressed in the travelling wave coordinates. The use of this transformation on both analytical cascade models and experimentally measure unsteady aerodynamic coefficients generally reveals that the dominant forces acting on a blade arise from the motion of the blade itself and its two adjacent neighbors. Hence, one would expect that any effective mistuning scheme will minimize the influence one blade has on its neighbors. This heuristic argument suggests that the alternate mistune pattern should be effective.

5. In an effort to better understand the mechanisms of mistuning, an inverse design procedure was developed which determines the optimal pattern of blade structural mistuning

for a required increase in aeroelastic stability margin. The optimal mistune pattern can achieve a given stability margin with a significantly lower level of mistuning than with the simple alternate mistuning. The success of optimal mistuning does not depend on an even number of blades being present, as similar results are found for rotors with odd and prime numbers of blades.

6. The optimal mistune pattern appears to have three salient features: First, in all optimal mistune patterns there is seen to be some features of the alternate mistune pattern, i.e., nearly every other blade is mistuned. This componant of the optimal mistune pattern serves to disrupt the dominant aerodynamic effects of the neighboring blades. Second, there are "break points" around the rotor which disrupt the alternate mistune pattern. It is thought that these break points prevent longer wavelength disturbances from travelling around the rotor. Third, those blades that are mistuned do not all have exactly the same amount of mistune. Rather, there is a subtle structure to the mistuning which is not possible to predict a priori.

7. The subtle detail in the mistune pattern appears to be very important to the effectiveness of the optimal mistuning. The optimal mistuning patterns were found to be very sensitive to small errors in mistuning due to the loss of this detailed structure. Alternate mistuning, on the other hand, was found to be relatively insensitive to errors in mistuning.

8. Another consequence of the importance of the subtle detail in the optimal mistune pattern is that any practical implementation of the mistune pattern using only a small number of different blade frequencies will not faithfully reproduce all the important features of the optimal mistune pattern. It was found that the practical suboptimal mistune patterns do not perform significantly better than alternate mistuning.

9. Three distinct regions of mistuning influence were identified. Starting from the tuned configuration, there is a first region were the stability boundary is insensitive to the addition of mistuning. It is thought that most present stages operate in this initial insensitive region, which explains why they behave similarly and can be analyzed as tuned rotors. After several percent of mistuning has been introduced, a region of approximately linear increase in stability with increasing optimal mistune is entered. Finally, an asymptotic limit on the ability of mistuning to increase stability is reached. It is apparent that to provide uniformity of performance of rotors in service, rotors should be designed assuming small amounts of mistuning (i.e. in the initial insensitive region), or if the rotor is to be deliberately mistuned for stability, a large amount of mistuning should be introduced so that the rotor operates in the latter region of insensitivity.

10. When studying the off design performance of a mistuned

rotor, it is useful to construct diagrams similar to the traditional V-g diagrams. The stability of the mistuned rotor, at least if the rotor can be modelled with a single degree of freedom per blade, will lie between two limiting curves. The worst possible case is the case of the tuned rotor. The mistuned rotor cannot be any less stable than this. On the other hand, the most stability one can achieve through the use of mistuning is limited by the blade self damping. This is the fundamental limitation to the usefulness of mistuning.

11. In order to perform the optimization discussed in Chapter 4, it was first necessary to develop a method of evaluating the eigenvalue and eigenvectors of the equations of motion which retains the identity of each eigenmode in a root locus sense. This was done by first determining the derivatives of the eigenvalues and eigenvectors as a function of the mistune of each blade. These derivatives were then integrated to determine the eigenvalues and eigenvectors of a given mistune pattern. This method of evaluating the eigenvalues and eigenvectors is reasonably efficient when used in the optimization procedure. Furthermore, the identities of the eigenmodes are not lost in their evaluation as the system is mistuned. The principle drawback of the method is that the integration scheme breaks down whenever two or more eigenvalues become nearly equal. This turned out to be the limiting factor in the ability to optimize the rotor. For

damping ratios of 0.002 and greater, the optimization routine did not converge due to problems in evaluating the eigenvalues and their derivatives.

References

1. Kaza, K.R.V., and Kielb, R.E., "Effect of Mistuning on Bending-Torsion Flutter and Response of a Cascade in Incompressible Flow," Presented at the AIAA Dynamics Specialists Conference, Atlanta, Georgia, April 9-11, 1981. (Also NASA Technical Memorandum 81674).

2. Kielb, R.E., and Kaza, K.R.V., "Aeroelastic Characteristics of a Cascade of Mistuned Blades in Subsonic and Supersonic Flows," Presented at the ASME Eighth Biennial Engineering Division Conference, Hartford, Connecticut, September 20-23, 1981. (Also NASA Technical Memorandum 82631).

3. Bendiksen, O.O., "Flutter of Mistuned Turbomachinery Rotors," Presented at the ASME 28th International Gas Turbine Conference and Exhibit, Phoenix, Arizona, March 27-31, 1983, Paper No. 83-GT-153.

4. Adamczyk, J.J., and Goldstein, M.E., "Unsteady Flow in a Supersonic Cascade with Subsonic Leading-Edge Locus," AIAA Journal, Vol. 16, No. 12, December, 1978.

5. Verdon, J.M., and McCune, J.E., "Unsteady Supersonic Cascade in Subsonic Axial Flow," AIAA Journal, Vol. 13, No. 2, February 1975.

6. Nagashima, T., and Whitehead, D.S., "Linearized Supersonic Unsteady Flow in Cascades," ARC Reports and Memoranda No. 3811, February 1977.

7. Samoylovich, G.S., "Nestatsionarnoye obtekaniye i aerouporugiye kolebaniya reshetok turbomashin," 1969, Moscow, Izd-Vo Nauka, pp 1-444. (Translated version "Unsteady Flow Around and Aeroelastic Vibrations in Turbomachine Cascades," Prepared by the Translation Division Foreign Technology Division, WP-AFB, Ohio, February 23, 1971, FTB-HT-23-242-70).

8. Srinivasan, A.V., "Influence of Mistuning on Blade Torsional Flutter," NASA CR-165137, August, 1980.

9. Hanamura, Y., Tanaka, H., and Yamaguchi, K., "A Simplified Method to Measure Unsteady Forces Acting on the Vibrating Blades in Cascade," Bulletin of the JSME, Vol. 23, No. 180, June 1980

10. Pierre, D.A., and Lowe, M.J., Mathematical Programming via Augmented Lagrangians: An Introduction with Computer Programs, Addison-Wesley, Reading, Massachusetts, 1975.

11. Vander Velde, W., Class notes from "Algorithms for Function Minimization and Optimal Control," MIT course 16.39, Department of Aeronautics and Astronautics, 1982.

12. Kielb, R.E., and Kaza, K.R.V., "Effects of Structural Coupling on Mistuned Cascade Flutter and Response," Presented at the ASME 28th International Gas Turbine Conference and Exhibit, Phoenix, Arizona, March 27-31, 1983, Paper No. 83-GT-117.

13. Dugundji, J., and Bundas, D.J., "Flutter and Forced Response of Mistuned Rotors Using Standing Wave Analysis," Presented at the 24th AIAA/ASME/ASCE/AHS Structures, Structural Dynamics and Materials Conference, Lake Tahoe, Nevada, May 2-4, 1983, AIAA Paper No. 83-0845.

14. Bundas, D.J., "Flutter and Forced Response of Mistuned Rotors Using Standing Wave Analysis," S.M. Thesis, MIT, 1983.

15. Smith, B.T., et al, Lecture Notes in Computer Science, Vol. 6, "Matrix Eigensystem Routines - EISPACK Guide," Second Edition, Springer-Verlag, New York, 1976.

16. Meirovitch, L., Analytical Methods in Vibrations, The Macmillan Co., London, 1967, pp 120-124.

17. Mathews, J., and Walker, R.L., Mathematical Methods of Physics, Second Edition, The Benjamin/Cummings Publishing Company, Menlo Park, California, 1970, pp 286-298.

18. Plaut, R.H., and Huseyin, K., "Derivatives of Eigenvalues and Eigenvectors in Non-Self-Adjoint Systems," AIAA Journal, Vol. 11, No. 2, February, 1973.

19. Carnahan, B., Luther, H.A., and Wilkes, J.O., Applied Numerical Methods, John Wiley and Sons, New York, 1969, pp 361-366.

20. Broyden, C.G., "The Convergence of a Class of Double-rank Minimization Algorithms," Journal of the Institute of Mathematics and Applications, Vol. 6, 1970, pp 76-90 and 222-231.

21. Dixon, L.C.W., "The Choice of Step Length, a Crucial Factor in the Performance of Variable Metric Algorithms," Presented at the Conference on Numerical Methods for Non-linear Optimization, University of Dundee, Scotland, June 28 to July 1, 1971.

22. Bertsekas, D.P., Notes on Nonlinear Programming and Discrete-Time Optimal Control, Laboratory for Information and Decision Systems, MIT, LIDS-R-919, July, 1979, pp 2-11 to 2-20.

23. Crawley, E.F., "Aerodynamic Damping Measurements in a Transonic Compressor," ASME Journal of Engineering for Power, Vol. 105, No. 3, July, 1983.

Table 2.1 Parameters of rotor at typical section at the aeroelastic design point.

Number of Blades	N	14
Solidity	σ	1.409
Mach number	M	1.317
Recuced frequency	k	0.495
Location of pitch axis	a	0.0
Mass ratio of reference blade	μ	181.9
Radius of gyration of blades	r	0.4731
Stagger angle at typical section	ξ	58.99°

C-2

Table 5.1 Two tone mistune patterns. Patterns 2a, 2b, and 2c were picked to approximate optimal mistune pattern.

	Percent mass mistuning of ith blade, ε_i			
Blade number	Optimal	2a	2b	2c
i = 1	0.00 %	0.00 %	0.00 %	0.00 %
2	0.94	0.00	0.00	6.00
3	0.00	0.00	0.00	0.00
4	4.27	6.00	6.00	6.00
5	0.00	0.00	0.00	0.00
6	5.81	6.00	6.00	6.00
7	0.00	0.00	0.00	0.00
8	5.09	6.00	6.00	6.00
9	3.47	0.00	6.00	6.00
10	7.05	6.00	6.00	6.00
11	0.00	0.00	0.00	0.00
12	4.76	6.00	6.00	6.00
13	0.00	0.00	0.00	0.00
14	6.26	6.00	6.00	6.00

Table 5.2 Three tone mistune patterns. Patterns 3a, 3b, 3c, 3d, 3e, 3f, and 3g were picked to approximate optimal mistune pattern.

	Percent mass mistuning of ith blade, ε_i			
Blade number	Optimal	3a	3b	3c
i = 1	0.00 %	0.00 %	0.00 %	0.00 %
2	0.94	0.00	0.00	6.00
3	0.00	0.00	0.00	0.00
4	4.27	5.00	6.00	6.00
5	0.00	0.00	0.00	0.00
6	5.81	6.00	7.00	7.00
7	0.00	0.00	0.00	0.00
8	5.09	5.00	6.00	6.00
9	3.47	5.00	0.00	0.00
10	7.05	6.00	7.00	7.00
11	0.00	0.00	0.00	0.00
12	4.76	5.00	6.00	6.00
13	0.00	0.00	0.00	0.00
14	6.26	6.00	7.00	7.00

Blade number	3d	3e	3f	3g
i = 1	0.00 %	0.00 %	0.00 %	0.00 %
2	0.00	0.00	6.00	0.00
3	0.00	0.00	0.00	0.00
4	6.00	6.00	6.00	6.00
5	0.00	0.00	0.00	0.00
6	7.00	8.00	8.00	9.00
7	0.00	0.00	0.00	0.00
8	6.00	6.00	6.00	6.00
9	6.00	6.00	6.00	6.00
10	7.00	8.00	8.00	9.00
11	0.00	0.00	0.00	0.00
12	6.00	6.00	6.00	6.00
13	0.00	0.00	0.00	0.00
14	7.00	8.00	8.00	9.00

Table 5.3 Four tone mistune patterns. Patterns 4a, 4b, 4c, and 4d were picked to approximate optimal mistune pattern.

	Percent mass mistuning of ith blade, ϵ_i				
Blade number i = 1	Optimal 0.00 %	4a 0.00 %	4b 0.00 %	4c 0.00 %	4d 0.00 %
2	0.94	2.00	4.00	4.00	5.00
3	0.00	0.00	0.00	0.00	0.00
4	4.27	6.00	6.00	6.00	6.00
5	0.00	0.00	0.00	0.00	0.00
6	5.81	9.00	9.00	8.00	9.00
7	0.00	0.00	0.00	0.00	0.00
8	5.09	6.00	6.00	6.00	6.00
9	3.47	2.00	4.00	4.00	5.00
10	7.05	9.00	9.00	8.00	9.00
11	0.00	0.00	0.00	0.00	0.00
12	4.76	6.00	6.00	6.00	6.00
13	0.00	0.00	0.00	0.00	0.00
14	6.26	6.00	9.00	9.00	9.00

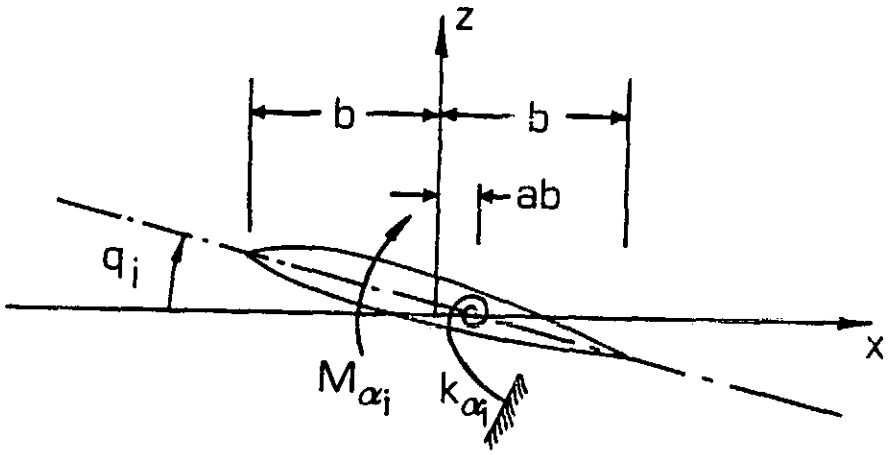

Figure 2.1 Geometry of the ith blade. Blade is modelled with a single torsional degree of freedom about the elastic axis.

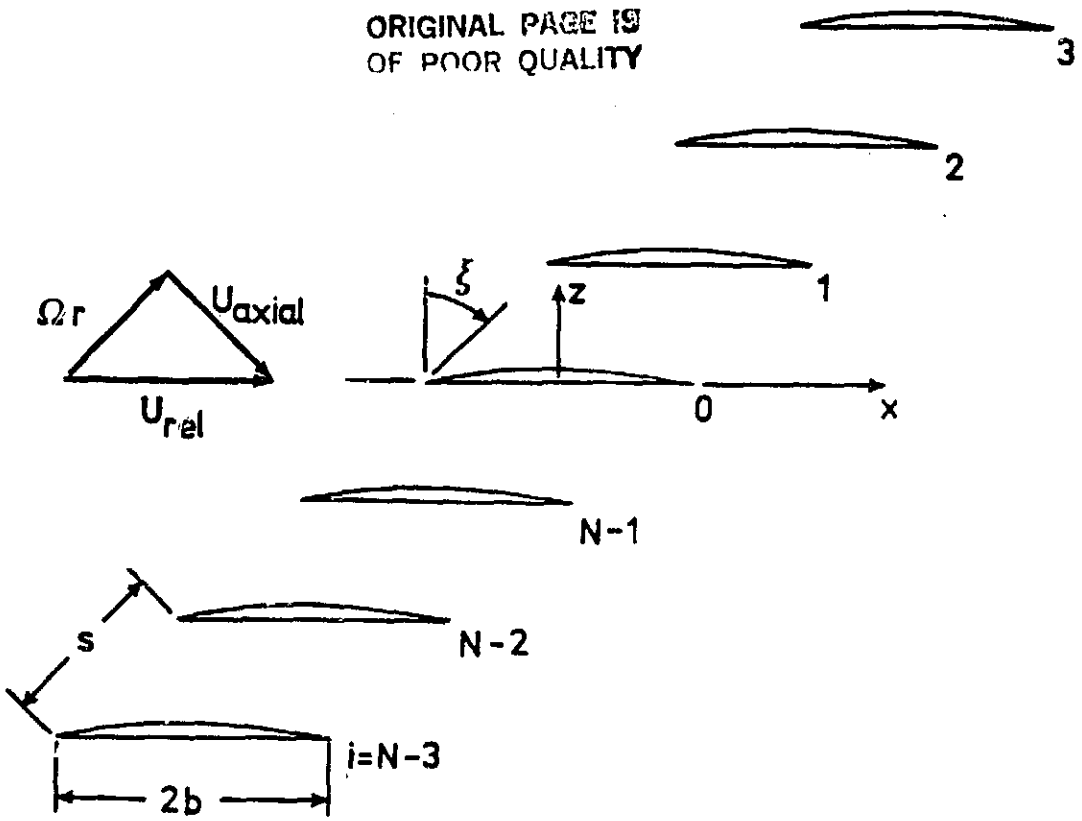

Figure 2.2 Geometry of the rotor at the typical section. Note the stagger angle and blade numbering definitions. The solidity of the rotor, σ, is equal to $2b/s$.

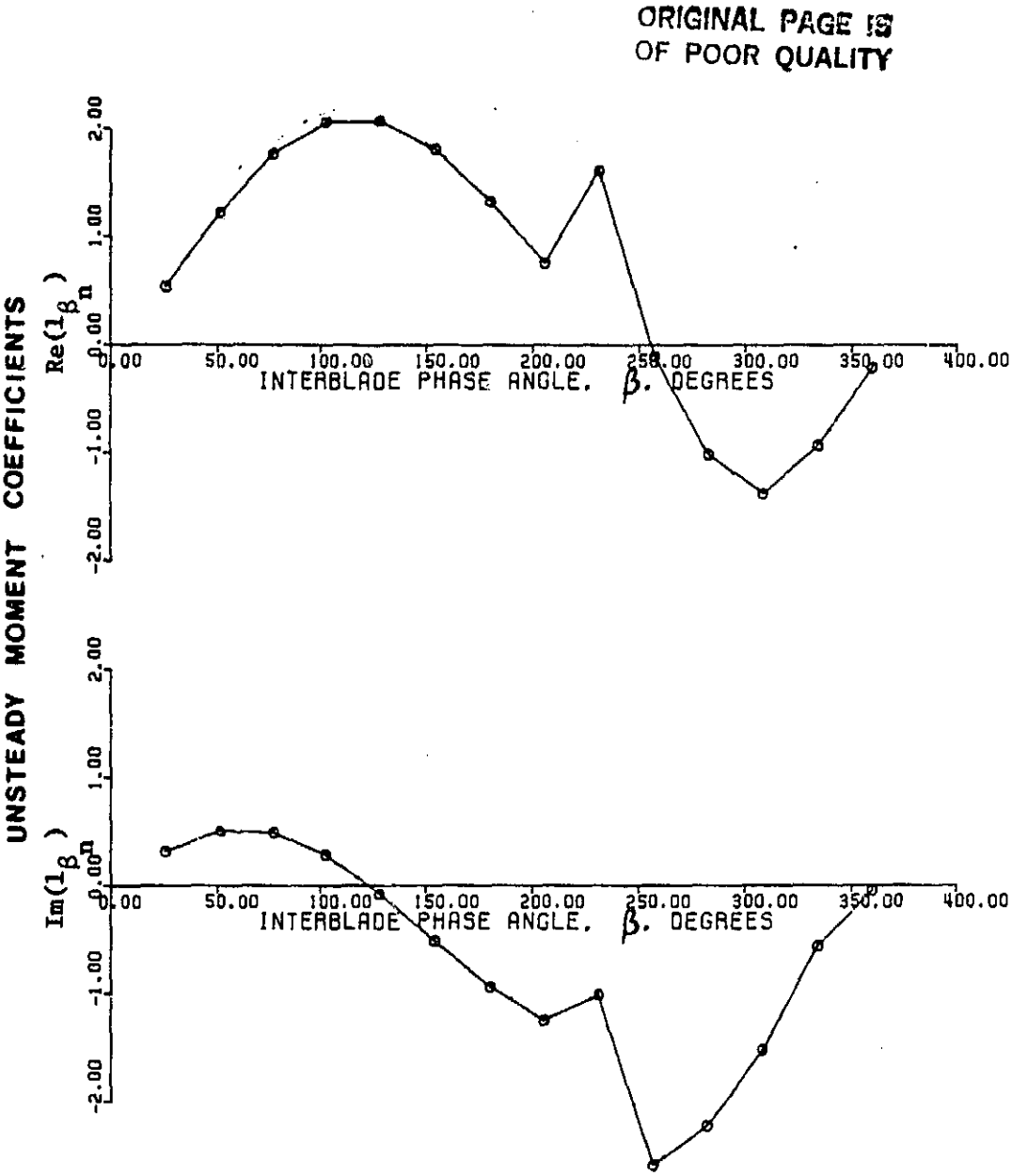

Figure 2.3 Unsteady moment coefficients acting on a reference blade for travelling wave motion of the blades.

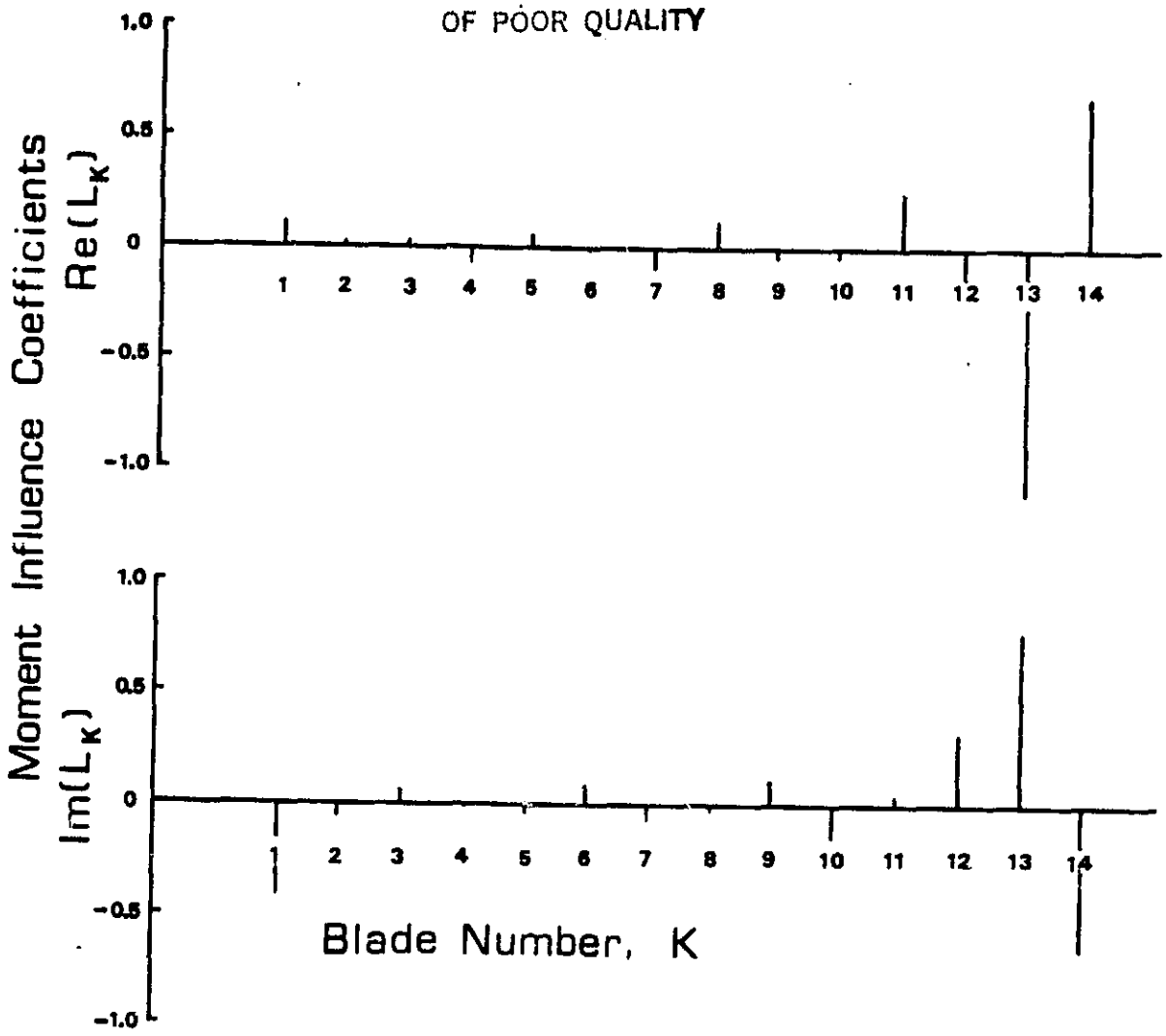

Figure 2.4 Unsteady moment coefficients in influence coefficient form. Note the four largest coefficients are L_{12}, L_{13}, L_{14}, and L_1, indicating that only neighboring blades have a significant influence on a given blade. Note also that $L_0 = L_{14}$.

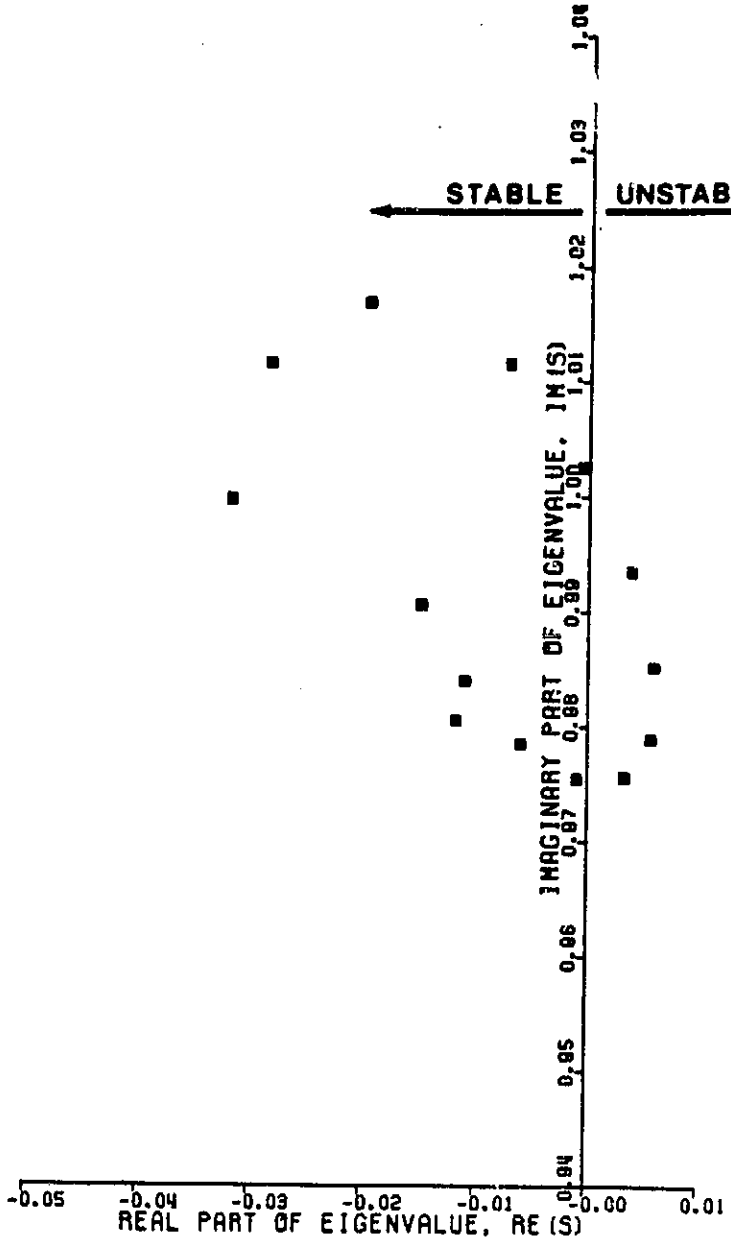

Figure 2.5 Eigenvalues of the tuned rotor. Notice that four of the 14 eigenvalues are unstable.

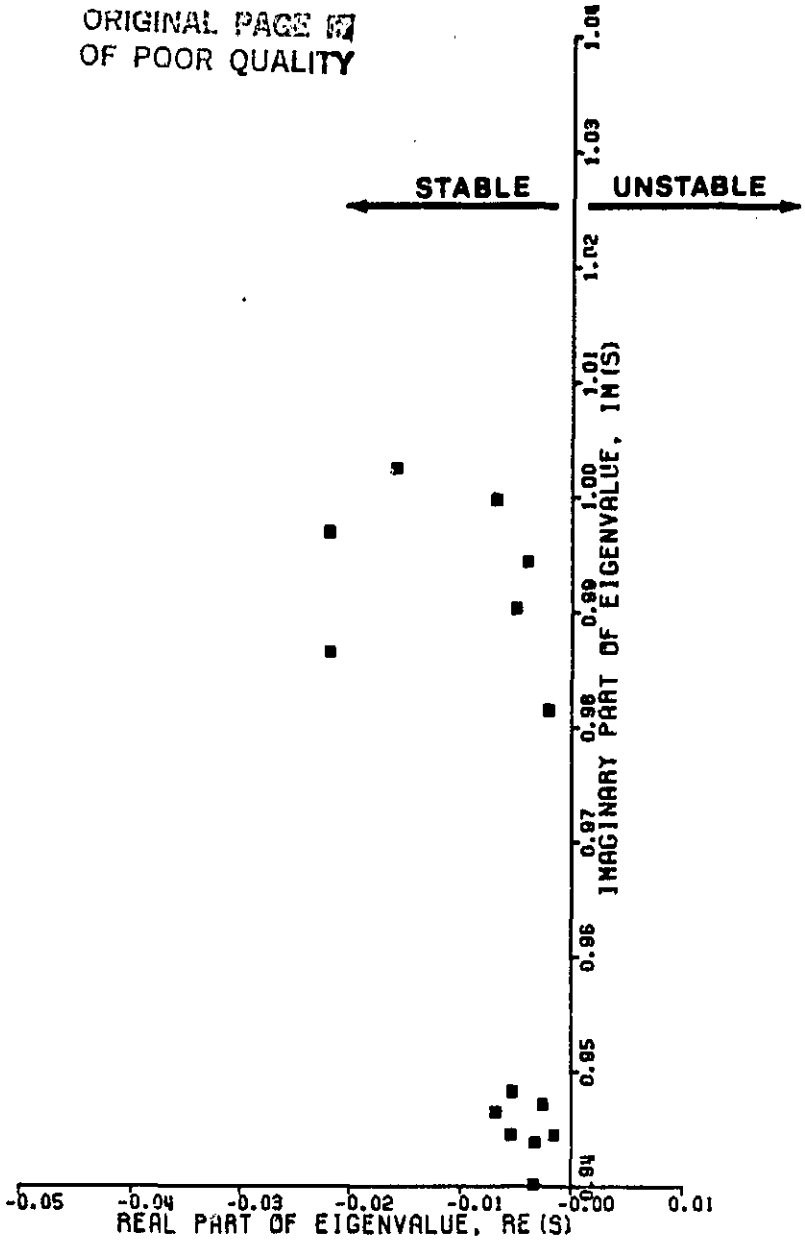

Figure 2.6 Eigenvalues of the alternately mistuned rotor. The even numbered blades have $\varepsilon_i = 0.0$ while the odd numbered blades have a mass mistune of $\varepsilon_i = 0.1$. For this case, the mistuning has stabilized an otherwise unstable rotor.

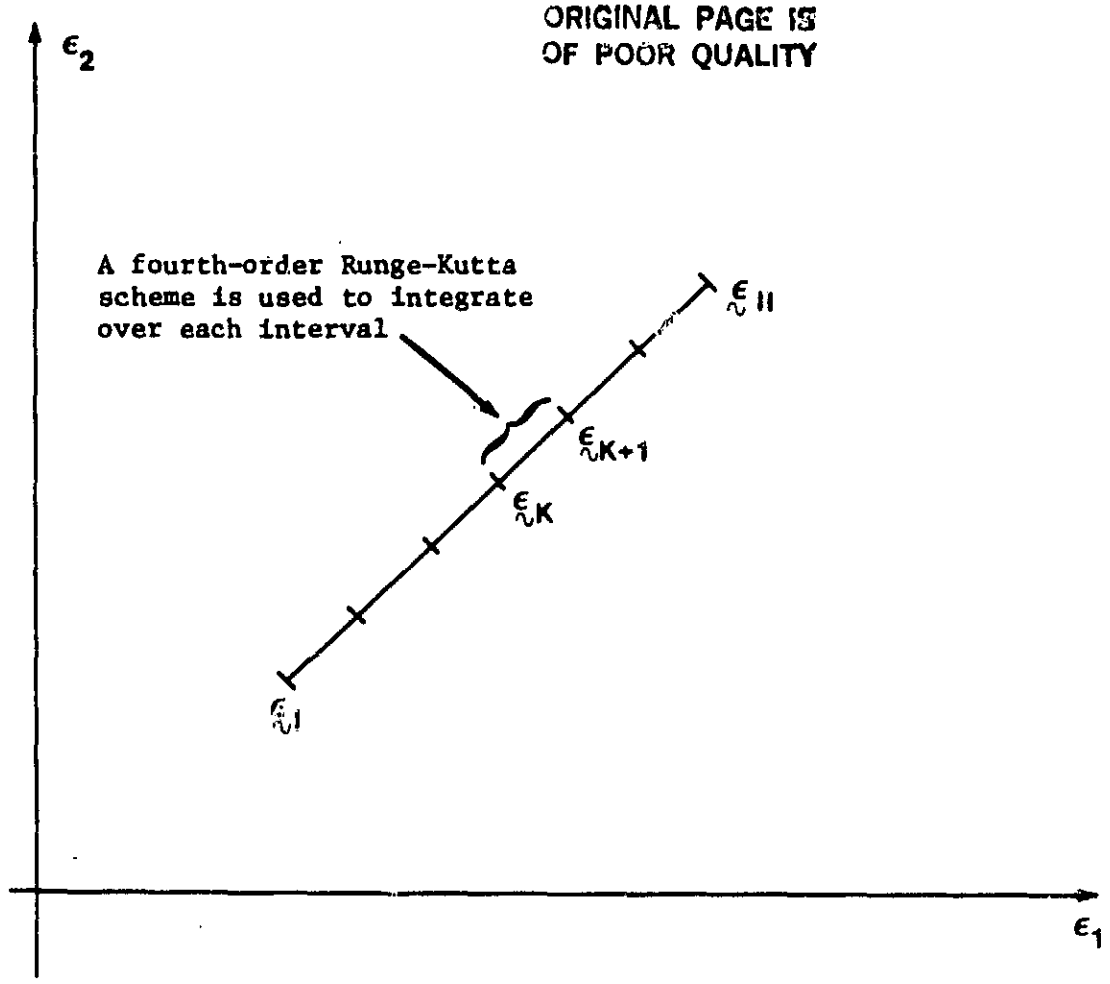

Figure 3.1 The path of integration for the evaluation of the eigenvalues and eigenvectors is chosen to be the straight line connecting the end points, $\underset{\sim}{\epsilon}_{I}$ and $\underset{\sim}{\epsilon}_{II}$. The path is then subdivided into I intervals. Over each interval, a fourth-order Runge-Kutta integration is performed.

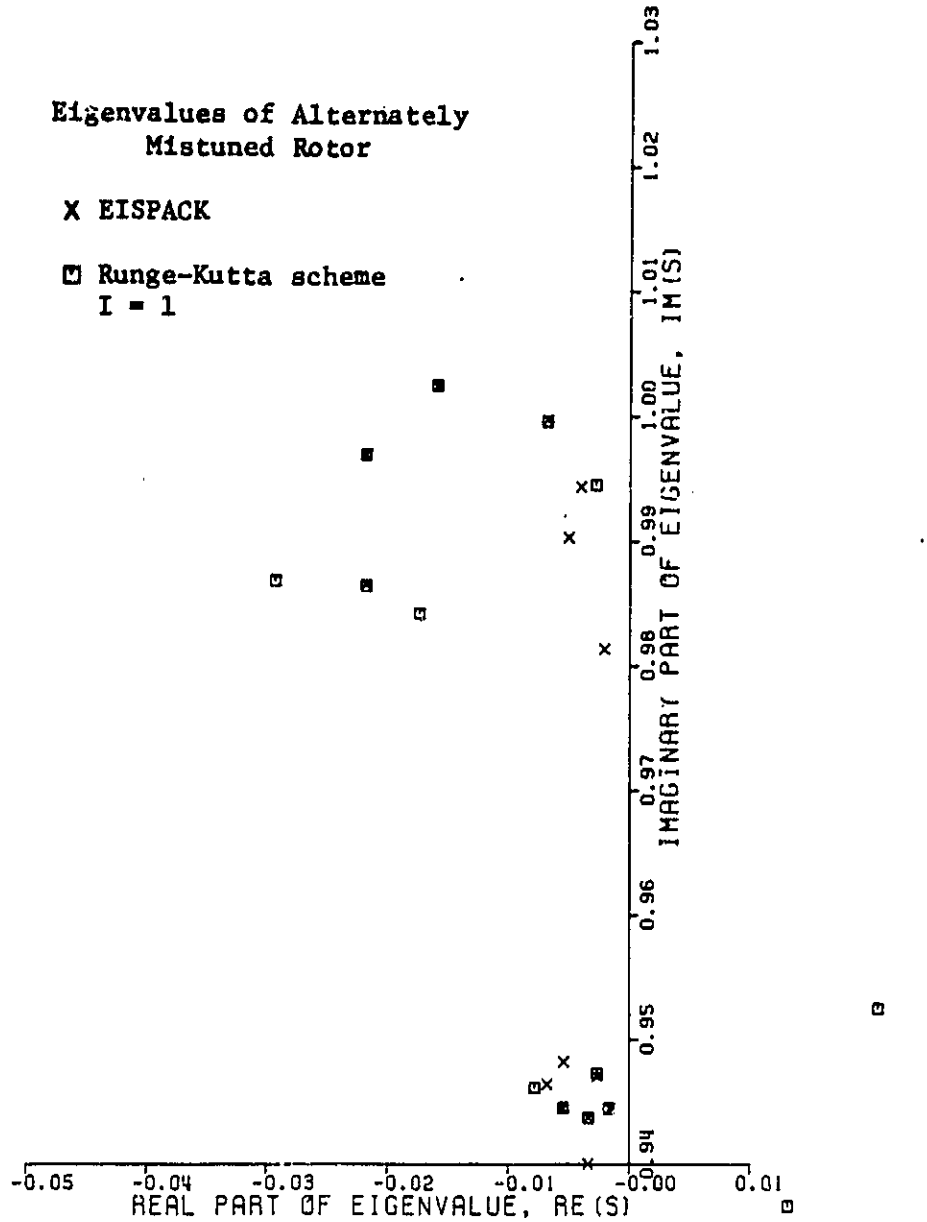

Figure 3.2 Evaluation of eigenvalues of alternately mistuned rotor via fourth-order Runge-Kutta integration. Number of integration steps = 1. Note the very poor agreement between the values determined by integration and those determined by EISPACK.

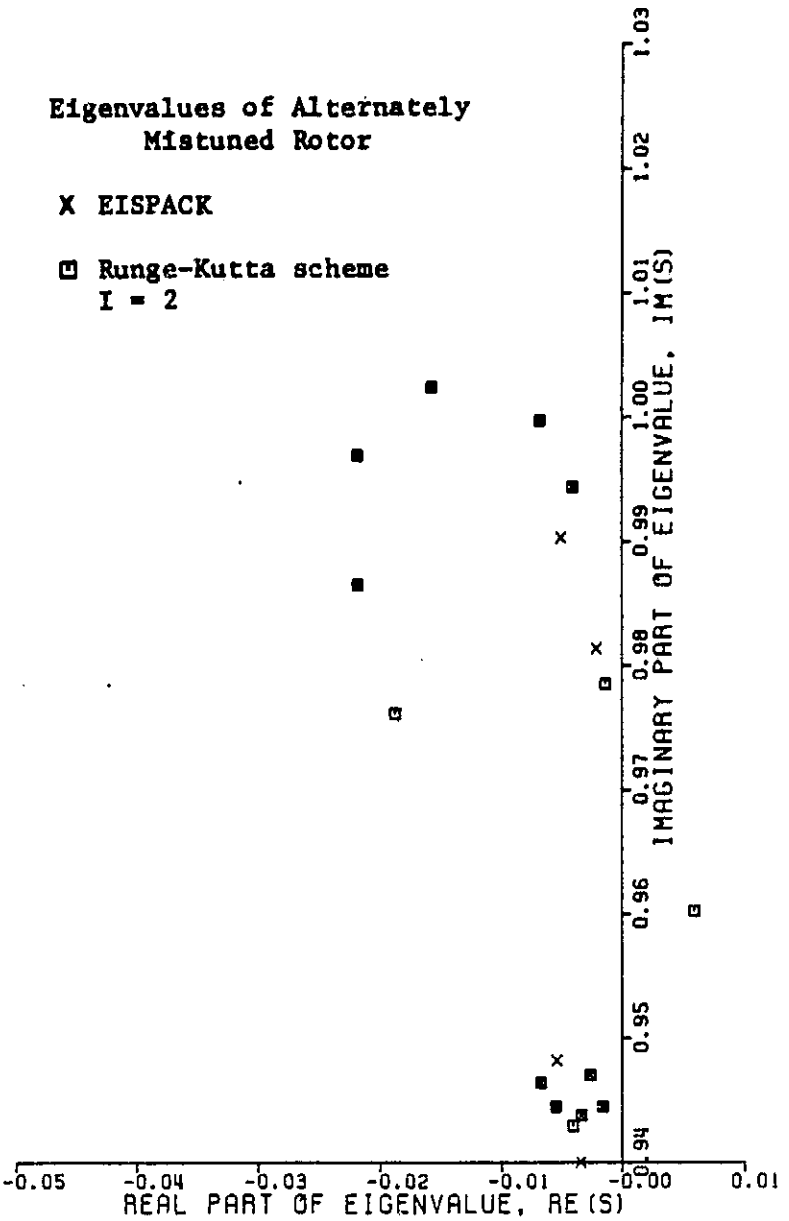

Figure 3.3 Evaluation of eigenvalues of alternately mistuned rotor via fourth-order Runge-Kutta integration. Number of integration steps = 2. Note the very poor agreement between the values determined by integration and those determined by EISPACK.

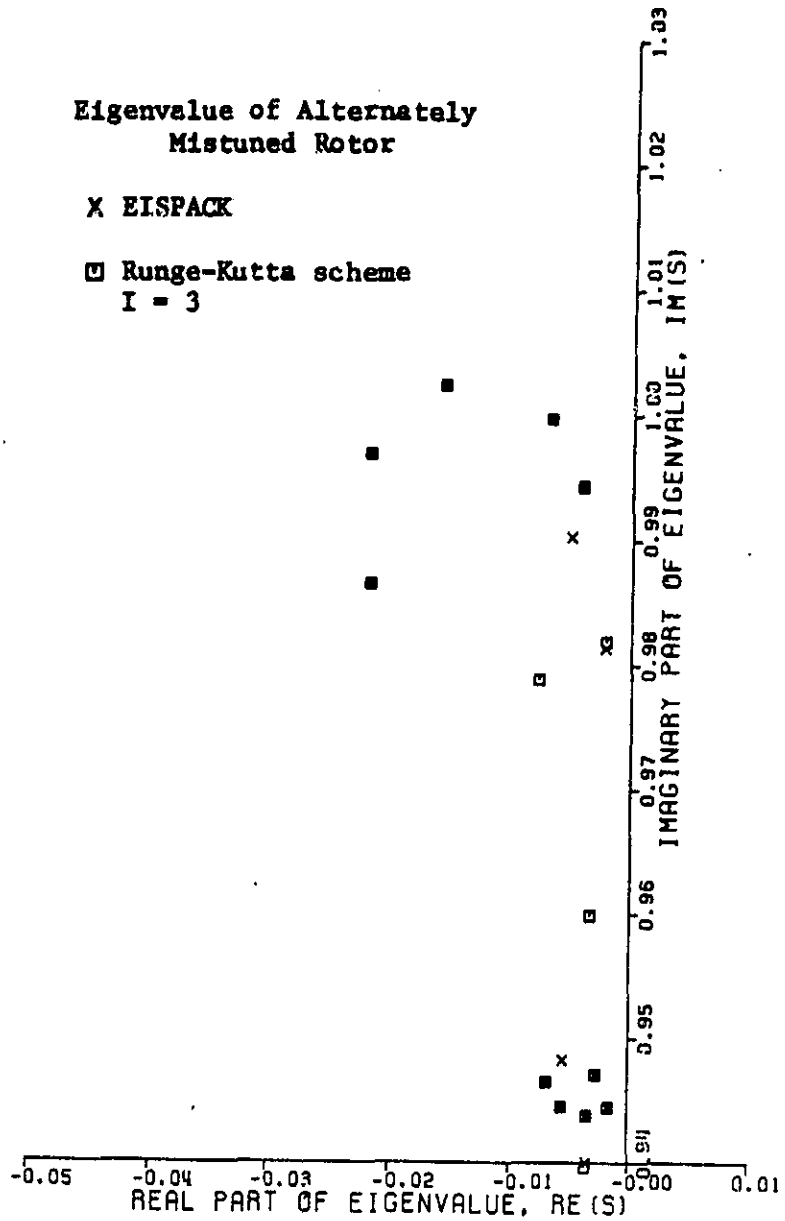

Figure 3.4 Evaluation of eigenvalues of alternately mistuned rotor via fourth-order Runge-Kutta integration. Number of integration steps = 3. Ten of the 14 eigenvalues determined by integration are in excellent agreement with those determined by EISPACK. However, four of the eigenvalues are not predicted well with three integration steps.

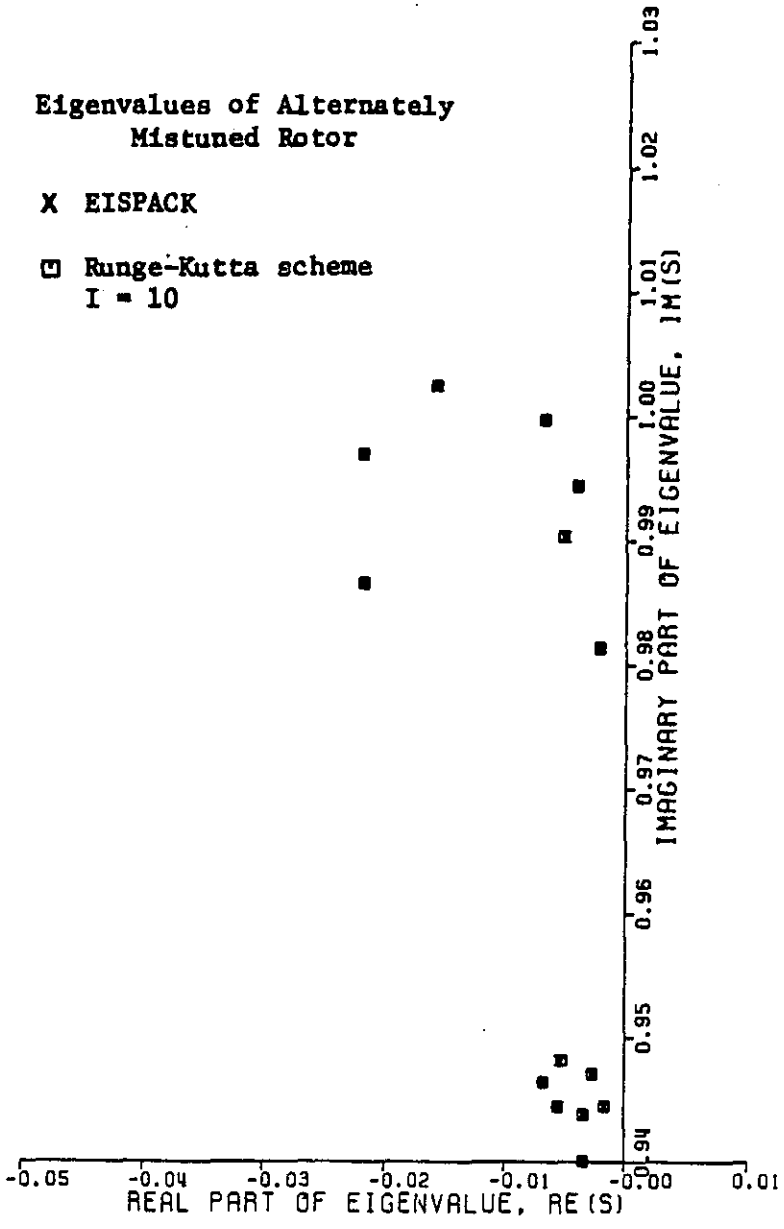

Figure 3.5 Evaluation of eigenvalues of alternately mistuned rotor via fourth-order Runge-Kutta integration. Number of integration steps = 10. With ten integration steps, the eigenvalues are correctly predicted using the Runge-Kutta integration scheme.

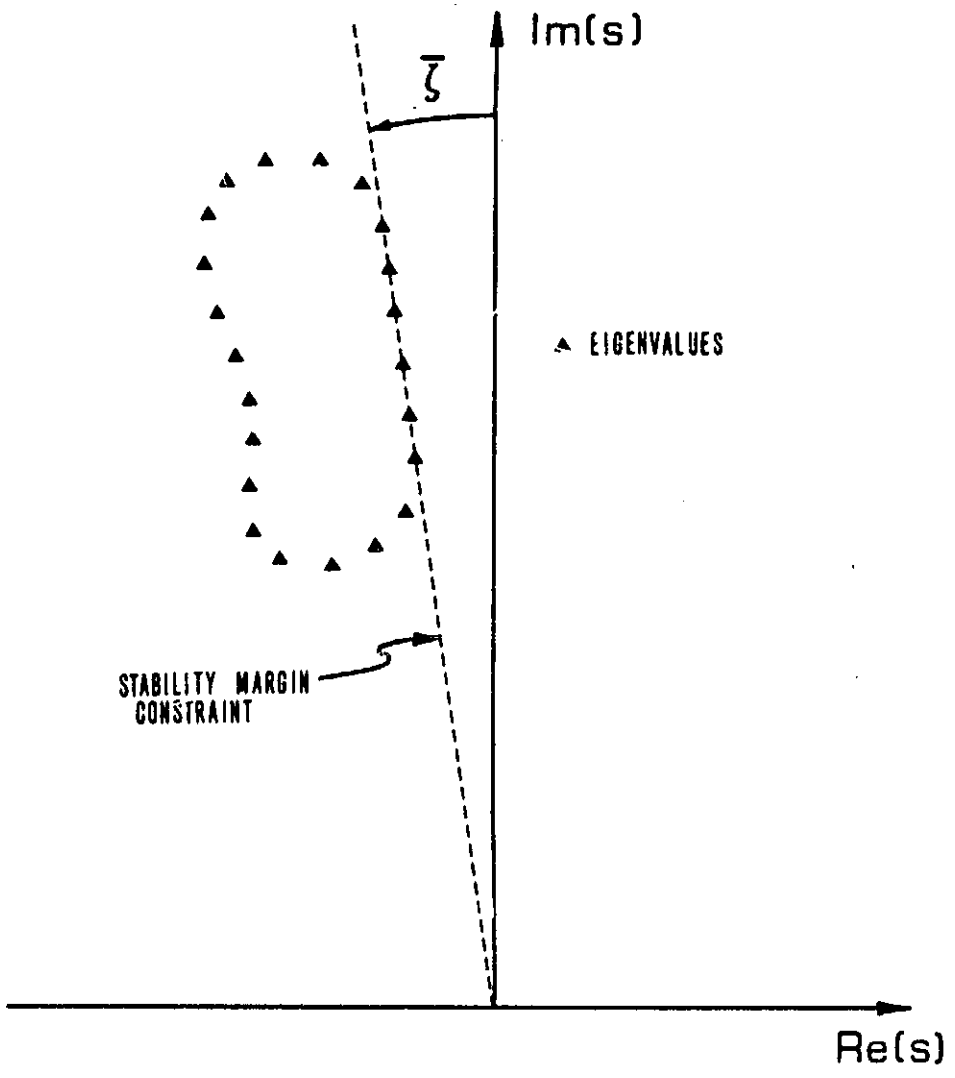

Figure 4.1 Graphic interpretation of stability margin constraint. Every eigenvalue must have a damping ratio greater than or equal to $\bar{\zeta}$.

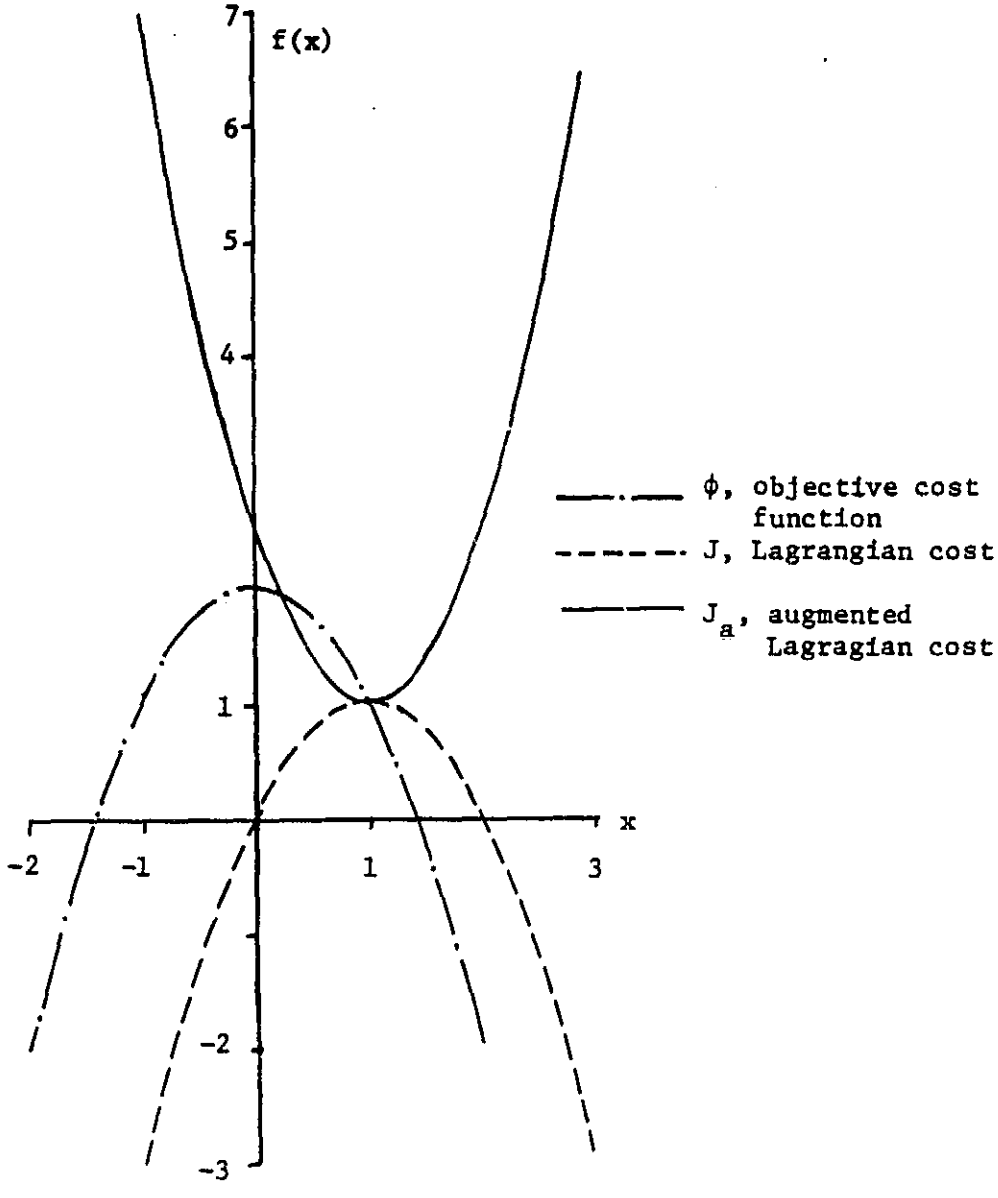

Figure 4.2 Relationship between cost, Lagrangian cost, and augmented Lagrangian cost. The constrained minimum is at x = 1. Note that at this point, all three cost functions have the same value. Furthermore, the slopes of the Lagrangian cost and the augmented Lagrangian cost curves are both zero. The augmented Lagrangian cost is positve definite at x = 1.

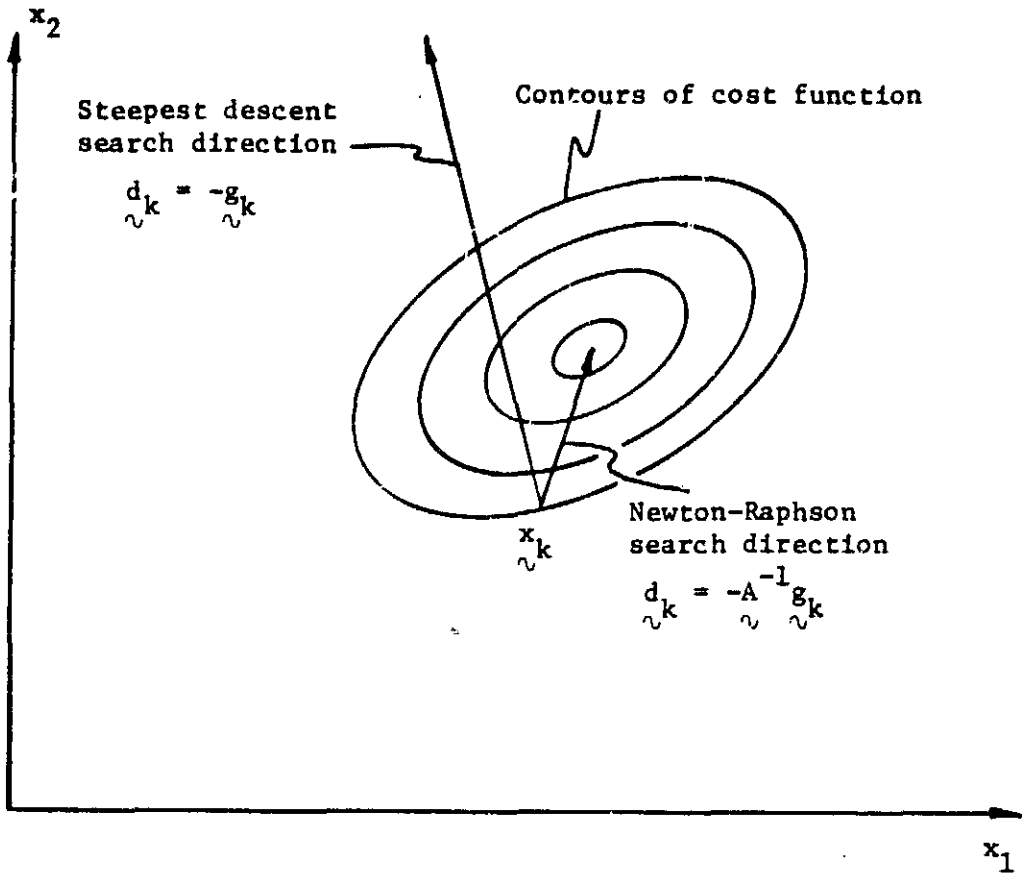

Figure 4.3 Near a minimum, a Newton-Raphson search vector points directly to the minimum of the cost function, both in direction and magnitude. On the other hand, a steepest descent search vector points in the direction of largest change in cost, which is not toward the minimum unless the cost contours are circular. Furthermore, the steepest descent vector contains no stepsize information.

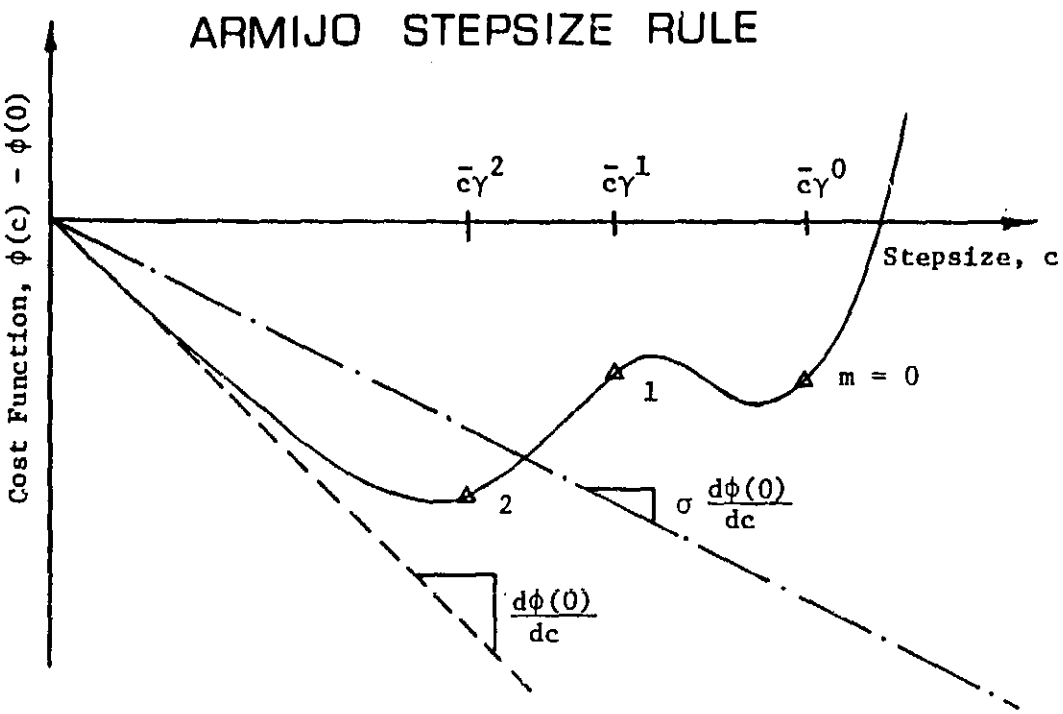

Figure 4.4 Graphical interpretation of the Armijo rule (from Reference [22]). The stepsize $c = \bar{c}\,\gamma^2$ is chosen since m = 2 is the smallest positive interger which results in a value of $\phi(c) - \phi(0)$ which is less than $c\sigma\frac{d\phi(0)}{dc}$.

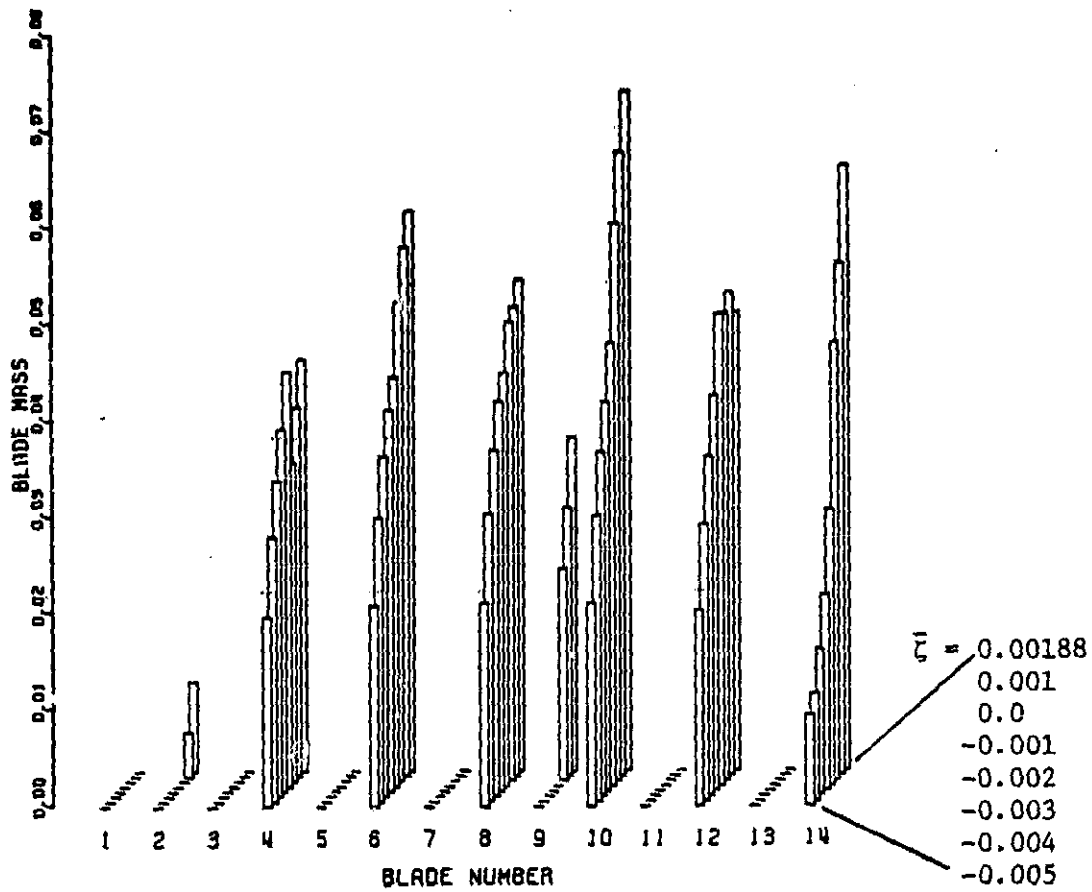

Figure 5.1 Mass mistuning vectors of the optimally mistuned rotor. Note that both the level of mistuning and the character of mistuning changes for increasing stability margin requirements.

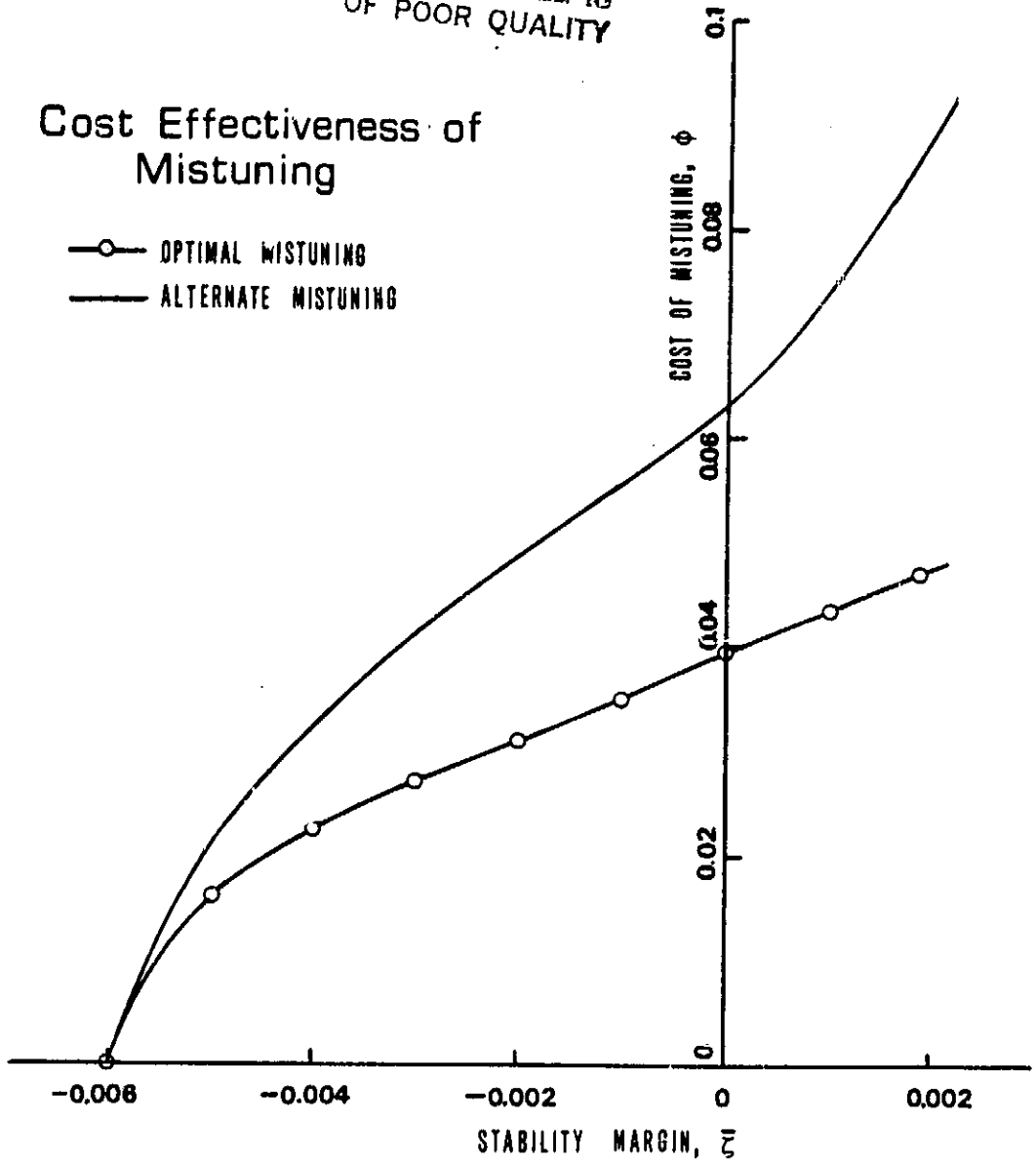

Figure 5.2 Cost effectiveness of optimal mistuning. Note that optimal mistuning can achieve a given stability margin for a low level of mistuning compared to the alternate mistune pattern.

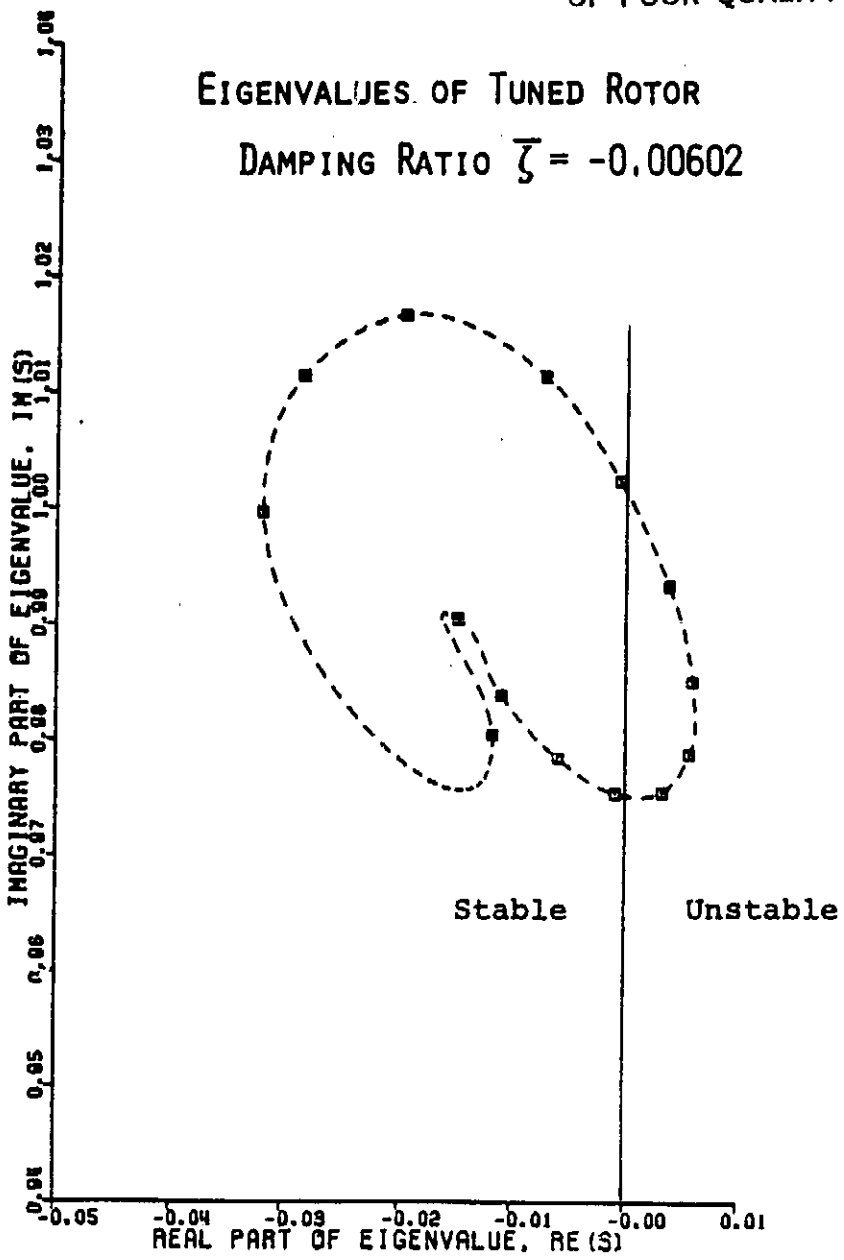

Figure 5.3a Eigenvalues of tuned rotor. Note that four of the 14 eigenvalues are unstable.

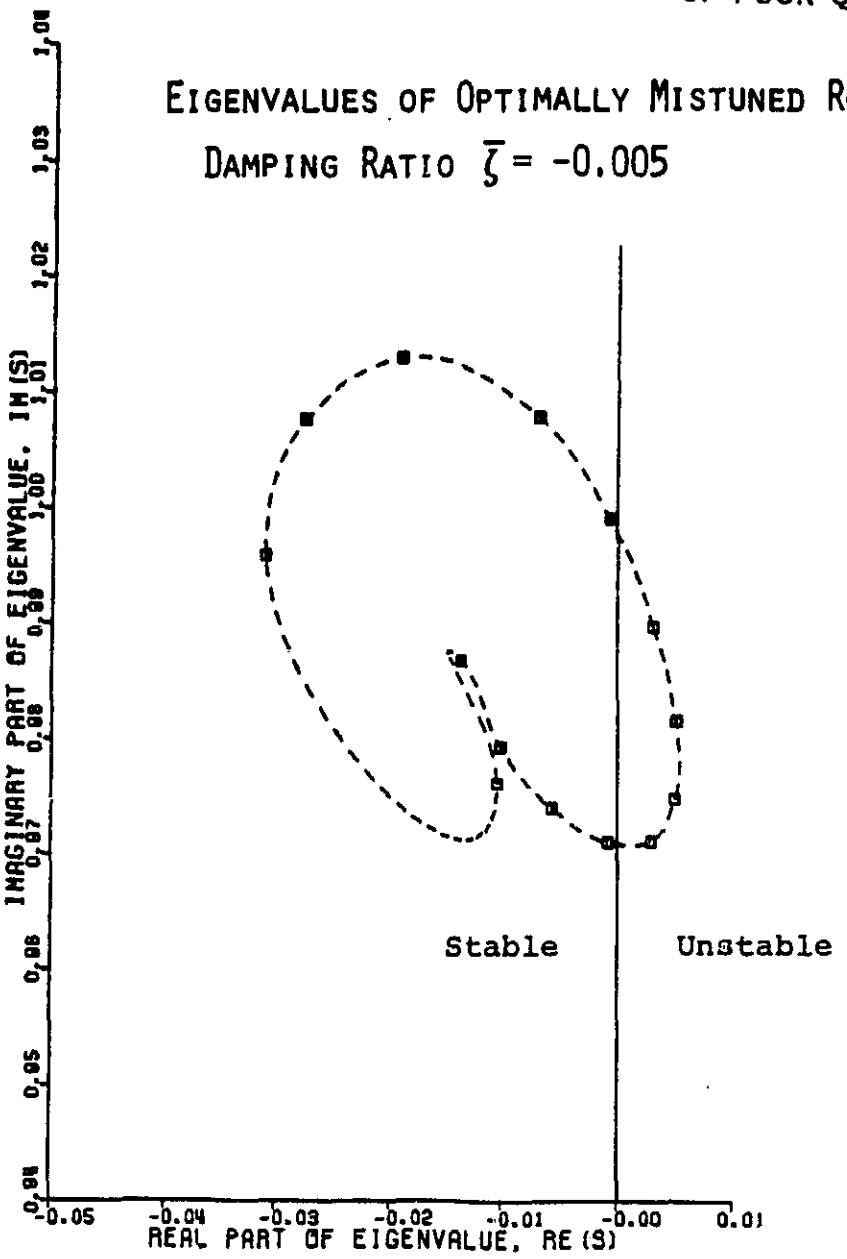

Figure 5.3b Eigenvalues of optimally mistuned rotor. The required stability margin is $\bar{\zeta}$ = -0.005.

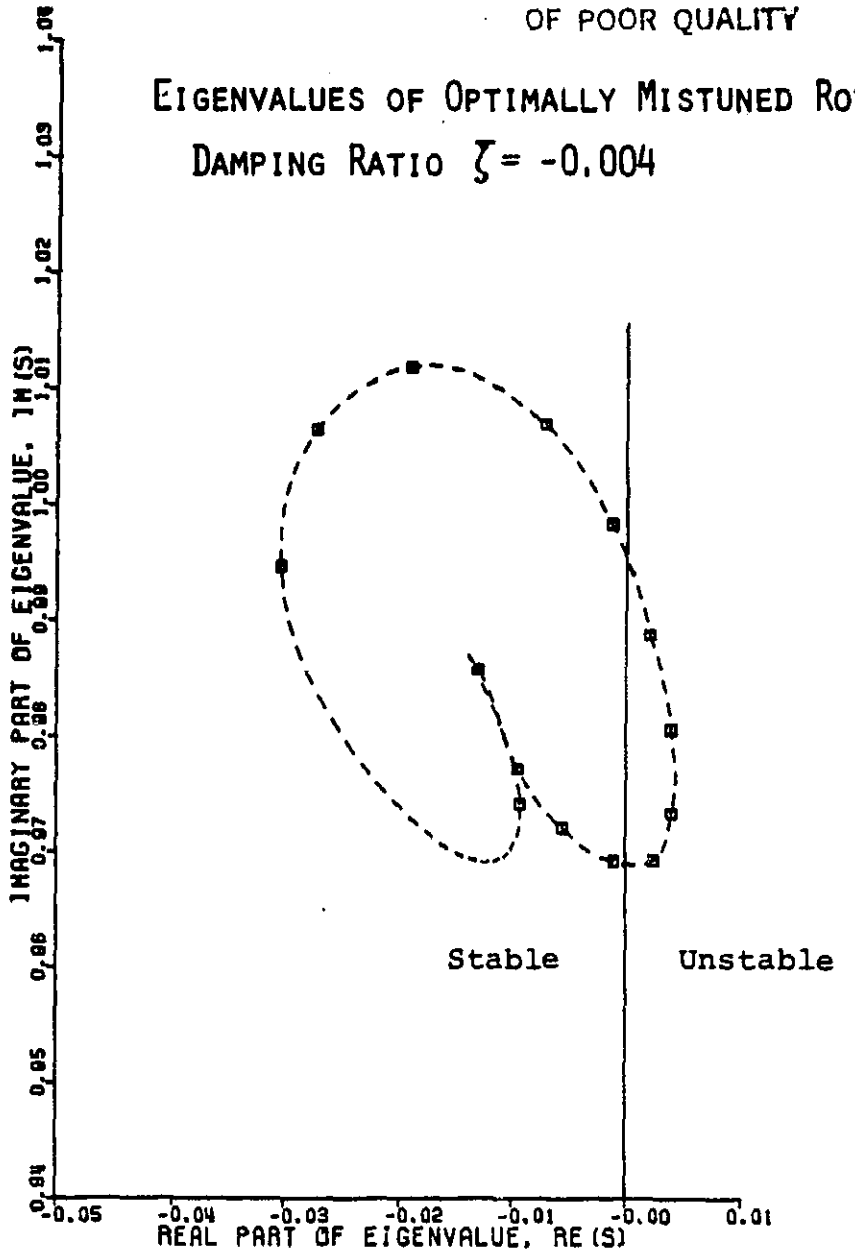

Figure 5.3c Eigenvalues of optimally mistuned rotor. The required stability margin is $\bar{\zeta}$ = -0.004.

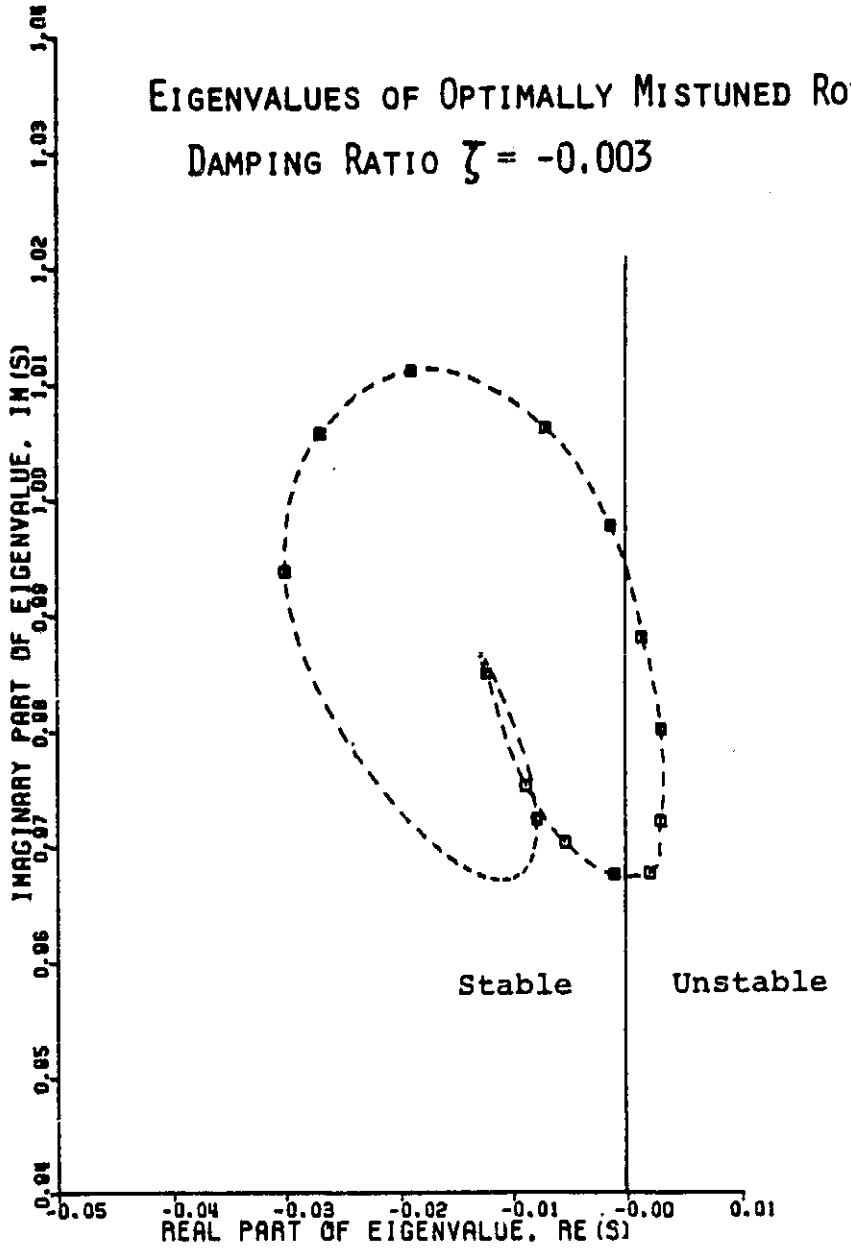

Figure 5.3d Eigenvalues of optimally mistuned rotor. The required stability margin is $\bar{\zeta} = -0.003$.

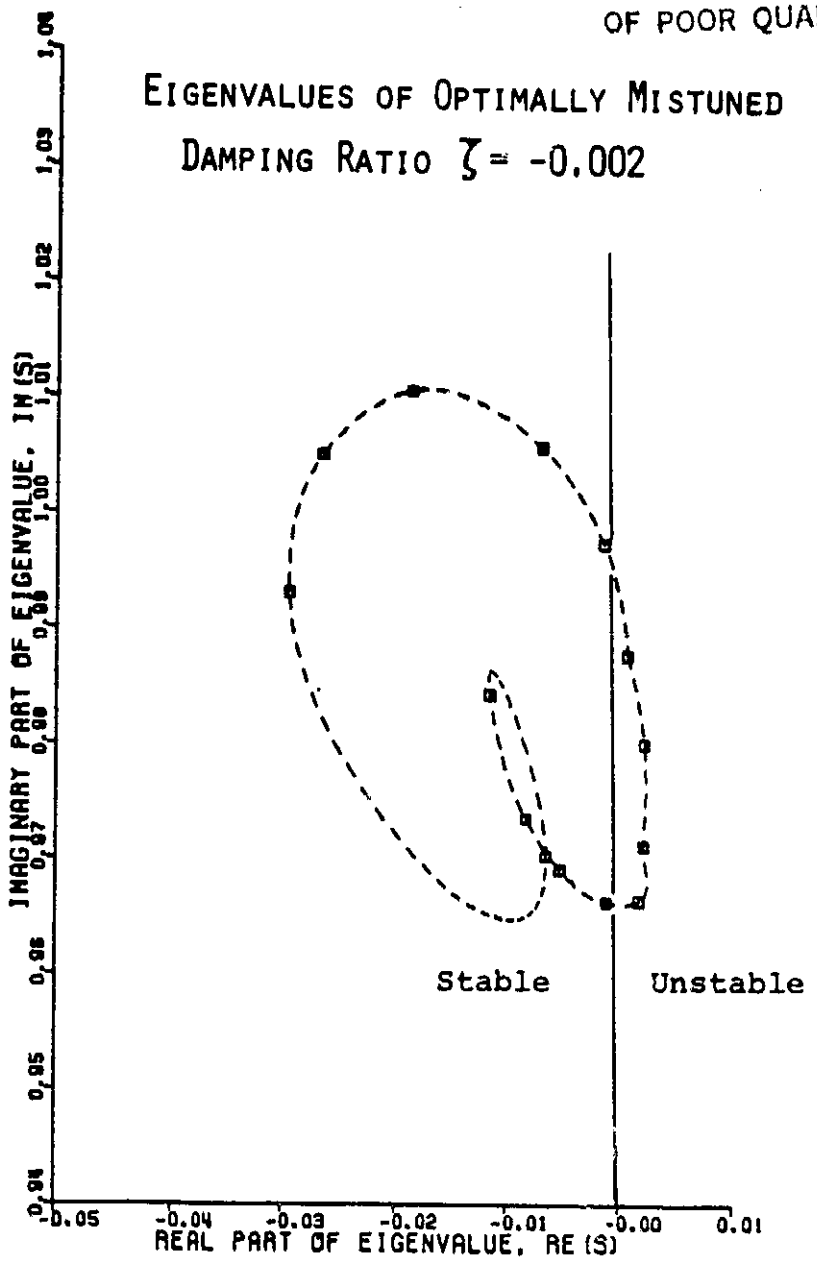

Figure 5.3e Eigenvalues of optimally mistuned rotor. The required stability margin is $\bar{\zeta} = -0.002$.

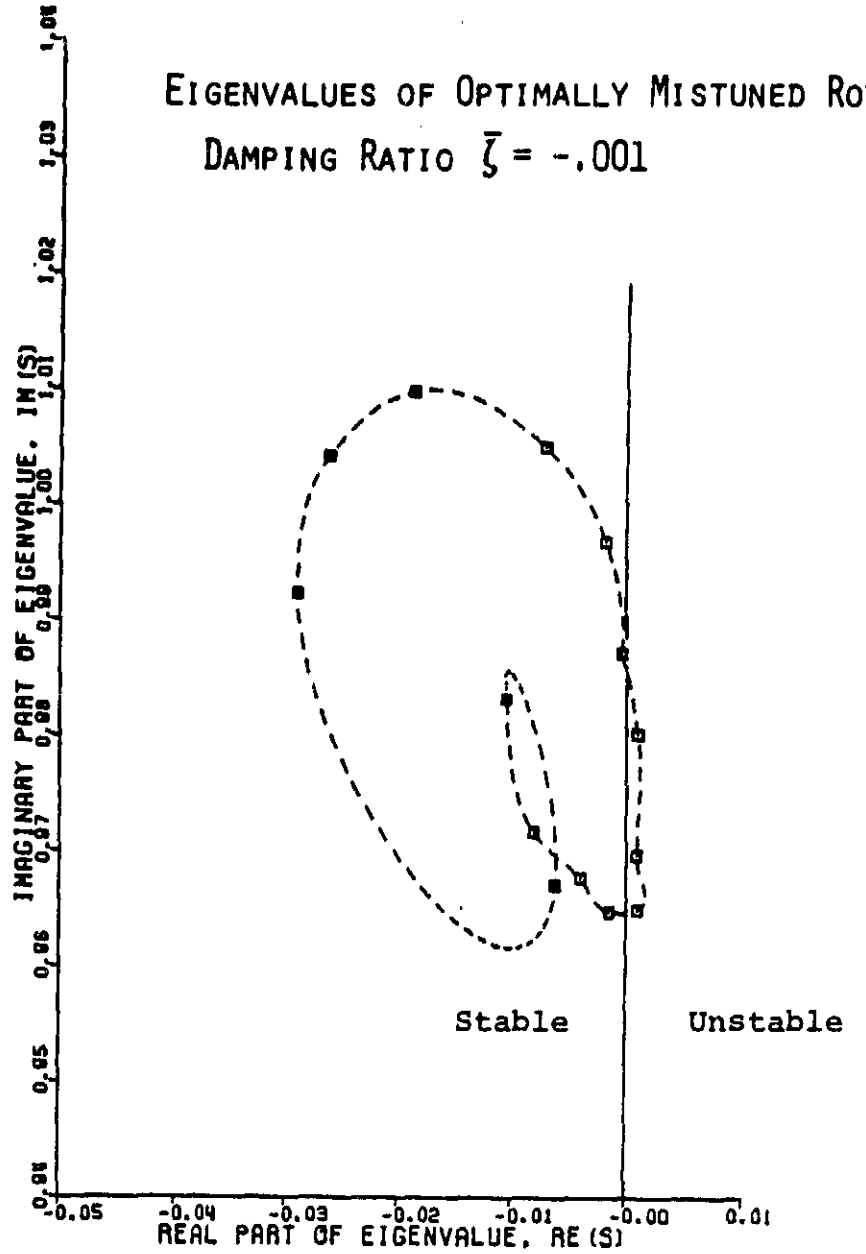

Figure 5.3f Eigenvalues of optimally mistuned rotor. The required stability margin is $\bar{\zeta}$ = -0.001.

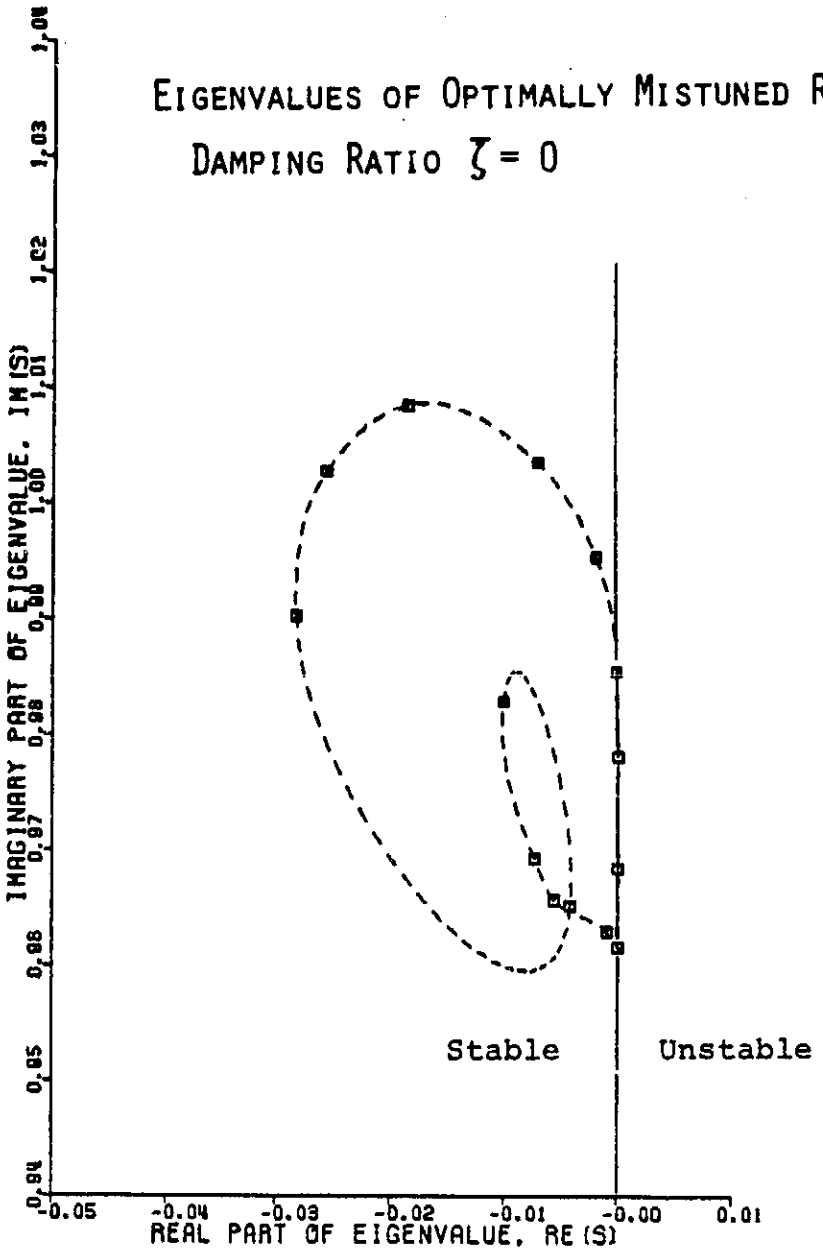

Figure 5.3g Eigenvalues of optimally mistuned rotor. The required stability margin is $\bar{\zeta} = 0$. Note that four of the 14 eigenvalues lie on the neutral stability line.

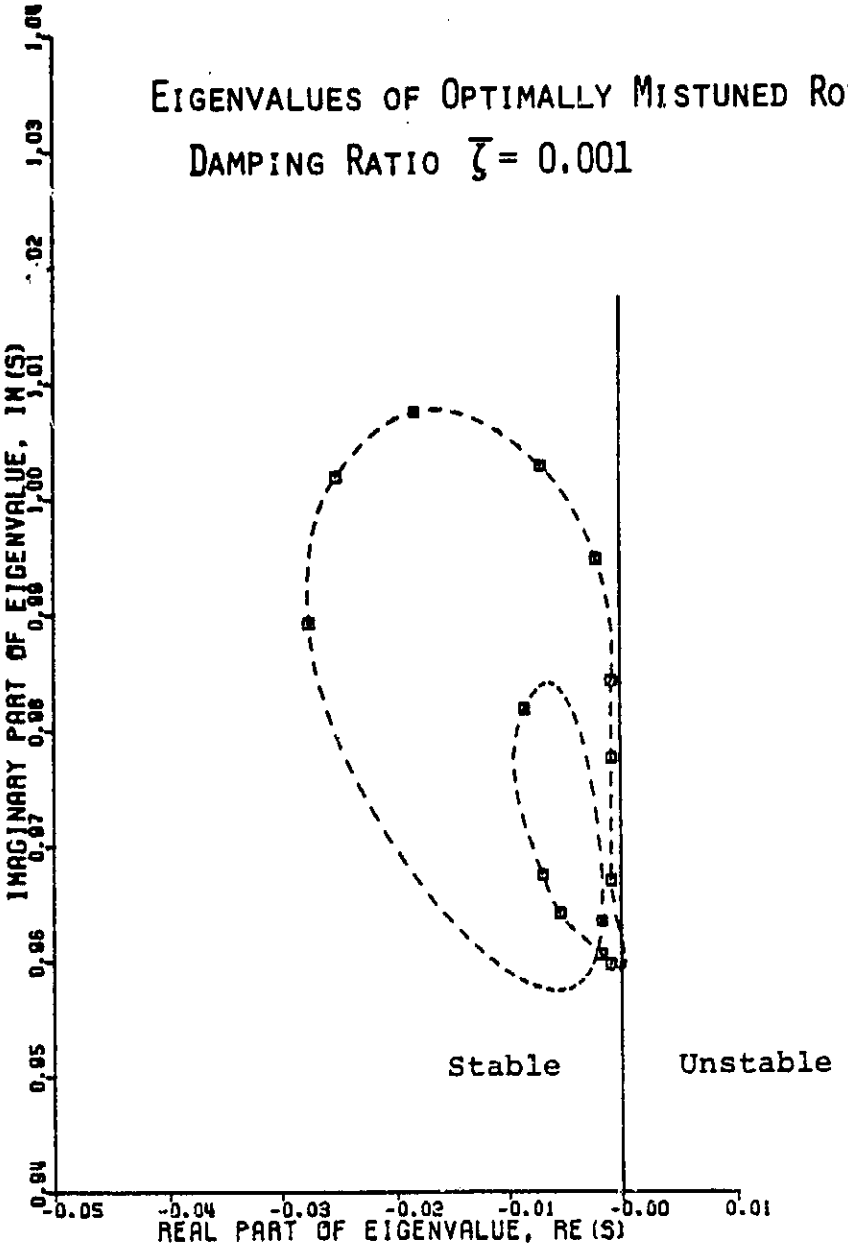

Figure 5.3h Eigenvalues of optimally mistuned rotor. The required stability margin is $\bar{\zeta}$ = 0.001.

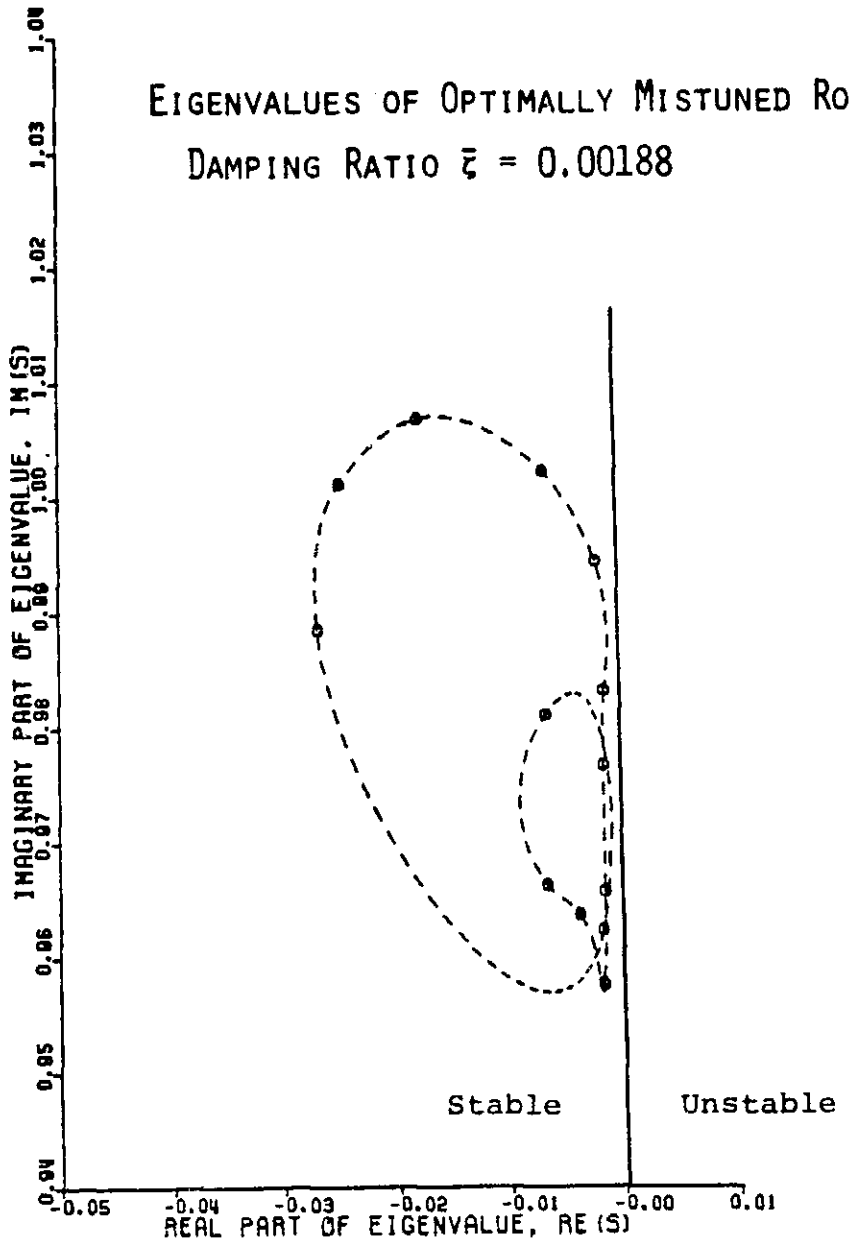

Figure 5.3i Eigenvalues of optimally mistuned rotor. The required stability is $\bar{\zeta} = 0.002$. However, for this case, the optimization procedure did not completely converge. The stability margin of the partially converged solution is $\bar{\zeta} = 0.00188$.

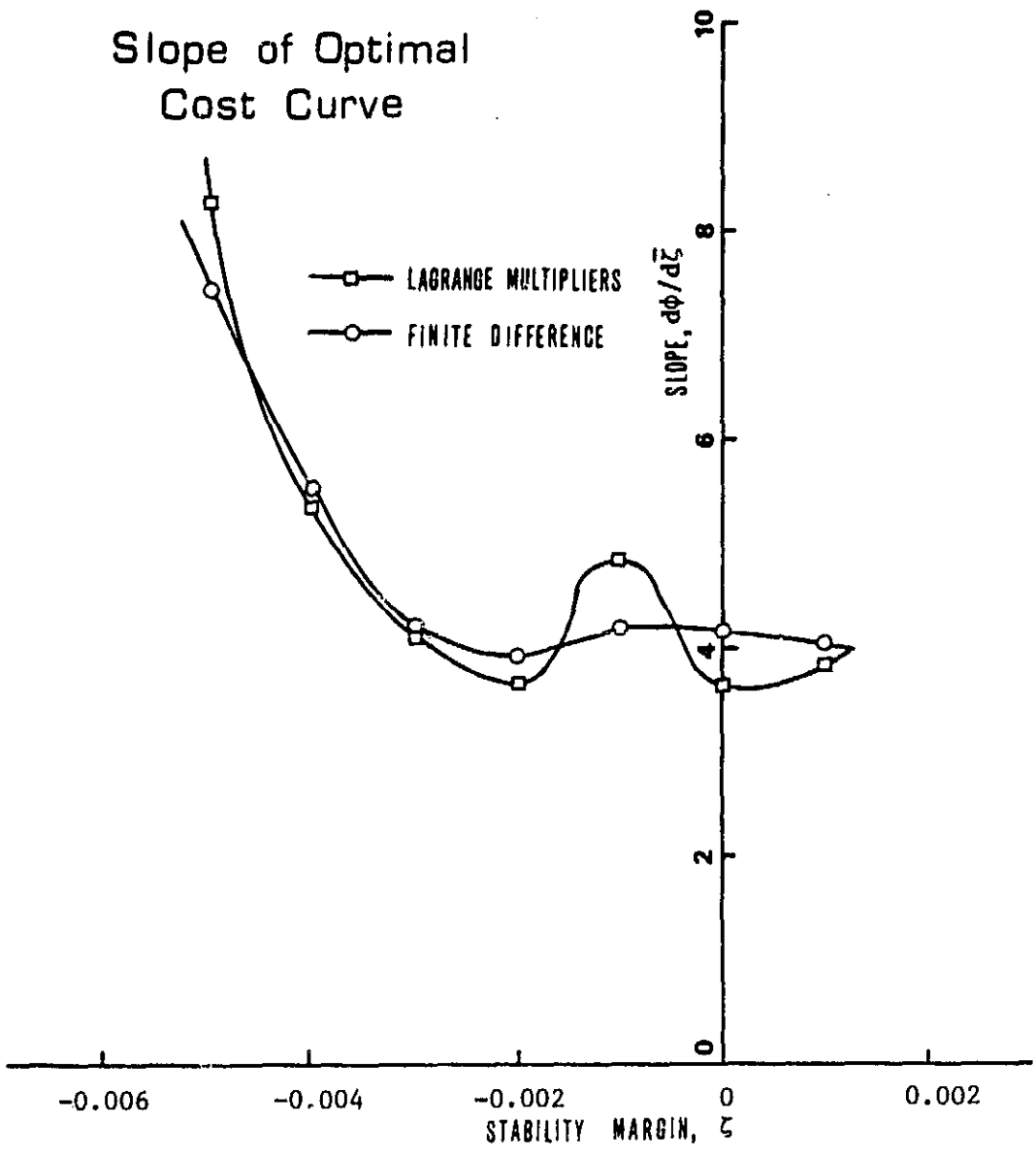

Figure 5.4 Slope of optimal cost versus stability margin curve. The slope of the optimal cost curve was evaluated from the Lagrange multiplies of the stability margin constraints, and by finite differncing the optimal cost curve.

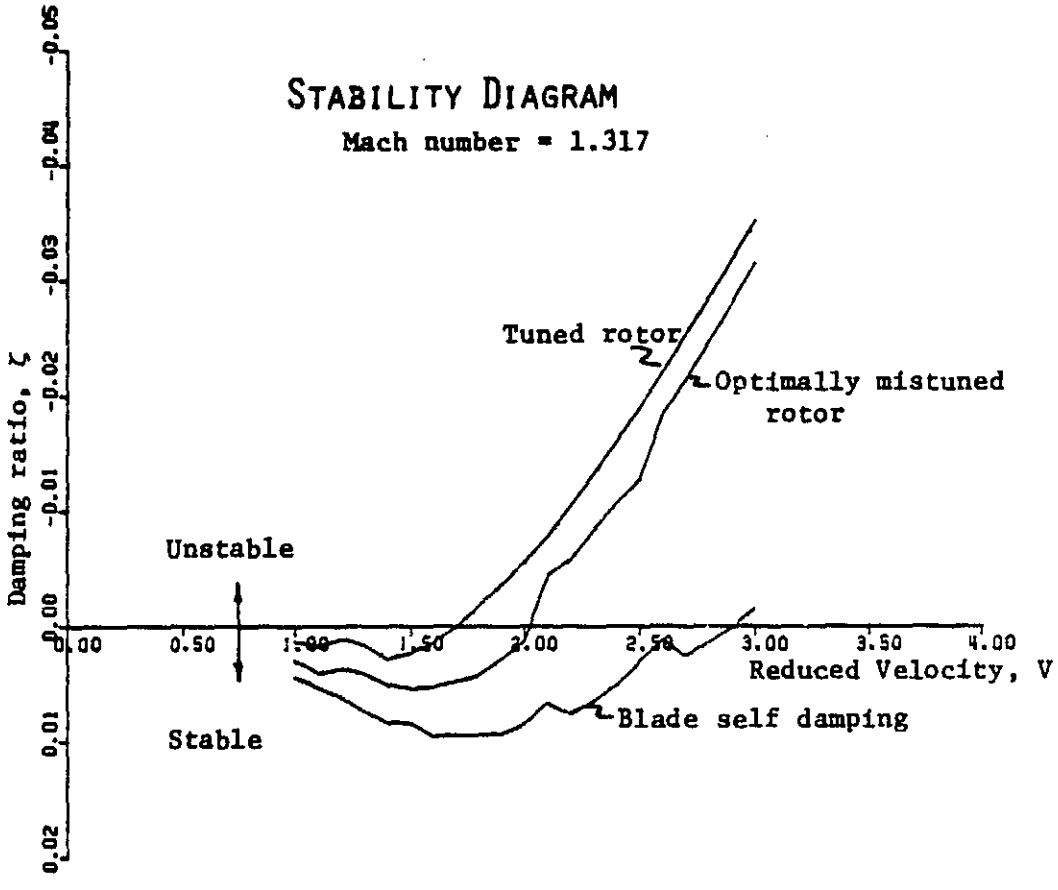

Figure 5.5 Stability margin of a rotor versus reduced velocity for the case of constant Mach number. Note the optimally mistuned rotor damping ratio lies between the blade self damping and the tuned rotor damping ratios.

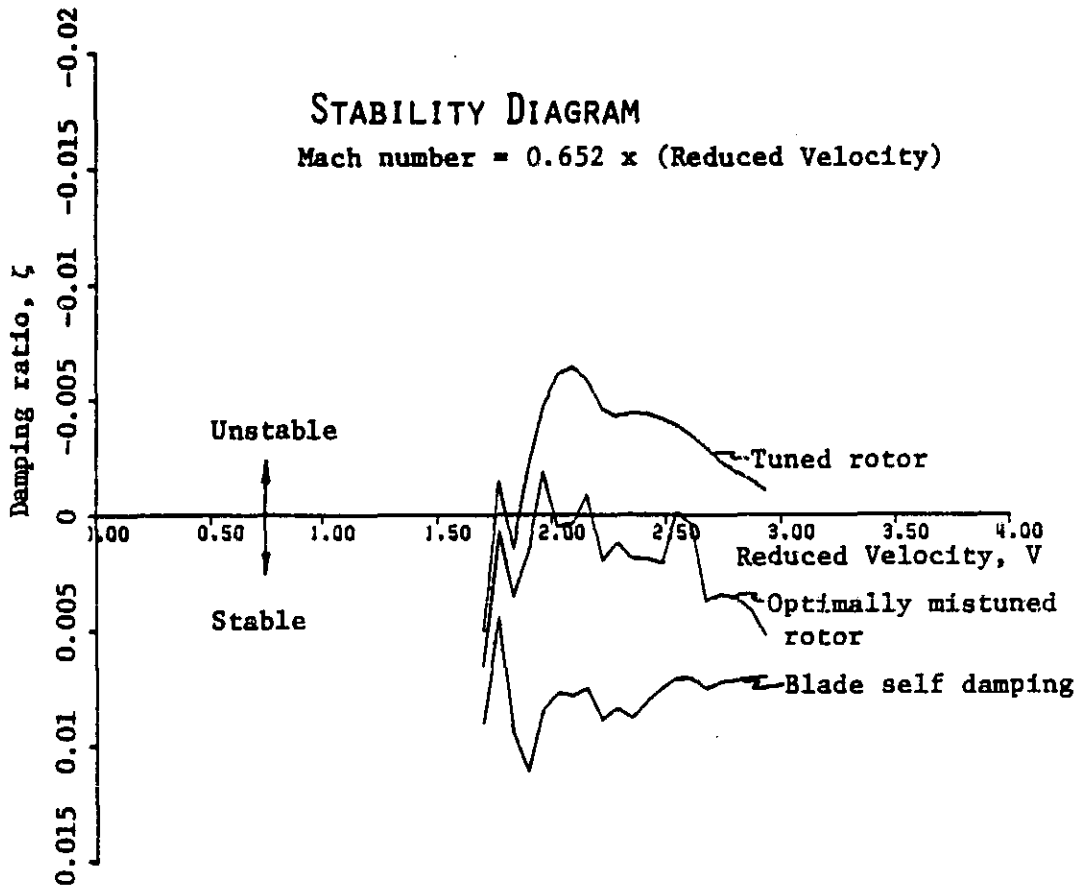

Figure 5.6 Stability margin of a rotor operating on its operating line. In this case, the Mach number is proportional to the reduced velocity.

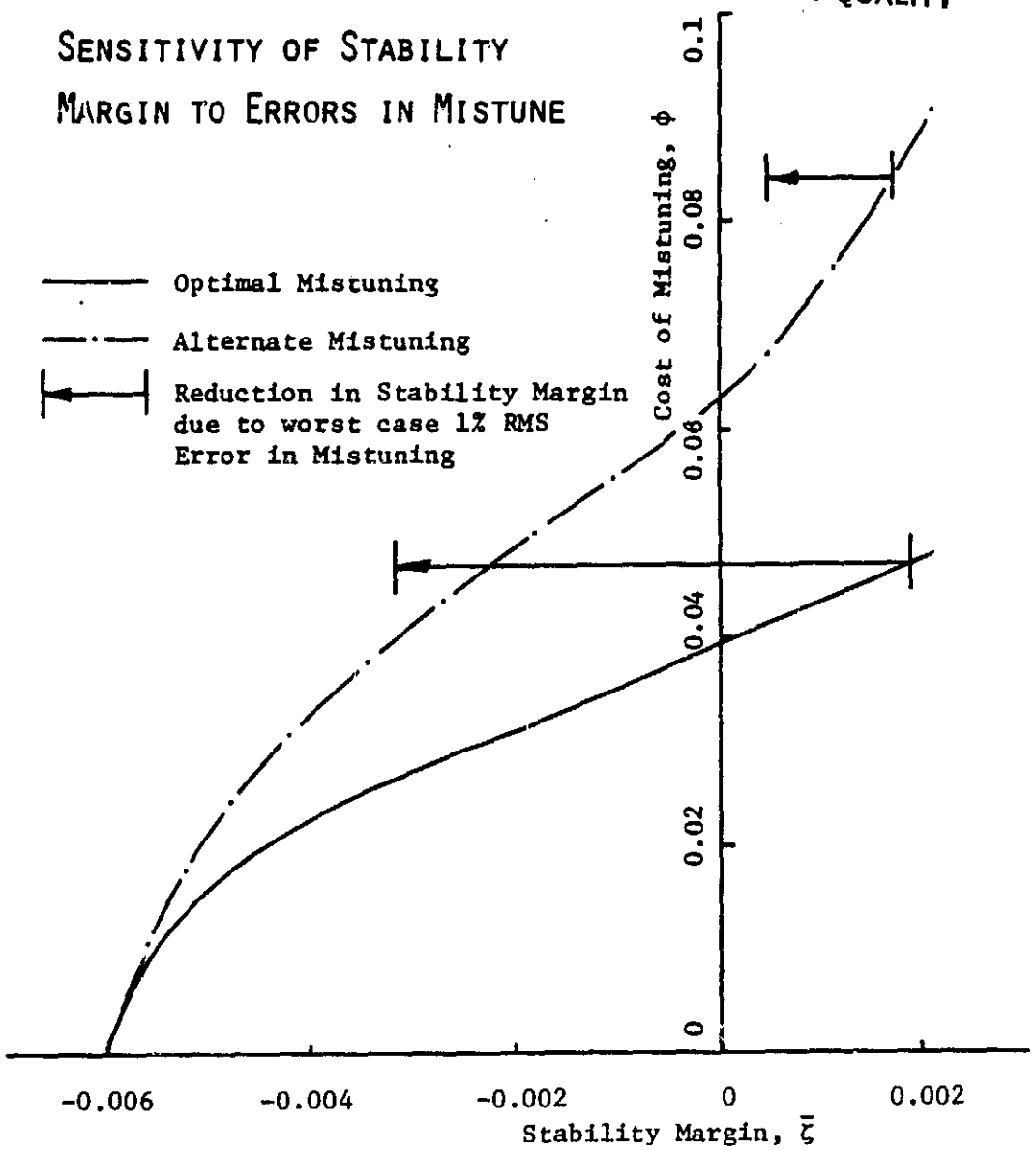

Figure 5.7 Sensitivity of the stability margin of a mistuned rotor to errors in mistuning. The arrows indicate the loss in stability due to mistuning errors of 1% root mean square introduced in the worst poosible direction. Note that optimal mistuning is much more sensitive to these errors than alternate mistuning.

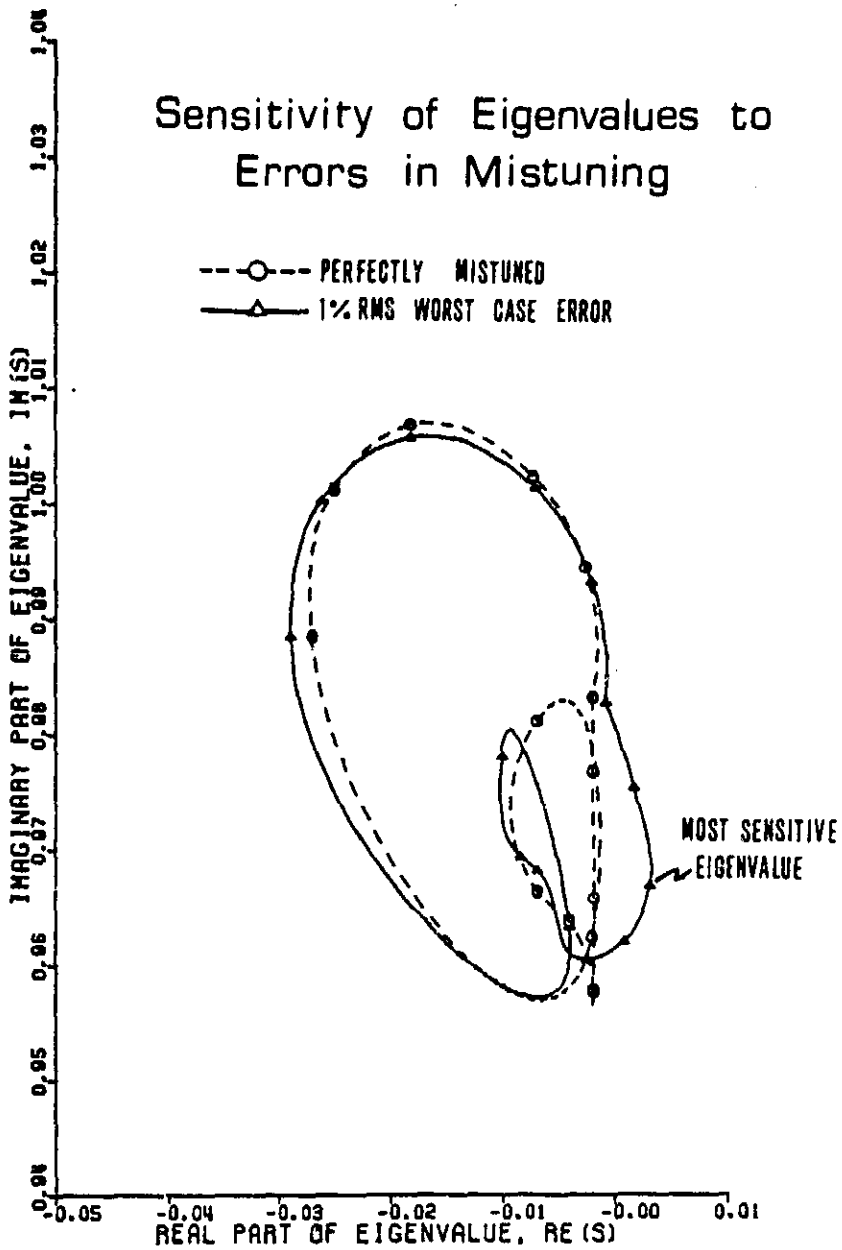

Figure 5.8 Sensitivity of eigenvalues of optimally mistuned rotor to errors in mistuning. The errors introduced into the system have a root mean square value of 0.01, and are introduced in the direction in mistune space which is most destabilizing.

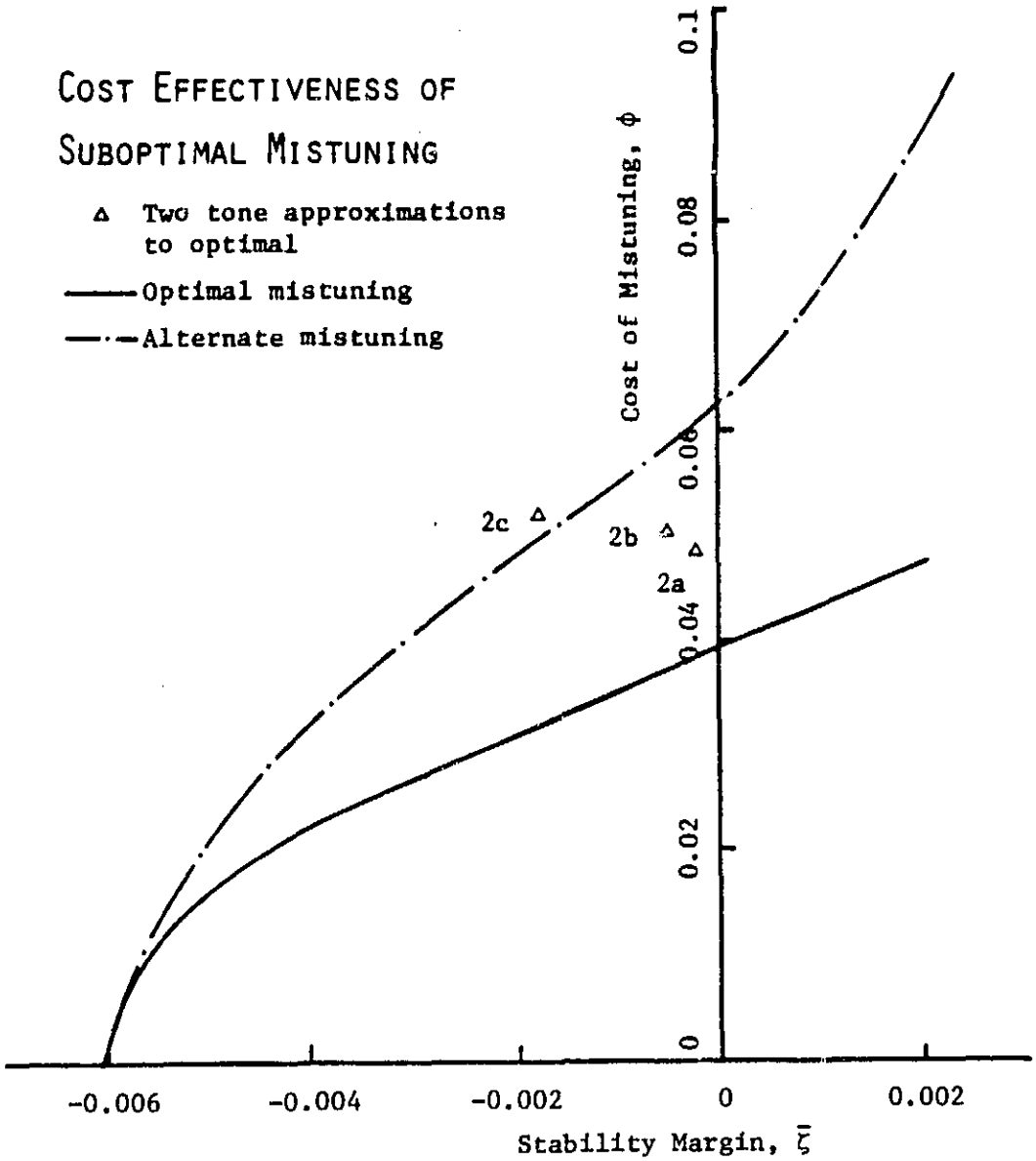

Figure 5.9 Cost effectiveness of two tone mistune patterns. Mistune patterns 2a, 2b, and 2c were chosen to approximate optimal mistune pattern for $\bar{\zeta} = 0.0018$.

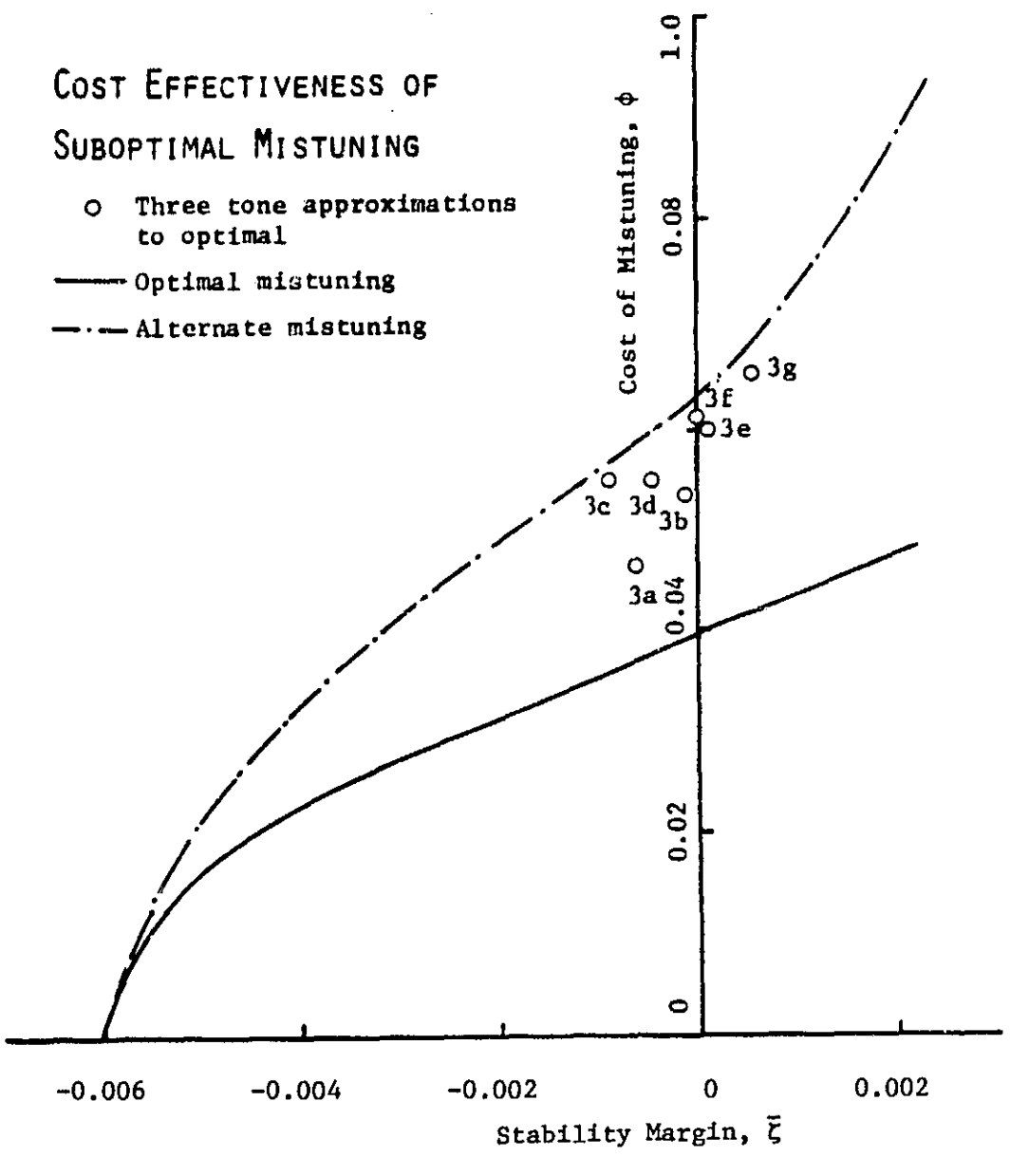

Figure 5.10 Cost effectiveness of three tone mistune patterns. Mistune patterns 3a, 3b, 3c, 3d, 3e, 3f, and 3g were chosen to approximate the optimal mistune pattern for $\bar{\zeta} = 0.0018$.

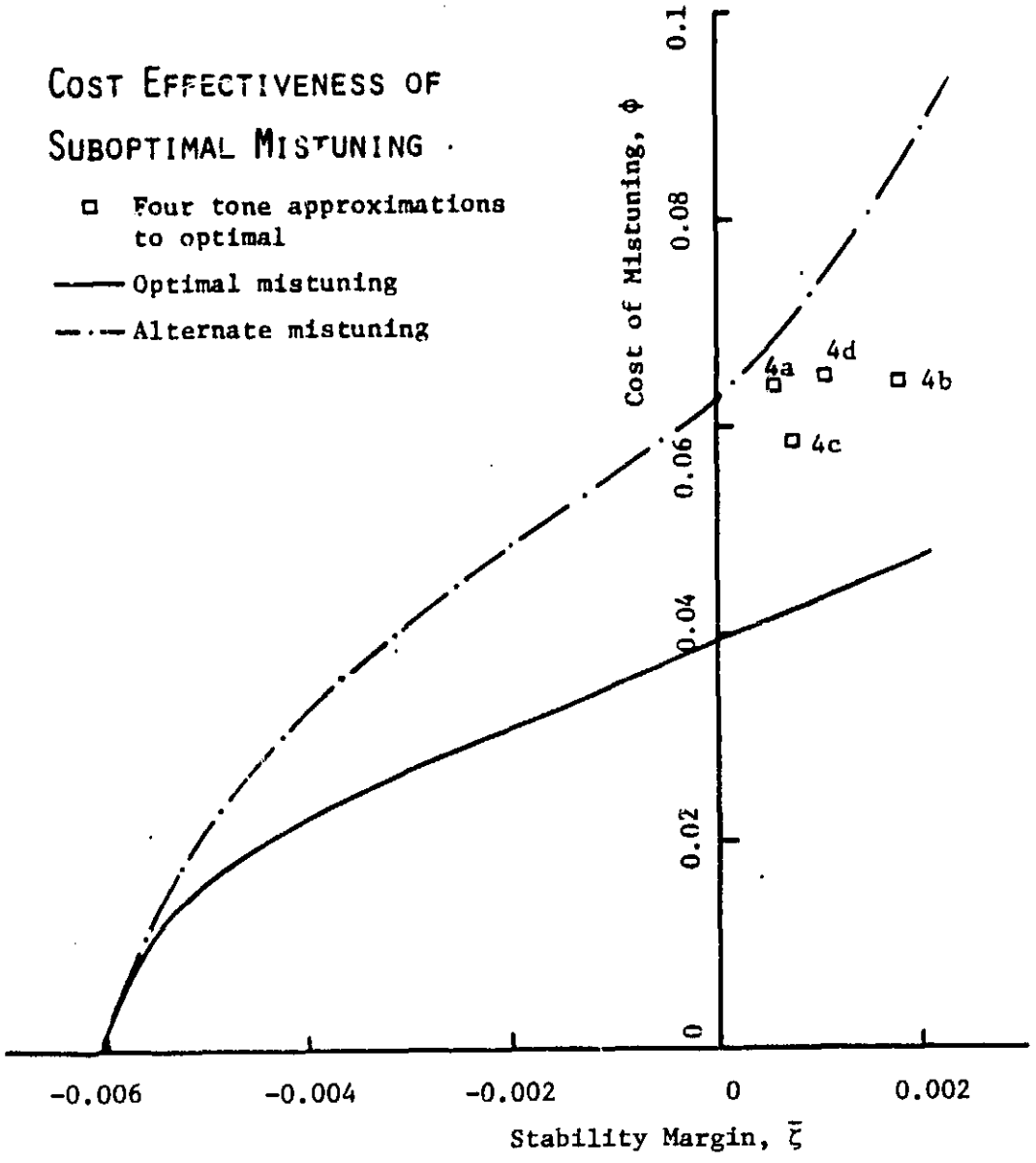

Figure 5.11 Cost effectiveness of four tone mistune patterns. Mistune patterns 4a, 4b, 4c, and 4d were chosen to approximate optimal mistune pattern for $\bar{\zeta} = 0.0018$.